Atlas of Formability

Haynes 230

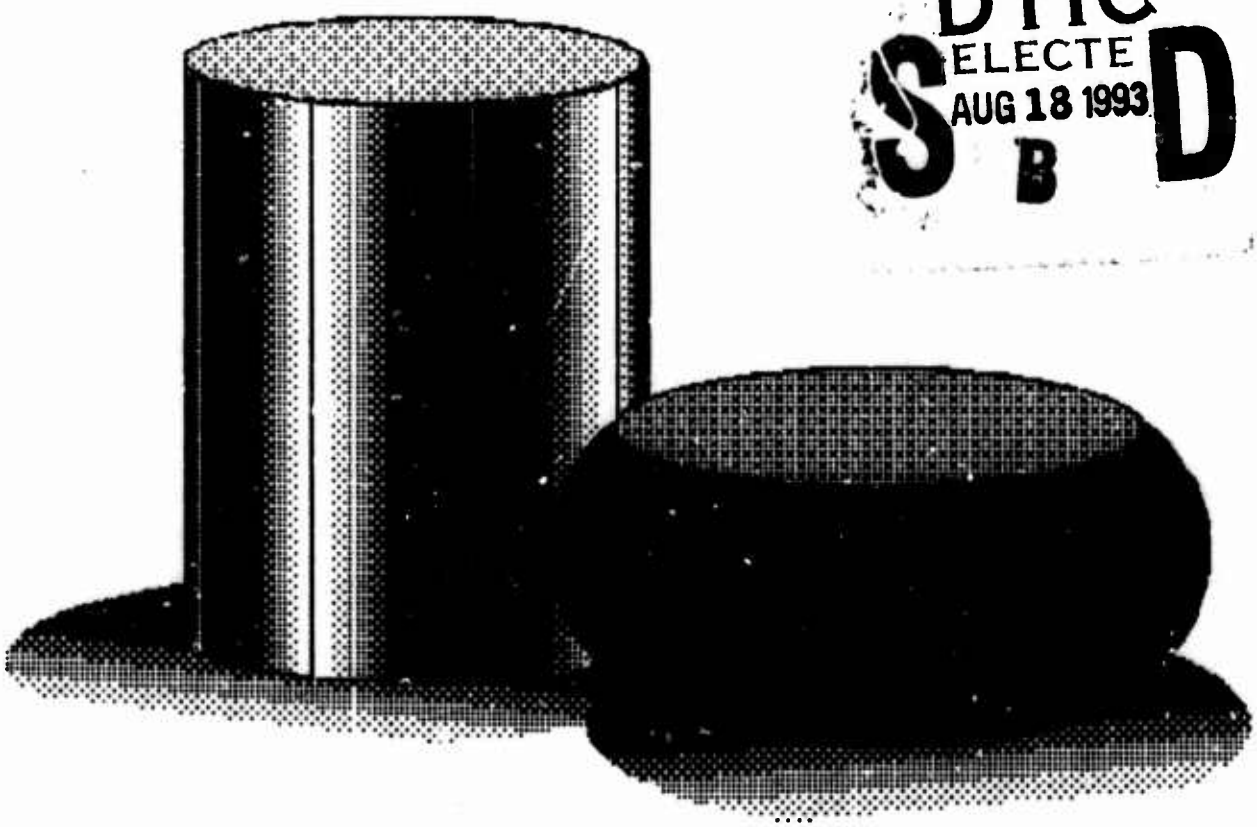

NCEMT

DISCLAIMER NOTICE

THIS DOCUMENT IS BEST QUALITY AVAILABLE. THE COPY FURNISHED TO DTIC CONTAINED A SIGNIFICANT NUMBER OF PAGES WHICH DO NOT REPRODUCE LEGIBLY.

ATLAS OF FORMABILITY

HAYNES 230

by

Prabir K. Chaudhury and Dan Zhao

National Center for Excellence in Metalworking Technology
1450 Scalp Avenue
Johnstown, PA 15904

for

Naval Industrial Resource Support Activity
Building 75-2, Naval Base
Philadelphia, PA 19112-5078

August 30, 1992

REPORT DOCUMENTATION PAGE

Form Approved
OMB No. 0704-0188

1. AGENCY USE ONLY (Leave blank)	2. REPORT DATE	3. REPORT TYPE AND DATES COVERED
	August 30, 1992	Final, 5/30/92-9/30/92

4. TITLE AND SUBTITLE
Atlas of Formability
Haynes 230

5. FUNDING NUMBERS
C-N00140-88-C-RC21

6. AUTHOR(S)
Prabir Chaudhury
Dan Zhao

7. PERFORMING ORGANIZATION NAME(S) AND ADDRESS(ES)
National Center for Excellence
Metalworking Technology (NCEMT)
1450 Scalp Avenue
Johnstown, PA 15904

8. PERFORMING ORGANIZATION REPORT NUMBER

9. SPONSORING/MONITORING AGENCY NAME(S) AND ADDRESS(ES)
Naval Industrial Resources Support Activity
Building 75-2, Naval Base
Philadelphia, PA 19112-5078

10. SPONSORING/MONITORING AGENCY REPORT NUMBER

11. SUPPLEMENTARY NOTES

12a. DISTRIBUTION/AVAILABILITY STATEMENT

12b. DISTRIBUTION CODE

13. ABSTRACT (Maximum 200 words)

In this investigation, flow behavior of Haynes 230 alloy was studied by conducting compression tests over a wide range of temperatures and stain rates. Constitutive relations were determined from the flow behavior, and a dynamic material modeling was performed on this alloy. Thus, the optimum processing condition in terms of temperature and during high temperature defromation were also characterized.

14. SUBJECT TERMS
Haynes 230, Deformation Processing
High temperature deformation, Processing Map, Metalworking

15. NUMBER OF PAGES
67

16. PRICE CODE

17. SECURITY CLASSIFICATION OF REPORT	18. SECURITY CLASSIFICATION OF THIS PAGE	19. SECURITY CLASSIFICATION OF ABSTRACT	20. LIMITATION OF ABSTRACT
Unclassified	Unclassified	Unclassified	

TABLE OF CONTENTS

LIST OF TABLE

Haynes 230

Introduction

Haynes alloy 230 finds extensive application in aerospace, chemical processing and industrial heating industries. This material has excellent high temperature properties and good corrosion resistance. The understanding of mechanical and microstructural behavior during high temperature deformation is very important for deformation processing of these alloys. In this investigation, flow behavior of Haynes alloy 230 was determined by conducting compression tests at various temperatures and strain rates. Constitutive relations were determined from the flow behavior, and a dynamic material modeling for this alloy was performed. Thus, the optimum processing condition in terms of temperature and strain rate was determined. Microstructural changes during high temperature deformation were also characterized to aid process design engineers to select processing conditions in terms of resulting microstructure.

Experimental Procedure

The material used in this investigation was commercially available Haynes 230 solution treated bars. The typical microstructure of the as-received materials had an equiaxed grain with an average size of 52 μm (ASTM 5.2), Figure 1. There are some large precipitates, possibly of M_6C type carbides, which remained in the microstructures even after high temperature deformation. The chemical composition of this alloy is as follows:

Element	Ni	Cr	W	Fe	Mo	Co	Mn	Si	Al	C
Wt. %	Bal	21.7	13.98	1.41	1.2	0.64	0.48	0.37	0.31	0.11

Cylindrical compression test specimens with a diameter of 12.7 mm and a height of 15.9 mm were machined from the bars. Isothermal compression testing was conducted on MTS testing machine under an inert environment. The test matrix was as follows:

Temperature, C (F): 950 (1742), 1000 (1832), 1050 (1922), 1100 (2012), 1150 (2102), 1175 (2147), and 1200 (2192)
Strain rate, s^{-1}: 0.001, 0.01, 0.05, 0.1, 0.5, 1, 5 and 20

The tests were conducted in vacuum. Load and stroke data from the tests were acquired by a computer and later converted to true stress-true strain curves. Immediately after the compression test, the specimens were quenched with forced helium gas in order to retain the deformed microstructure. Longitudinal and transverse sections of the specimens were examined using optical microscope. The photomicrographs presented were taken from the center of the longitudinal section of the specimens.

Results

Table 1 is a list of the figures, test conditions and the observed microstructures. The true stress-true strain flow curves are shown in Figure 2 to Figure 57 with the corresponding deformed microstructures in some of these figures to understand microstructural changes under the processing conditions. True stress versus strain rate was plotted in log-log scale in Figure 58 at a true strain of 0.3. The slope of the plot gives the strain rate sensitivity m, which is not constant over the range of strain rate tested. Log stress vs. 1/T at the same true strain is shown in Figure 59. A processing map at this strain was developed for the Haynes alloy 230 and is shown in Figure 60. The optimum processing condition from the map can be obtained by selecting the temperature and strain rate combination which provides the maximum efficiency in the stable region. This condition is approximately 1100 C and 0.001 s^{-1} for this material. The precipitates in the as-received material remain after test at all test conditions.

Table 1. List of figures, testing conditions and microstructural observations for Haynes 230

Fig. No.	Temperature C(F)	Strain Rate S^{-1}	Microstructure Optical Microscopy	Page No
1			As received, heat treated and aged wrought bars Equiaxed grains of 52 µm (ASTM 5.2) Some twins observed. Precipitates present and remain for all the test conditions below.	4
2	950(1742)	0.001	Twinned elongated grains (aspect ratio ~3.1) showing some necklacing.	5
3	950(1742)	0.01		6
4	950(1742)	0.05	Elongated grains showing some necklacing.	7
5	950(1742)	0.10	Elongated grains (aspect ratio ~3.5) with starting necklacing at the grain boundaries.	8
6	950(1742)	0.50		9
7	950(1742)	1.0	Elongated grains, extensive necklacing and about 25% of recrystallized equiaxed grains (~4µm).	10
8	950(1742)	5.0		11
9	950(1742)	20.0	Elongated grains (aspect ratio ~2.1) with some twins and possibly slip lines.	12
10	1000(1832)	0.001	Elongated grains showing twins and, ~3% necklacing is also present.	13
11	1000(1832)	0.01	Elongated grains and extensive necklacing with ~10% of recrystallized equiaxed grains (3.4 µm). Some twins and possibly slip bands are present.	14
12	1000(1832)	0.05		15
13	1000(1832)	0.10	same as above (11).	16
14	1000(1832)	0.50		17
15	1000(1832)	1.0	Elongated grains with some twins and, very fine necklacing at grain boundaries. There is also some subgranular structure within deformed grains.	18
16	1000(1832)	5.0		19
17	1000(1832)	20.0	Elongated grains with some twins and possibly slip bands.	20
18	1050(1922)	0.001	Elongated grains with some twins and, very fine necklacing. There is also some subgranular structure within deformed grains.	21
19	1050(1922)	0.01		22
20	1050(1922)	0.05	Elongated grains with extensive necklacing, recrystallized grains, some twins , slip lines, and, there is also some subgranular structure within deformed grains.	23
21	1050(1922)	0.1	Same as above.	24
22	1050(1922)	0.5		25

23	1050(1922)	1	Elongated grains with extensive necklacing, recrystallized grains, some twins , slip lines, and, there is also some subgranular structure (~60% equiaxed grains of 7 μm) within deformed grains.	26
24	1050(1922)	5		27
25	1050(1922)	20	Elongated grains (aspect ratio ~3 1)with necklacing and a sub granular structure.	28
26	1100(2012)	0.001	Equiaxed dynamically recrystallized grains (~40% with a average size of 12 μm) and some elongated deformed grains. Fine grain boundary precipitation	29
27	1100(2012)	0.01	Elongated and ~45% equiaxed recrystallized grains of 8.5 μm. There are deformation twins and possibly slip bands. Fine grain boundary precipitation	30
28	1100(2012)	0.05		31
29	1100(2012)	0.1	Extensively deformed grains with necklacing and subgranular structure ~45% (equiaxed grains with an average size of 8 μm). Fine precipitation at grain boundaries is also present.	32
30	1100(2012)	0.5		33
31	1100(2012)	1	Elongated grains with a subgranular structure and fine precipitation at grain boundaries	34
32	1100(2012)	5		35
33	1100(2012)	20	Elongated grains with a subgranular structure ~90% (equiaxed grains with an average size of 11 μm). Fine precipitation at grain boundaries is also present.	36
34	1150(2102)	0.001	Large recrystallized equiaxed grains with some twinning.	37
35	1150(2102)	0.01		38
36	1150(2102)	0.05	Recrystallized equiaxed grains.	39
37	1150(2102)	0.1		40
38	1150(2102)	0.5		41
39	1150(2102)	1	Small recrystallized grains (duplex size) with some twinning.	42
40	1150(2102)	5		43
41	1150(2102)	20	Small recrystallized grains (duplex size) with some twinning.	44
42	1175(2147)	0.001	Recrystallized equiaxed grains (duplex size).	45
43	1175(2147)	0.01	Recrystallized equiaxed grains (duplex size).	46
44	1175(2147)	0.05		47
45	1175(2147)	0.1	Recrystallized equiaxed grains, and few grown grains.	48
46	1175(2147)	0.5		49
47	1175(2147)	1	Equiaxed recrystallized grains with some twins.	50
48	1175(2147)	5		51
49	1175(2147)	20	Small recrystallized equiaxed grains.	52
50	1200(2192)	0.001	Large recrystallized equiaxed grains (~47 μm), there are no twins present and the large precipitates are finer than at lower temperatures.	53
51	1200(2192)	0.01		54

52	1200(2192)	0.05	Large recrystallized equiaxed recrystallized grains, there are no twins present and the large precipitates are finer than at lower temperatures.	55
53	1200(2192)	0.1	Recrystallized equiaxed grains (~17.1 μm), there are some twins present and the large precipitates are finer than at lower temperatures.	56
54	1200(2192)	0.5		57
55	1200(2192)	1	Recrystallized equiaxed grains.	58
56	1200(2192)	5		59
57	1200(2192)	20	Recrystallized equiaxed grains.	60

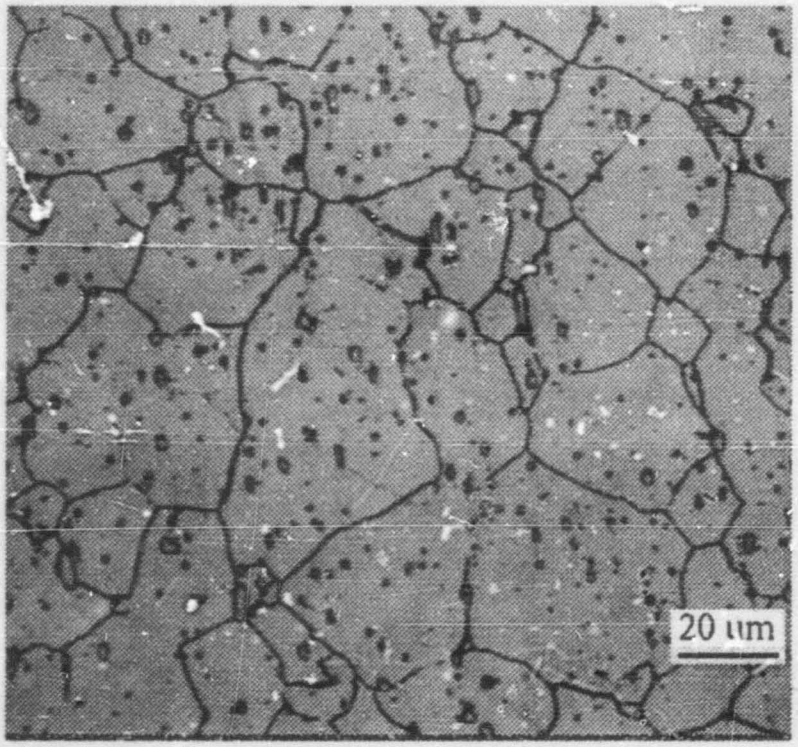

Figure 1. As-received microstructure of Haynes 230.

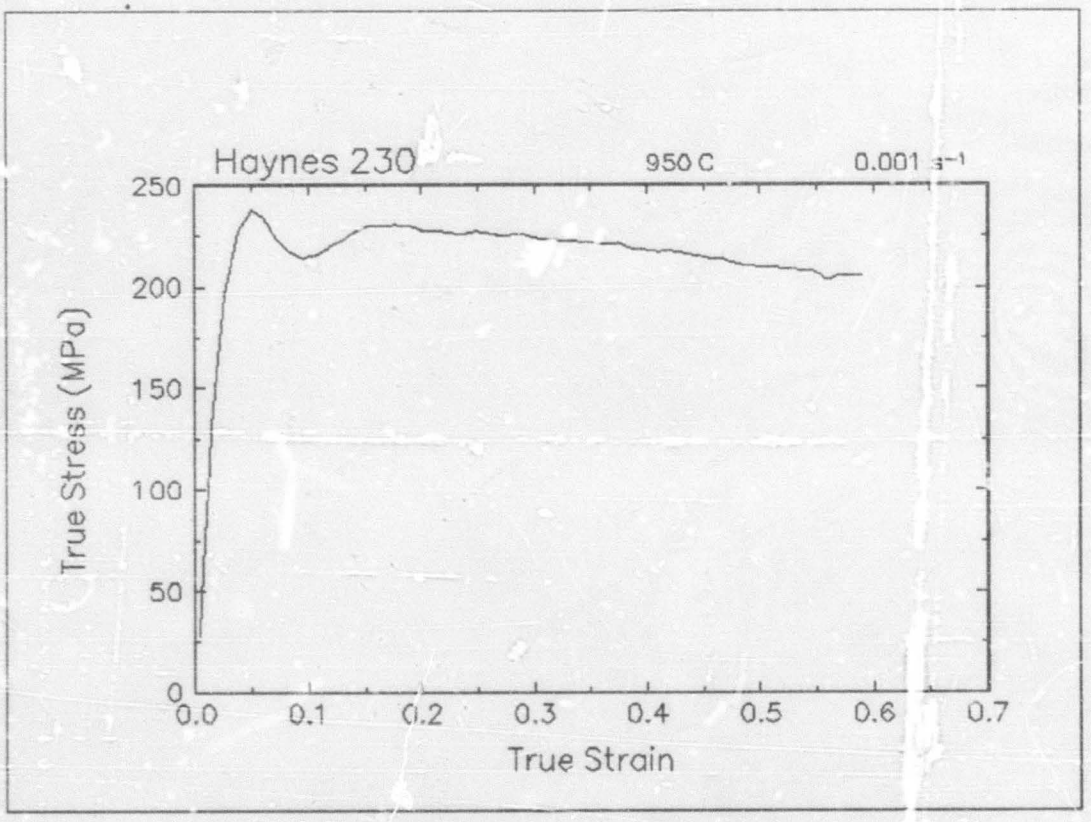

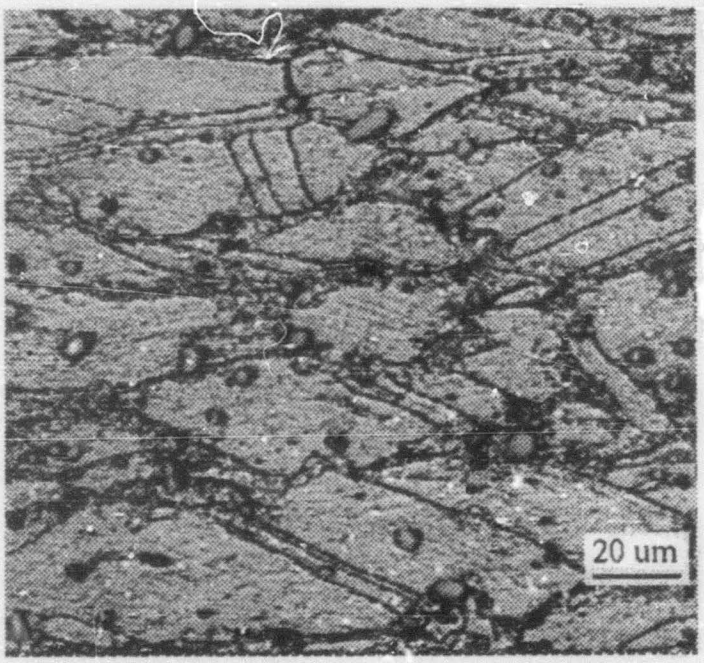

Figure 2. True stress-true strain curve and an optical micrograph from the center of the compressed sample cut through the compression axis, 950 C and 0.001 s^{-1}.

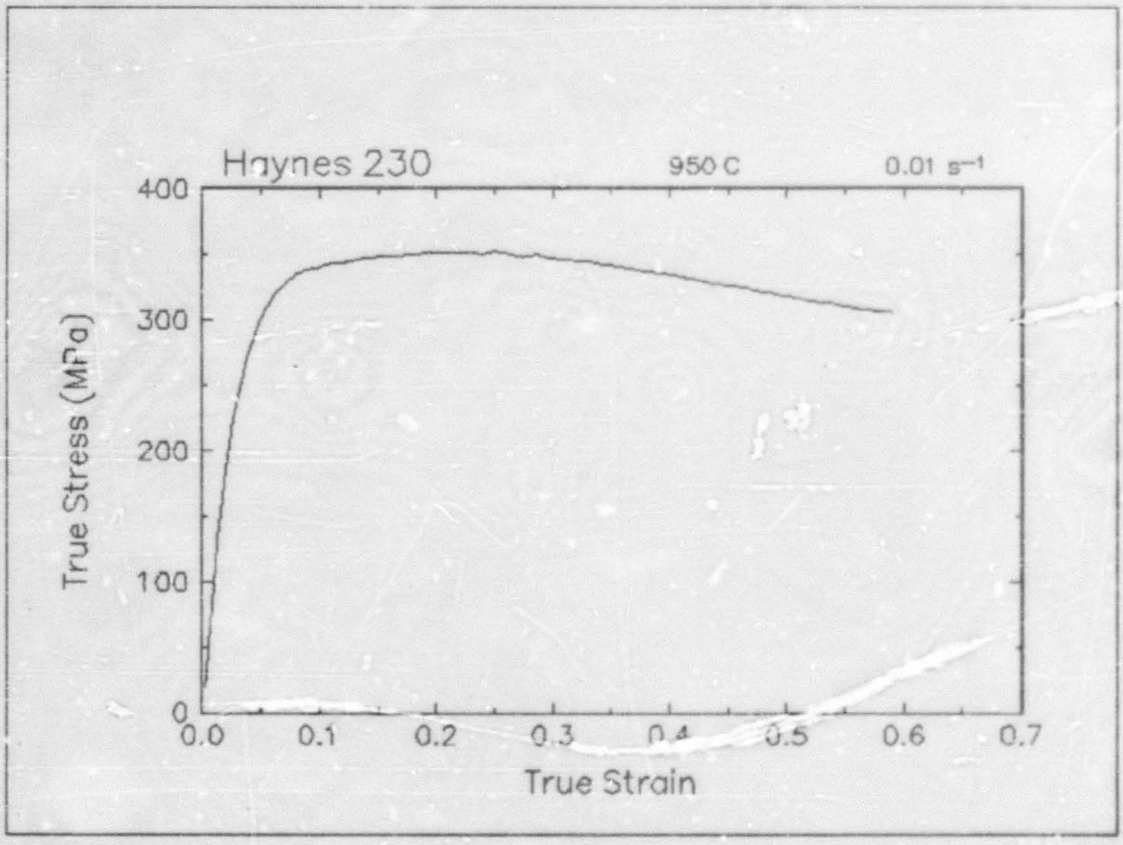

Figure 3. True stress-true strain curve, 950 C and 0.01 s^{-1}

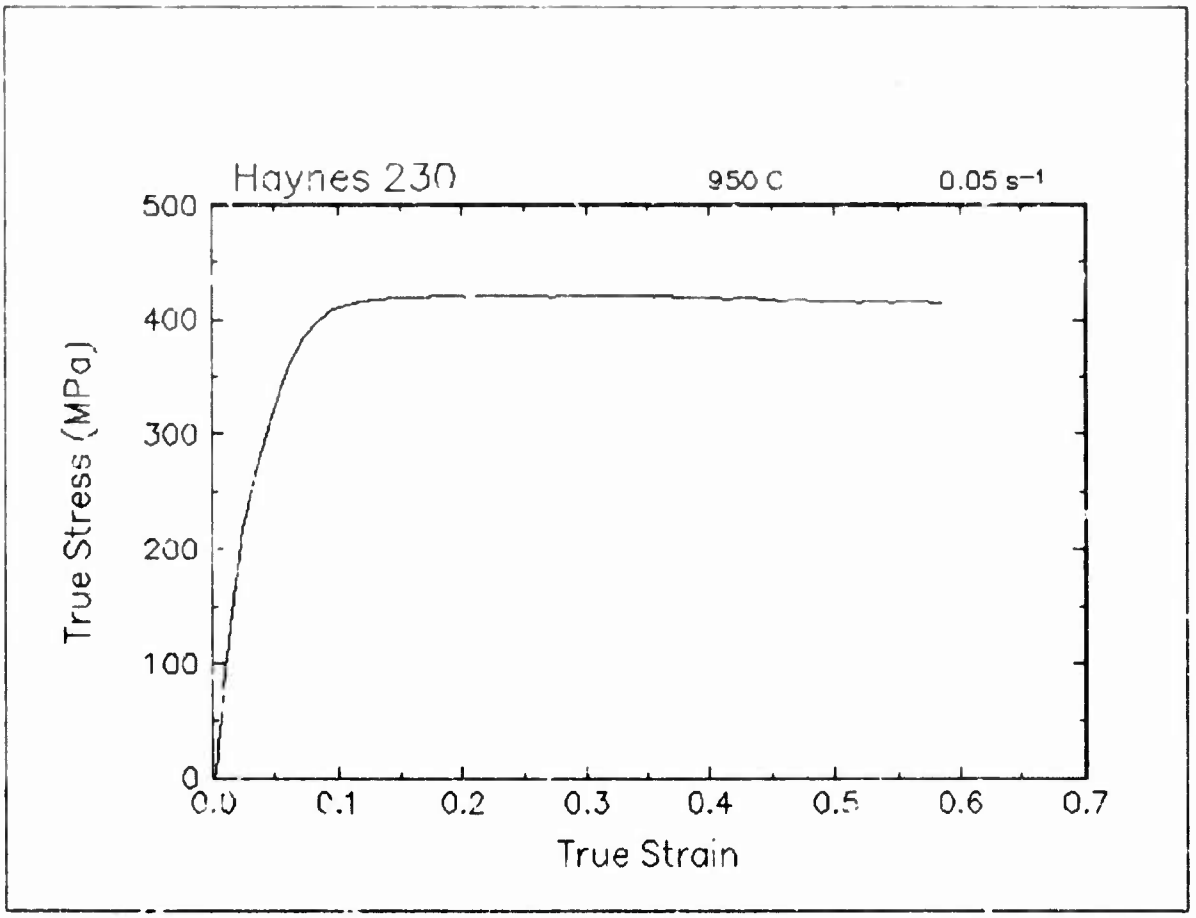

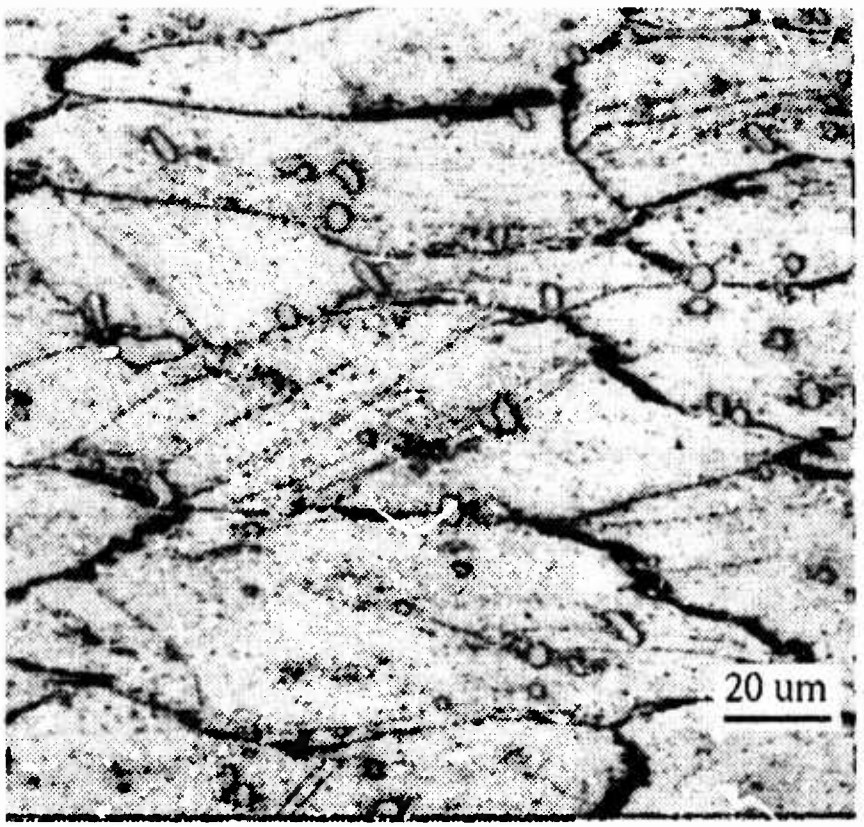

Figure 4. True stress-true strain curve and an optical micrograph from the center of the compressed sample cut through the compression axis, 950 C and 0.05 s^{-1}

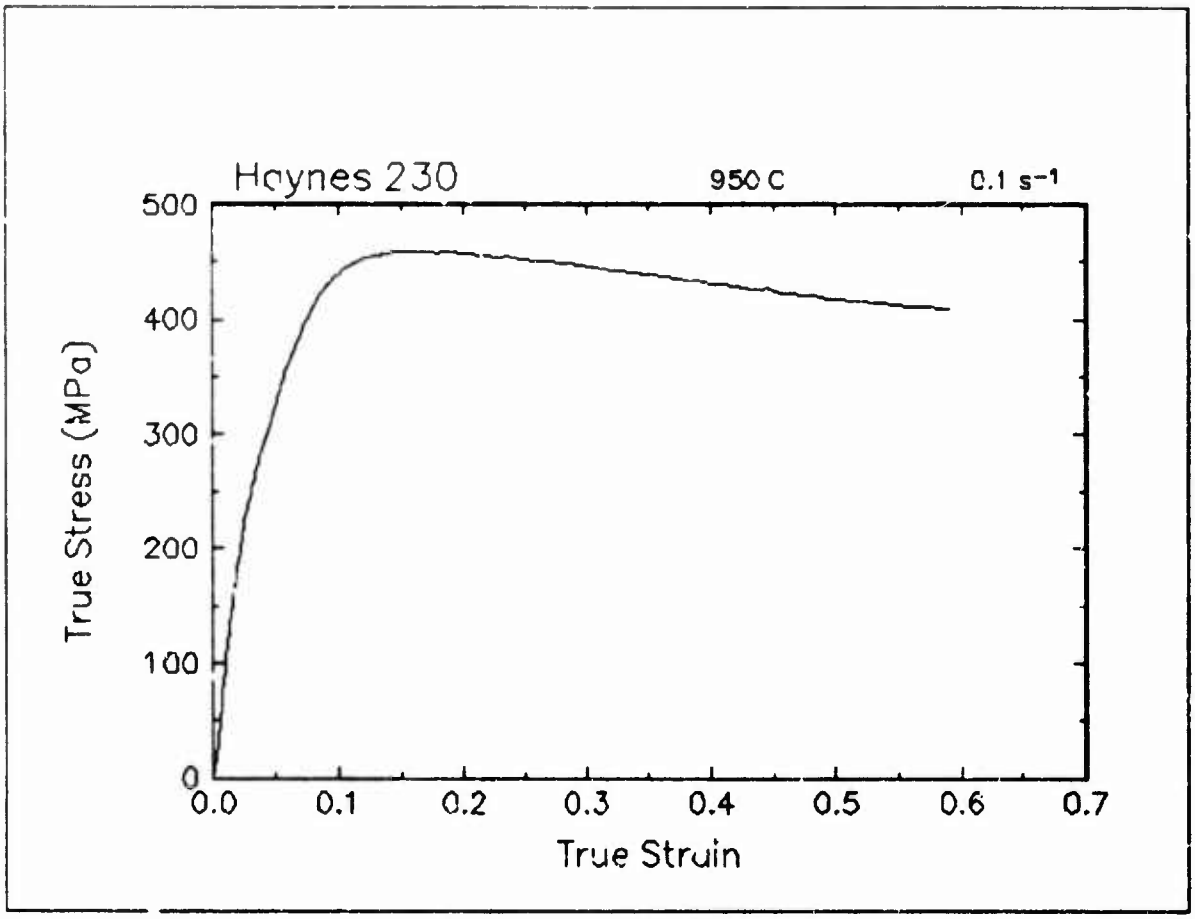

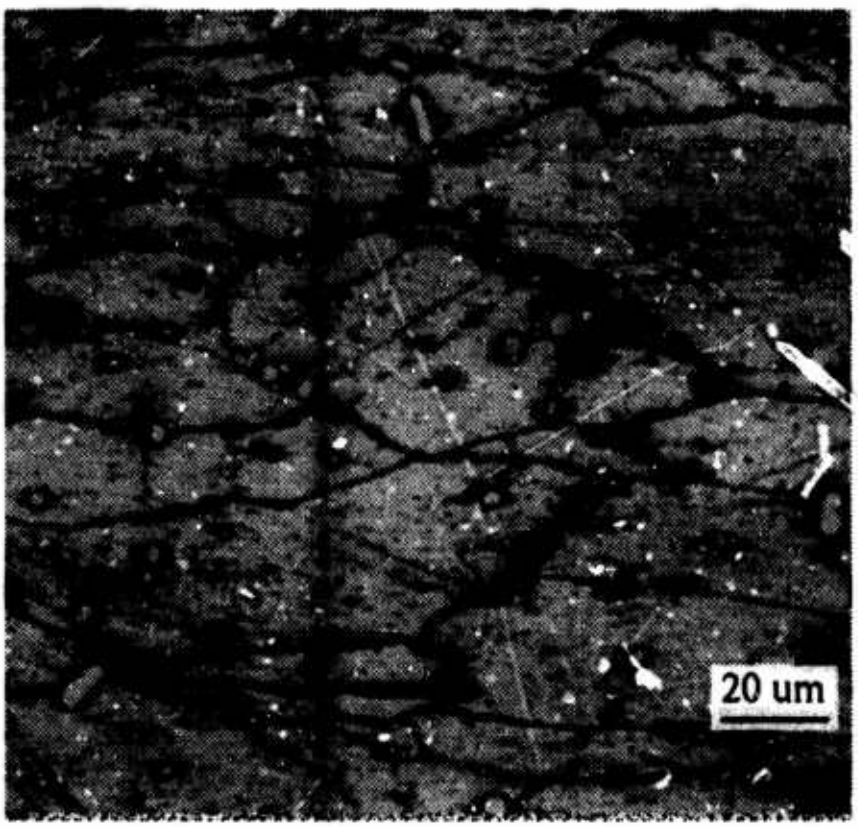

Figure 5. True stress-true strain curve and an optical micrograph from the center of the compressed sample cut through the compression axis, 950 C and 0.1 s^{-1}.

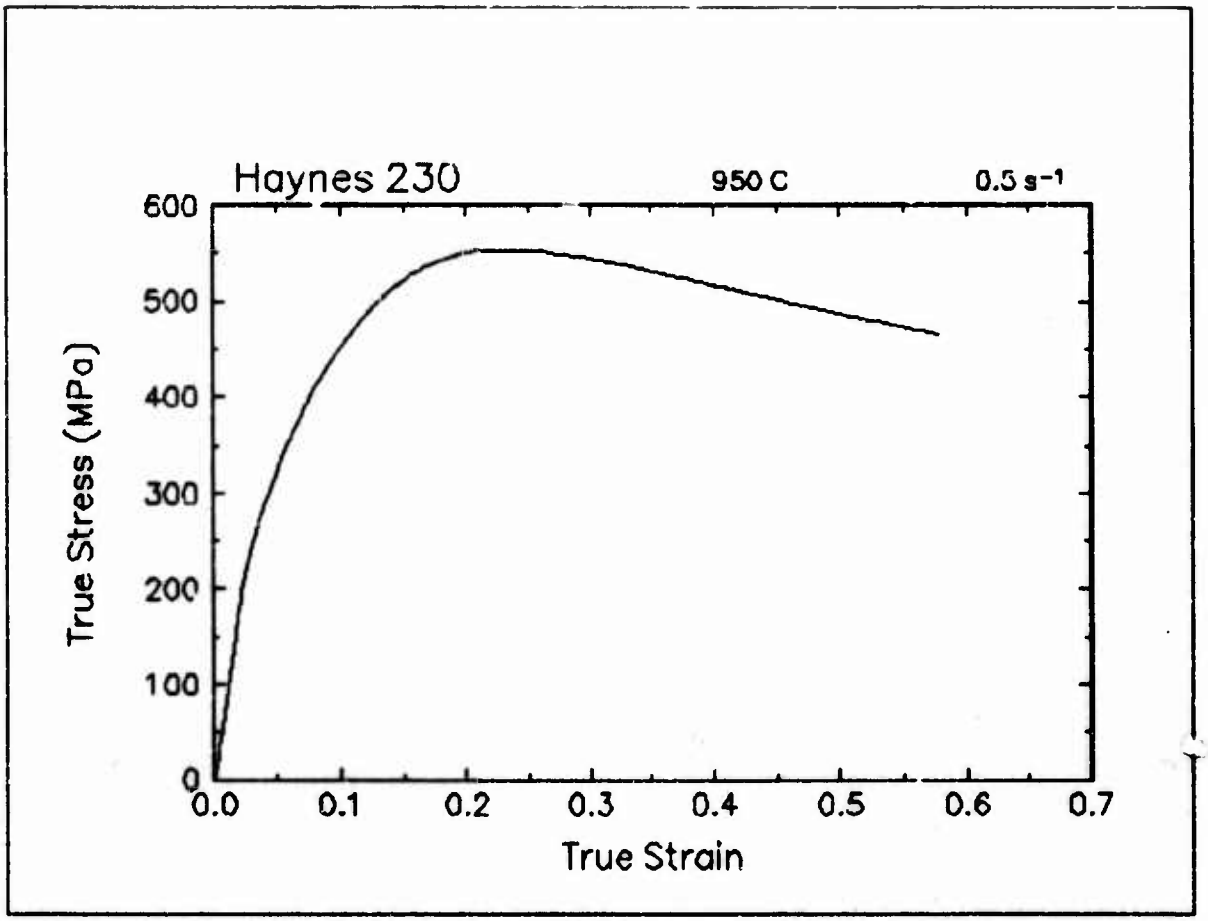

Figure 6. True stress-true strain curve, 950 C and 0.5 s^{-1}.

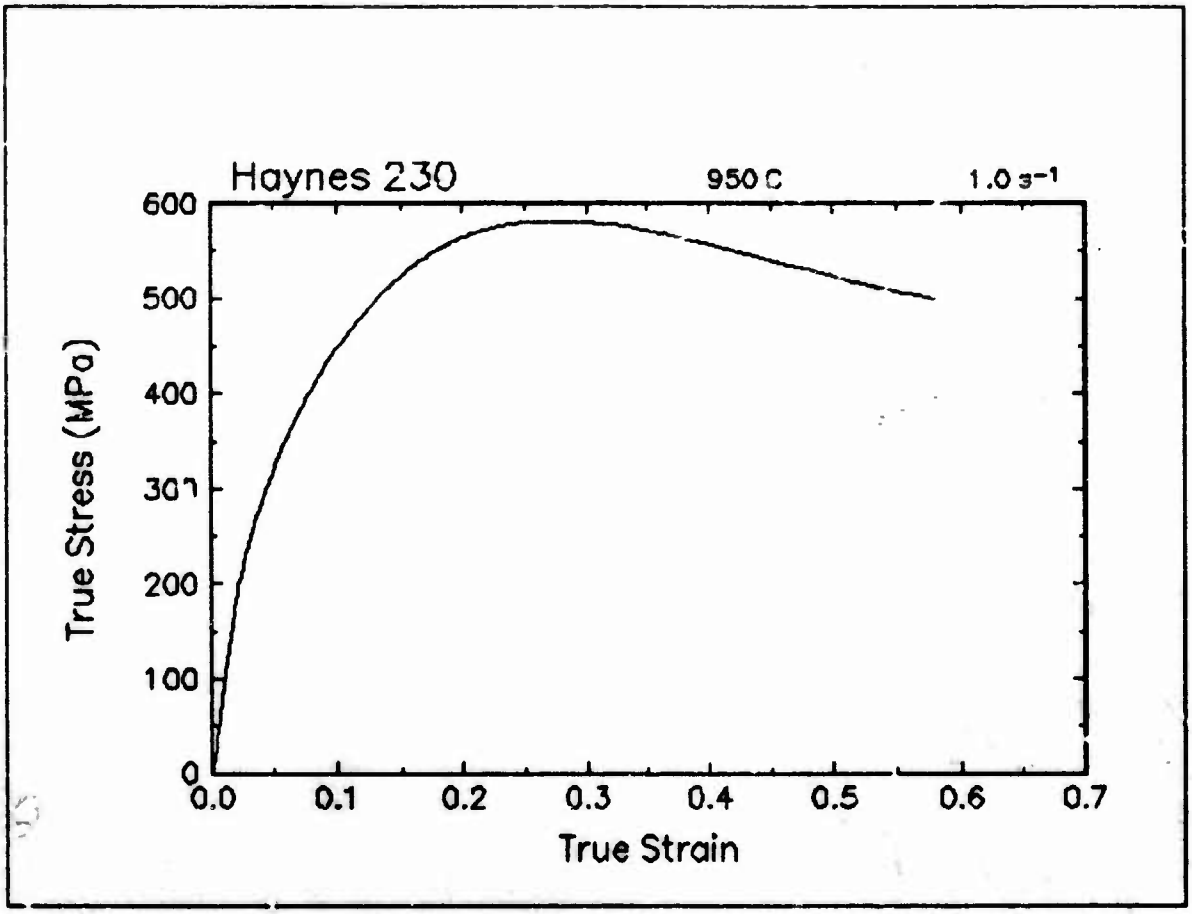

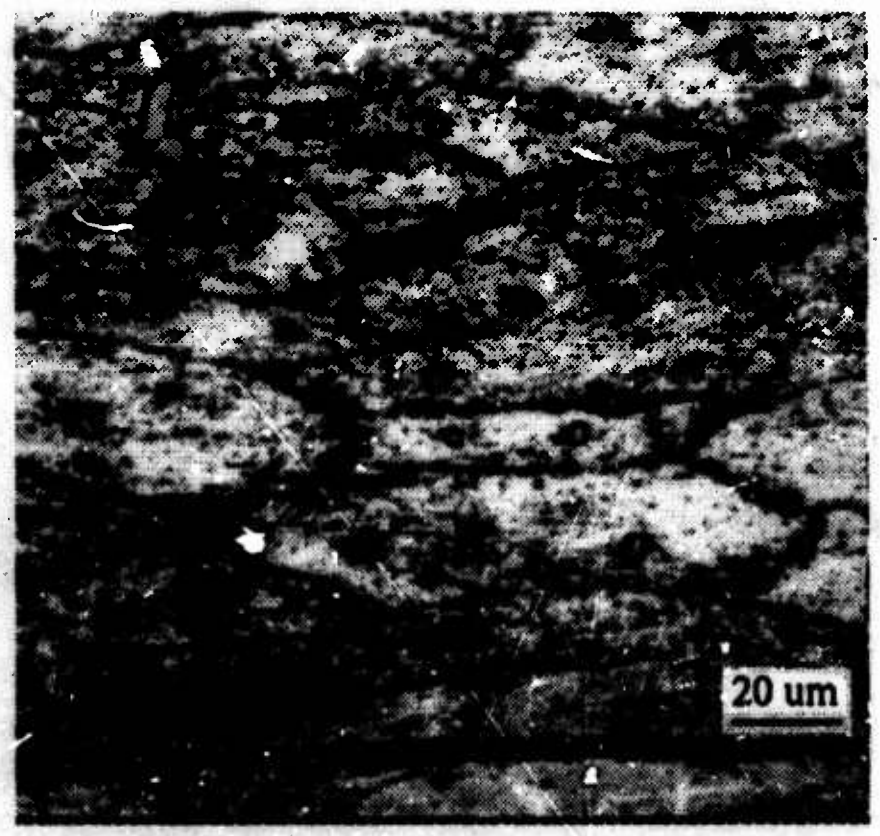

Figure 7. True stress-true strain curve and an optical micrograph from the center of the compressed sample cut through the compression axis, 950 C and 1 s^{-1}.

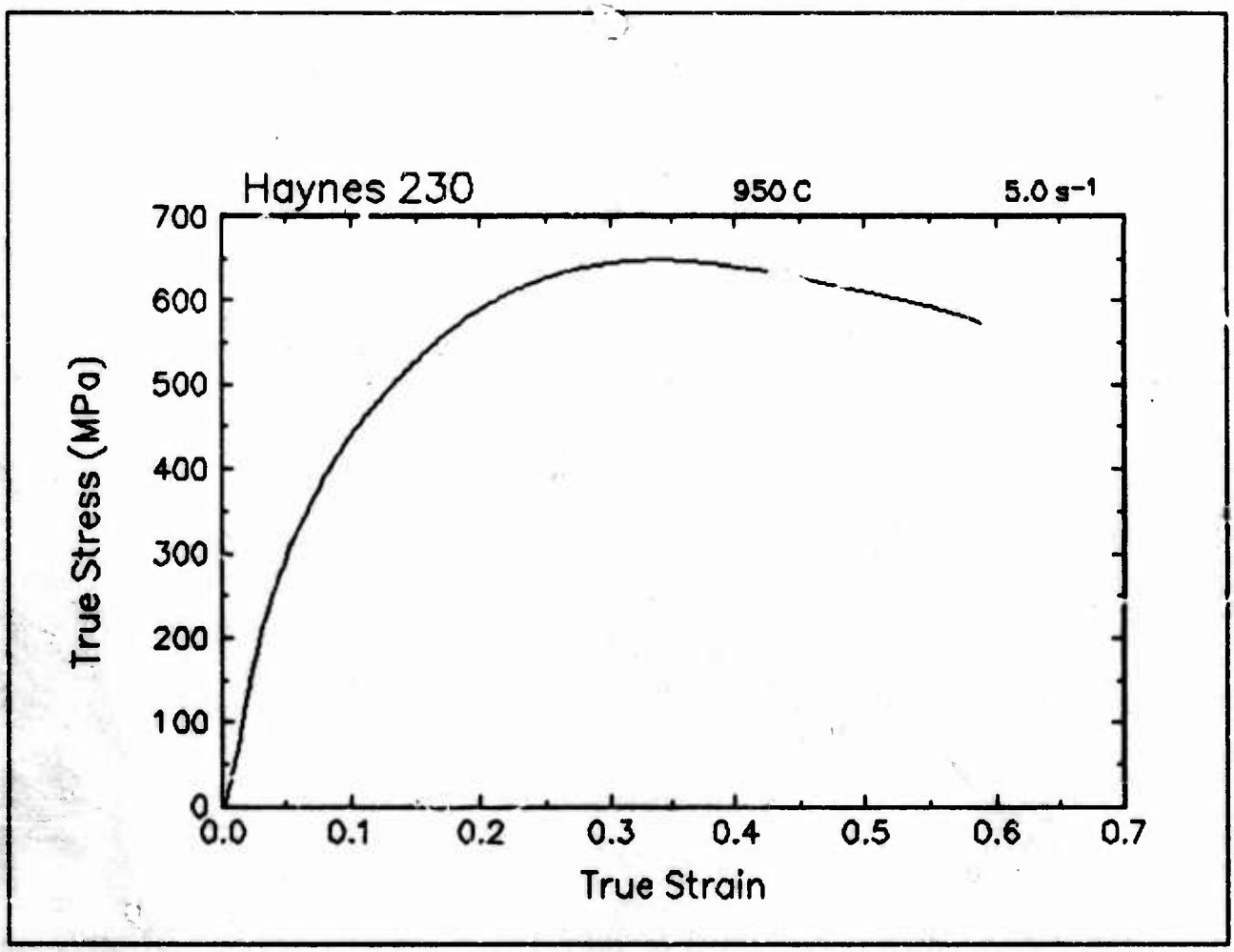

Figure 8. True stress-true strain curve, 950 C and 5 s^{-1}.

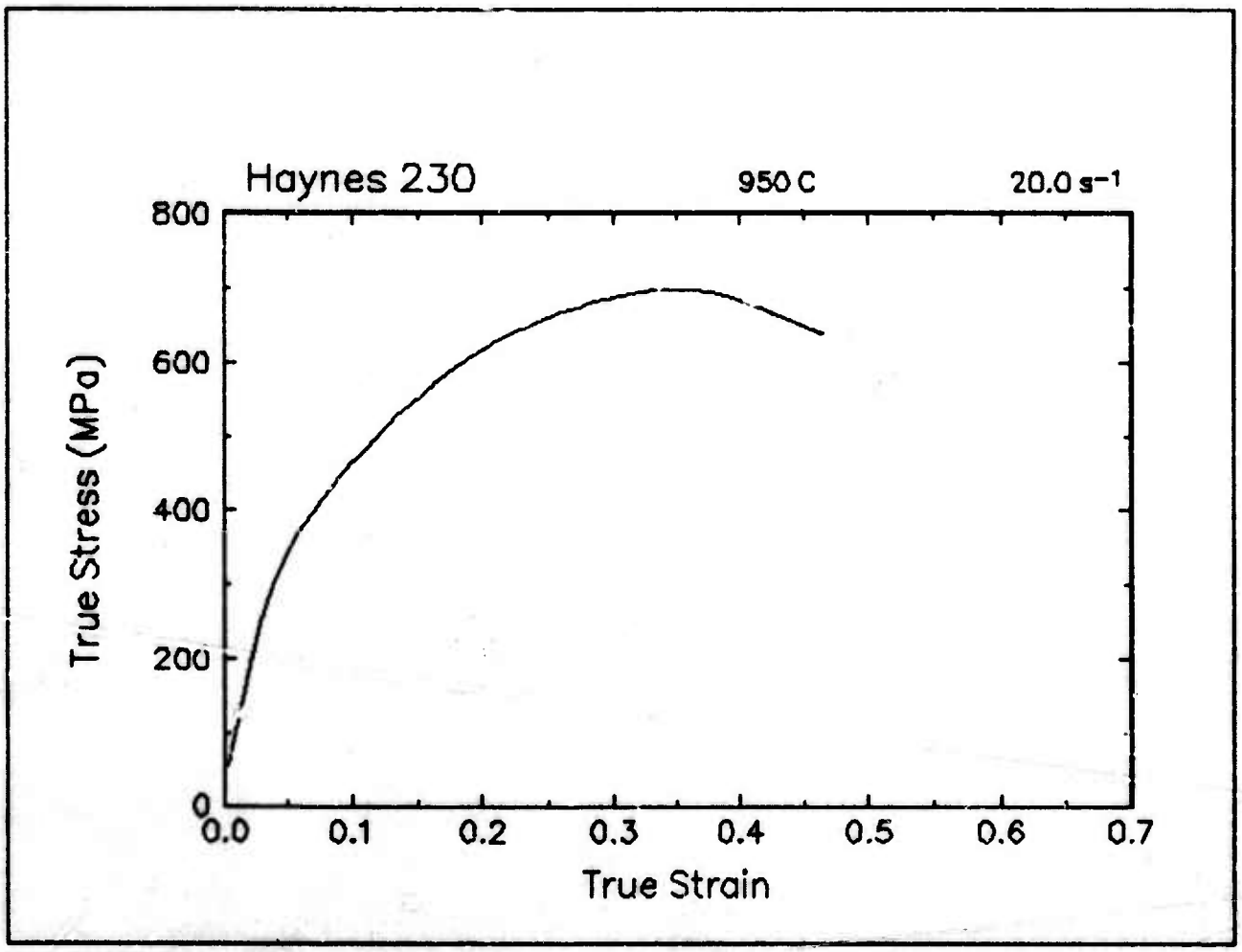

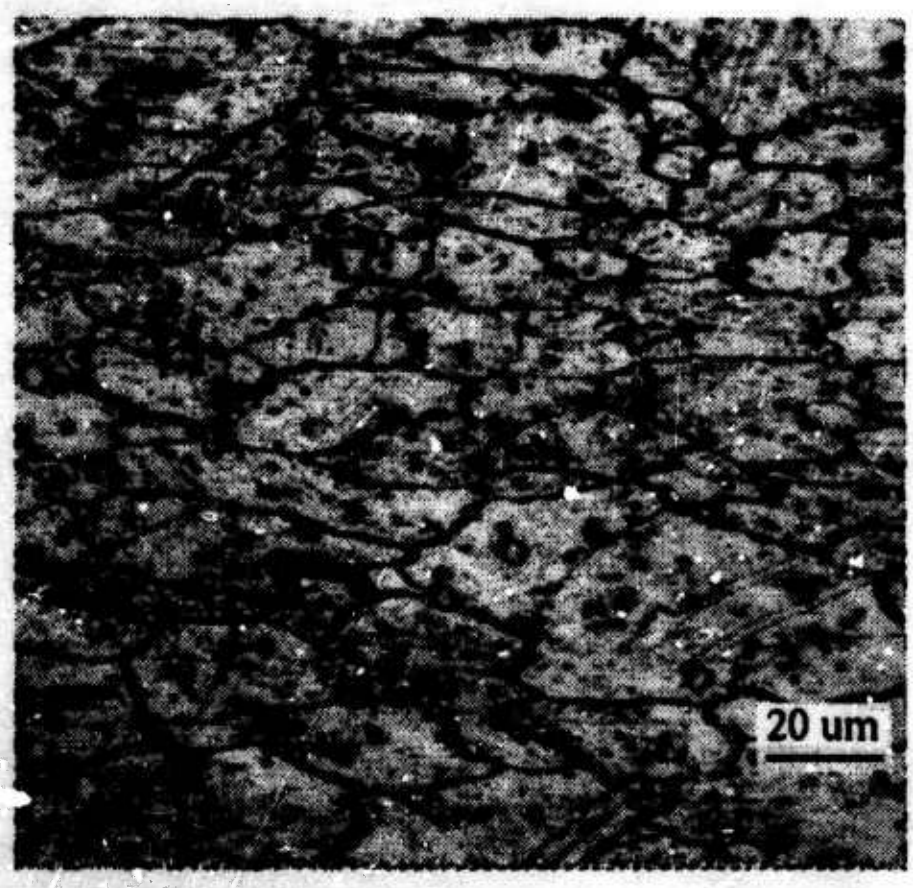

Figure 9. True stress-true strain curve and an optical micrograph from the center of the compressed sample cut through the compression axis, 950 C and 20 s^{-1}.

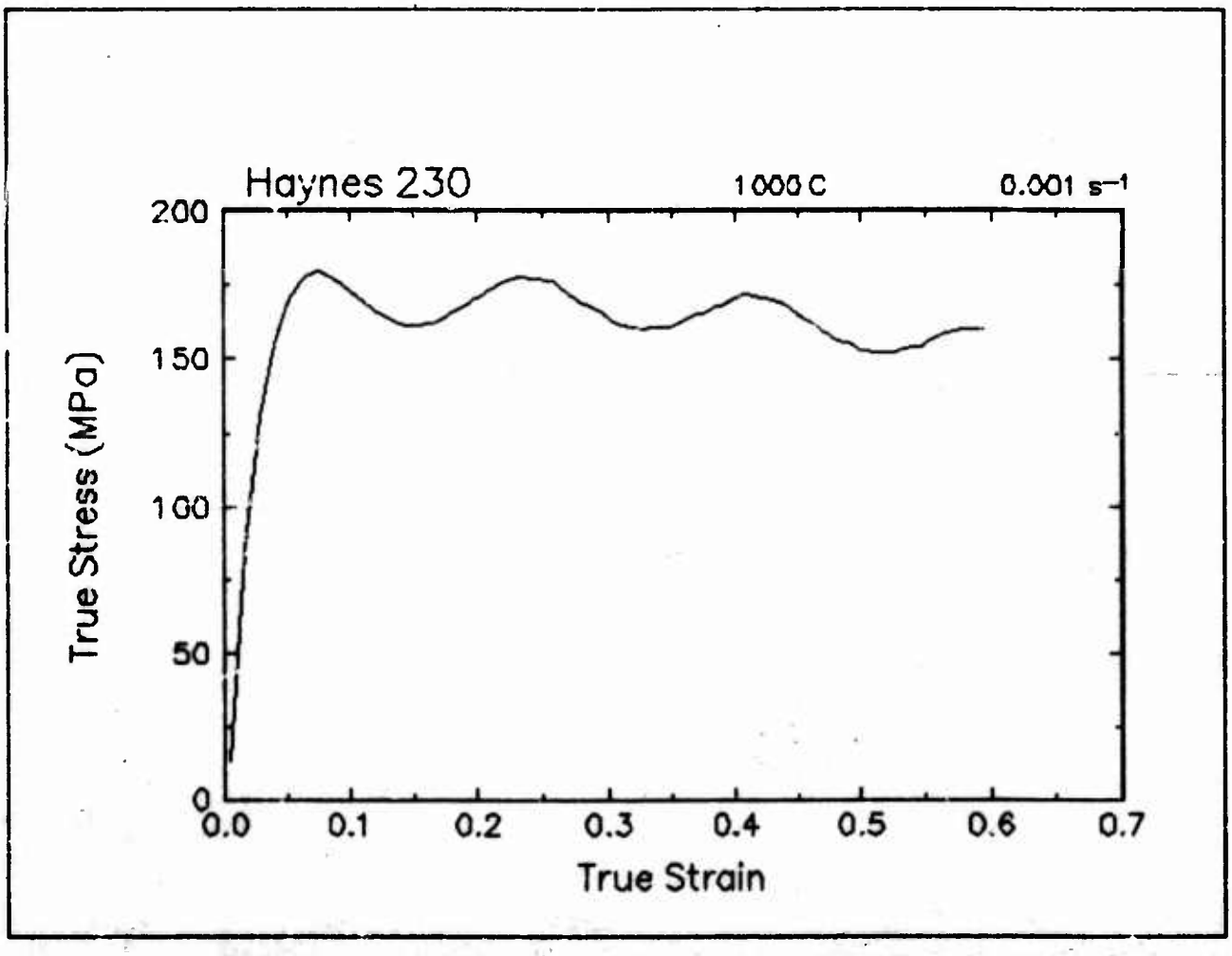

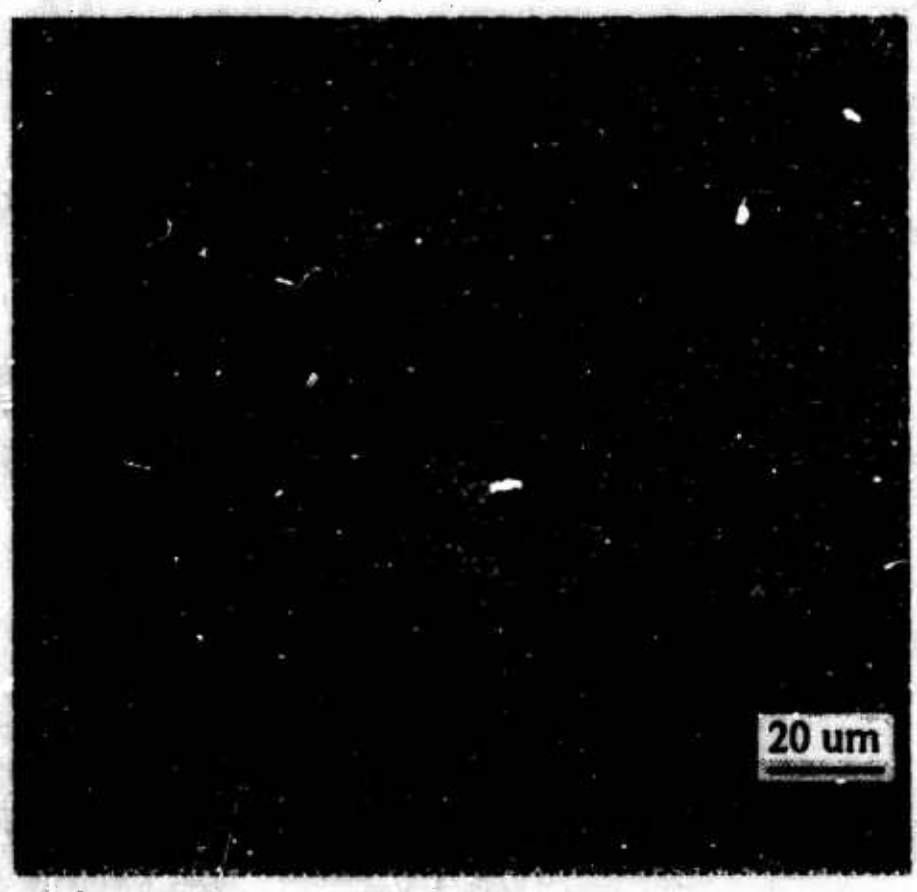

Figure 10. True stress-true strain curve and an optical micrograph from the center of the compressed sample cut through the compression axis, 1000 C and 0.001 s^{-1}.

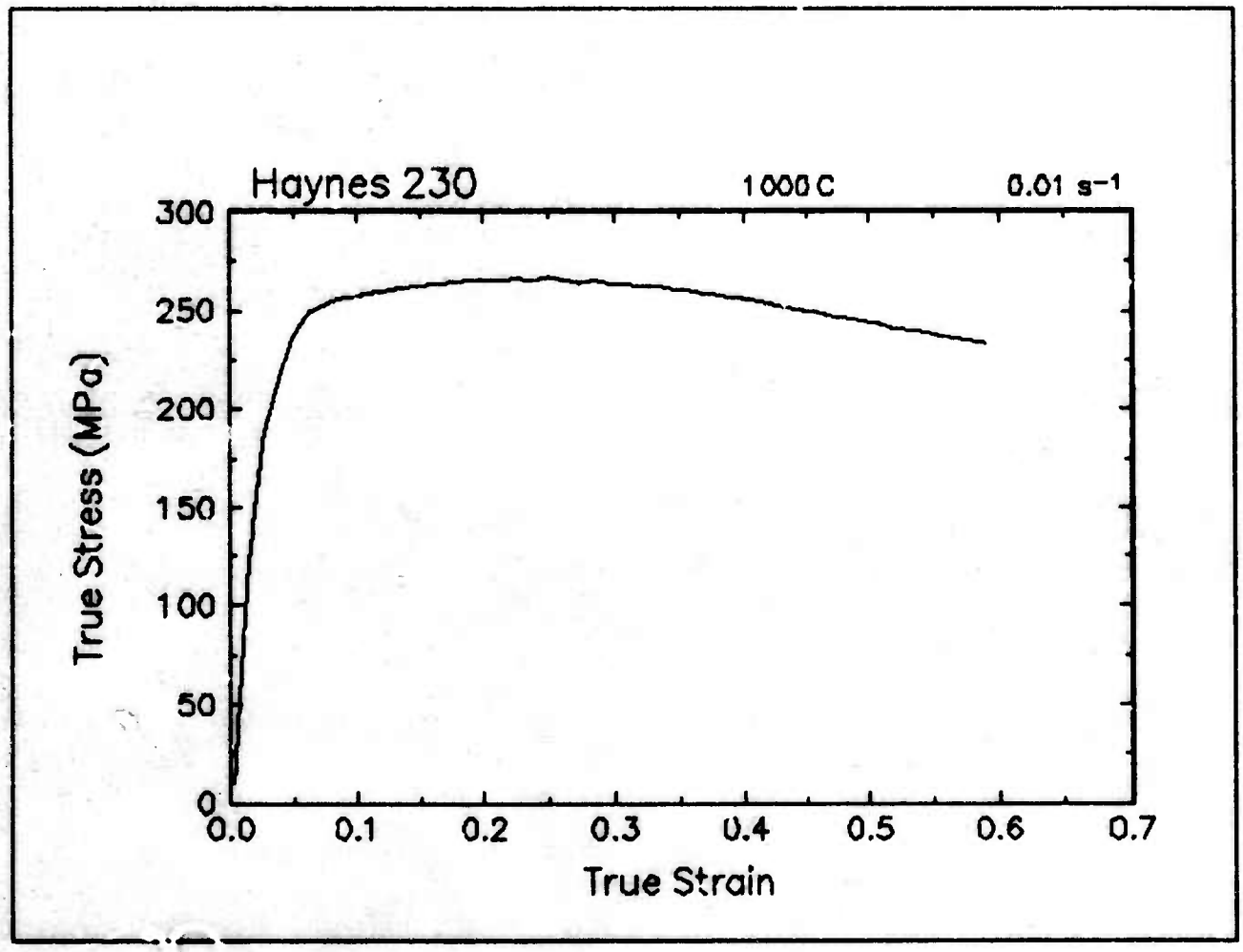

Figure 11. True stress-true strain curve, 1000 C and 0.01 s^{-1}.

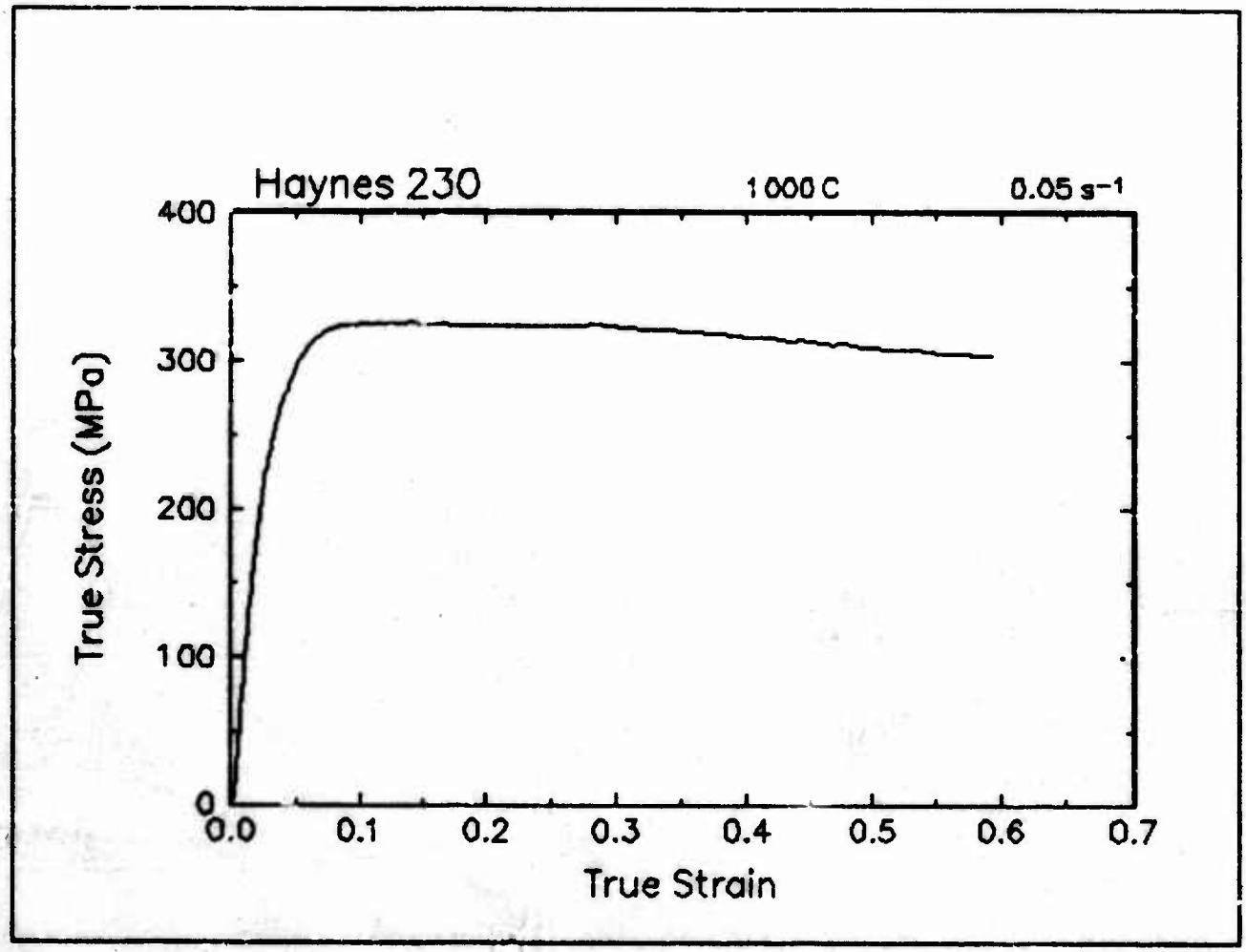

Figure 12. True stress-true strain curve, 1000 C and 0.05 s^{-1}.

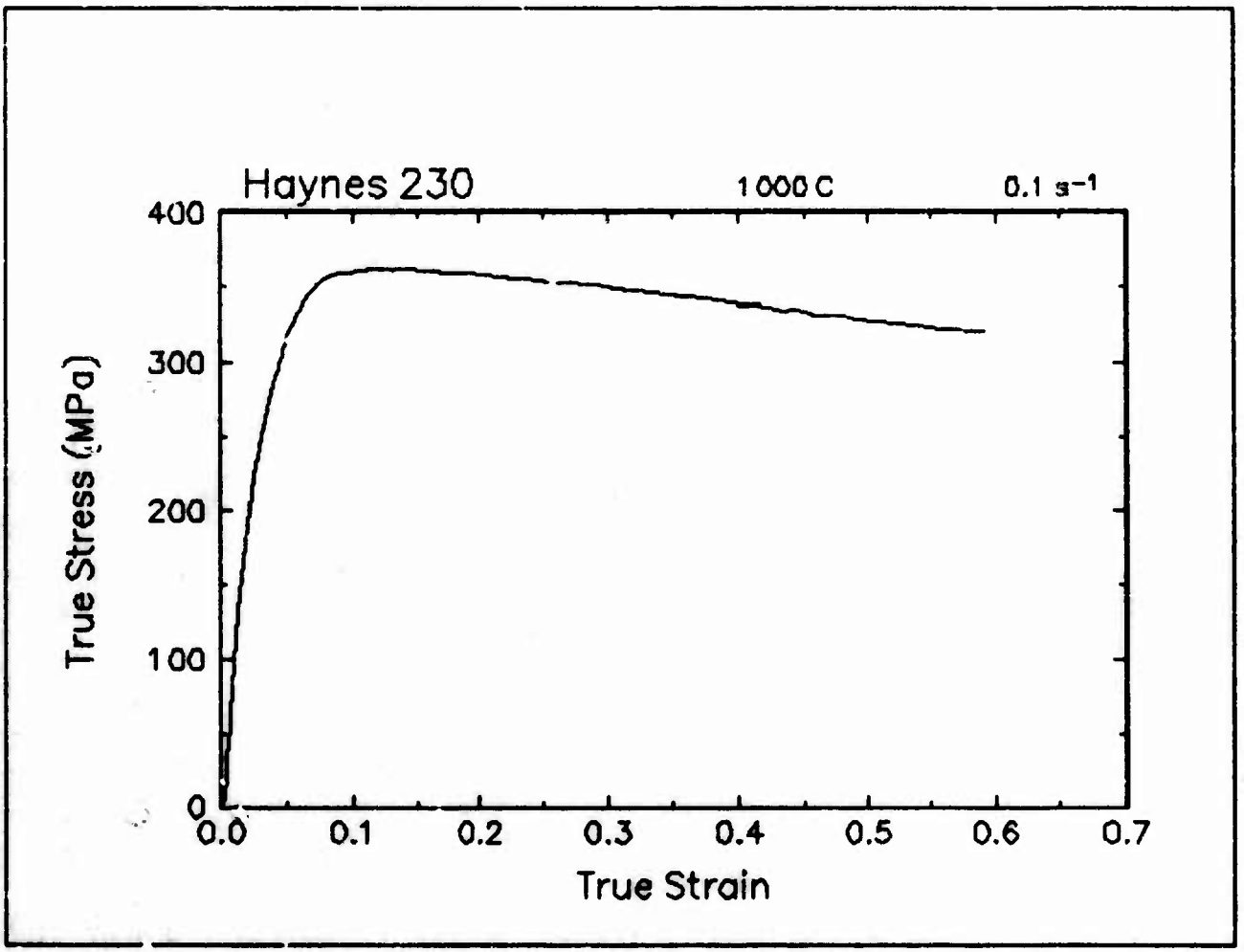

Figure 13. True stress-true strain curve, 1000 C and 0.1 s^{-1}.

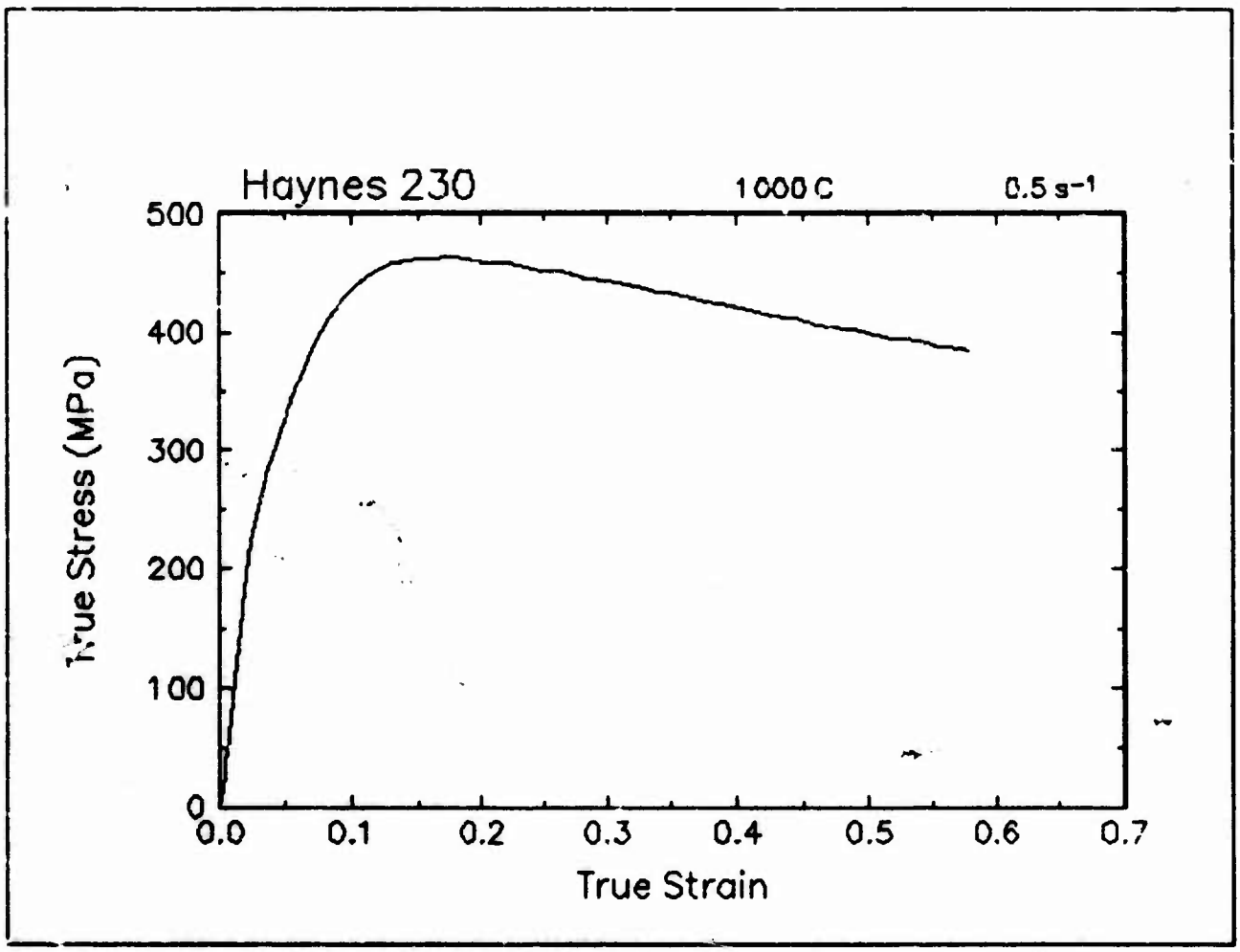

Figure 14. True stress-true strain curve, 1000 C and 0.5 s^{-1}.

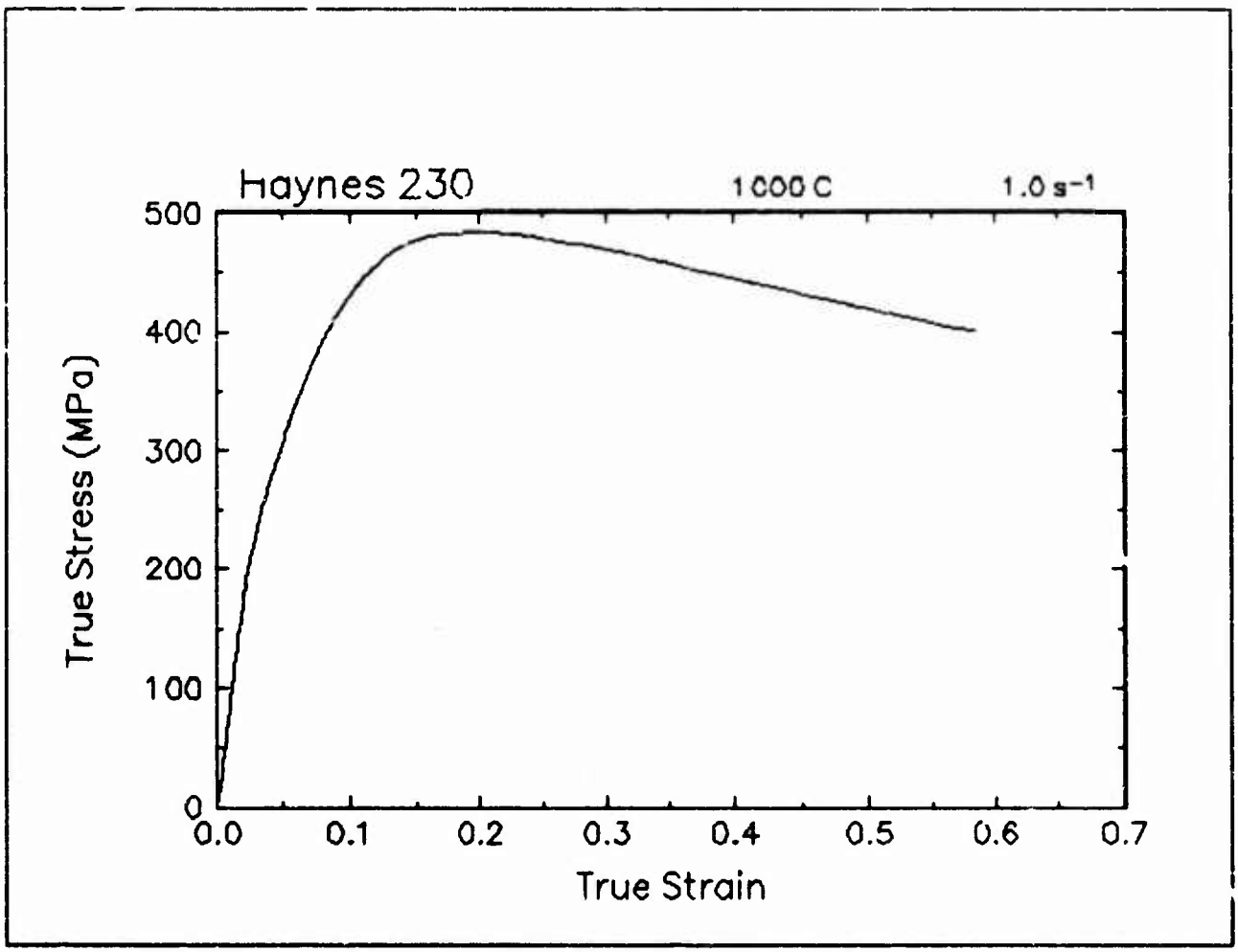

Figure 15. True stress-true strain curve, 1000 C and 1 s^{-1}.

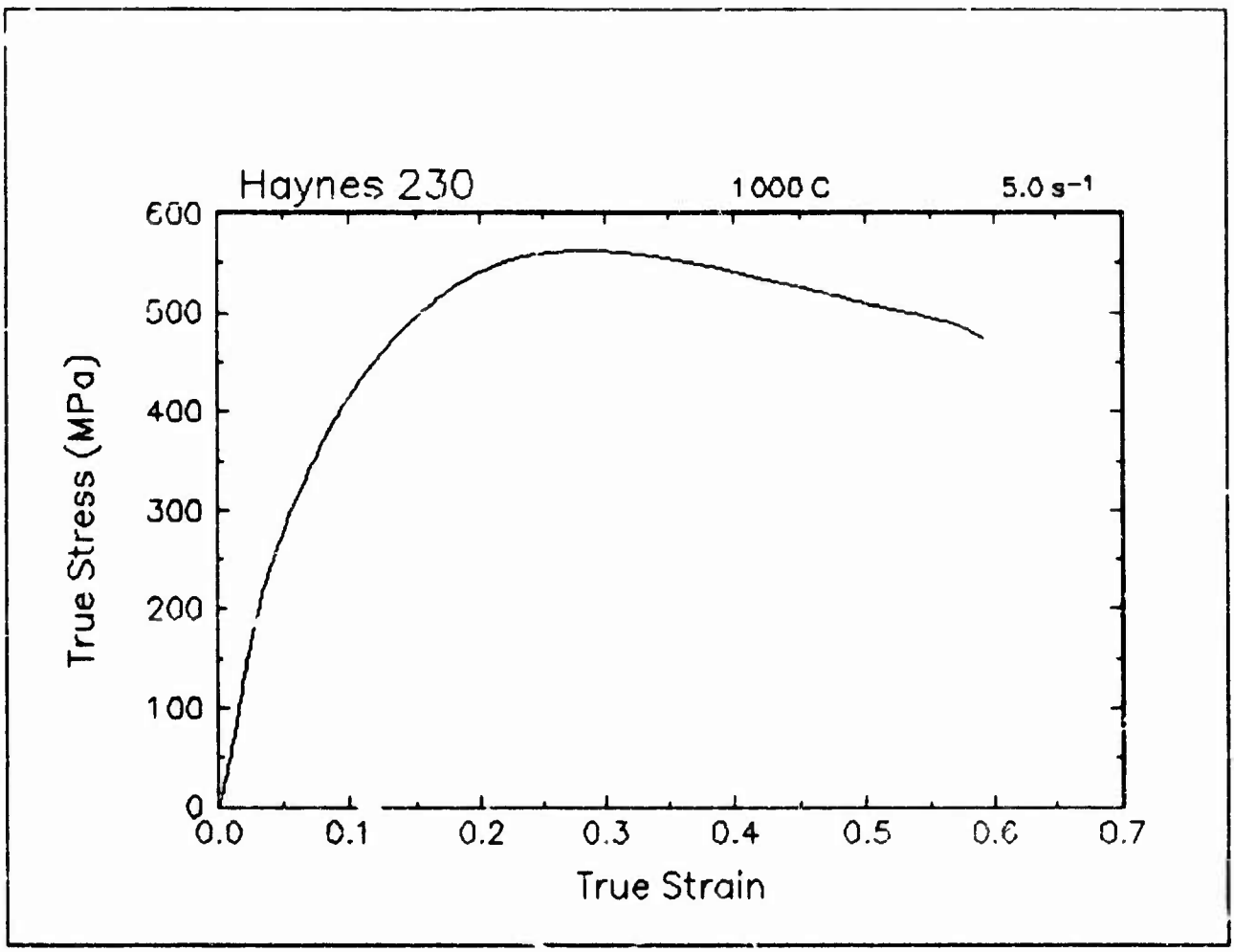

Figure 16. True stress-true strain curve, 1000 C and 5 s^{-1}.

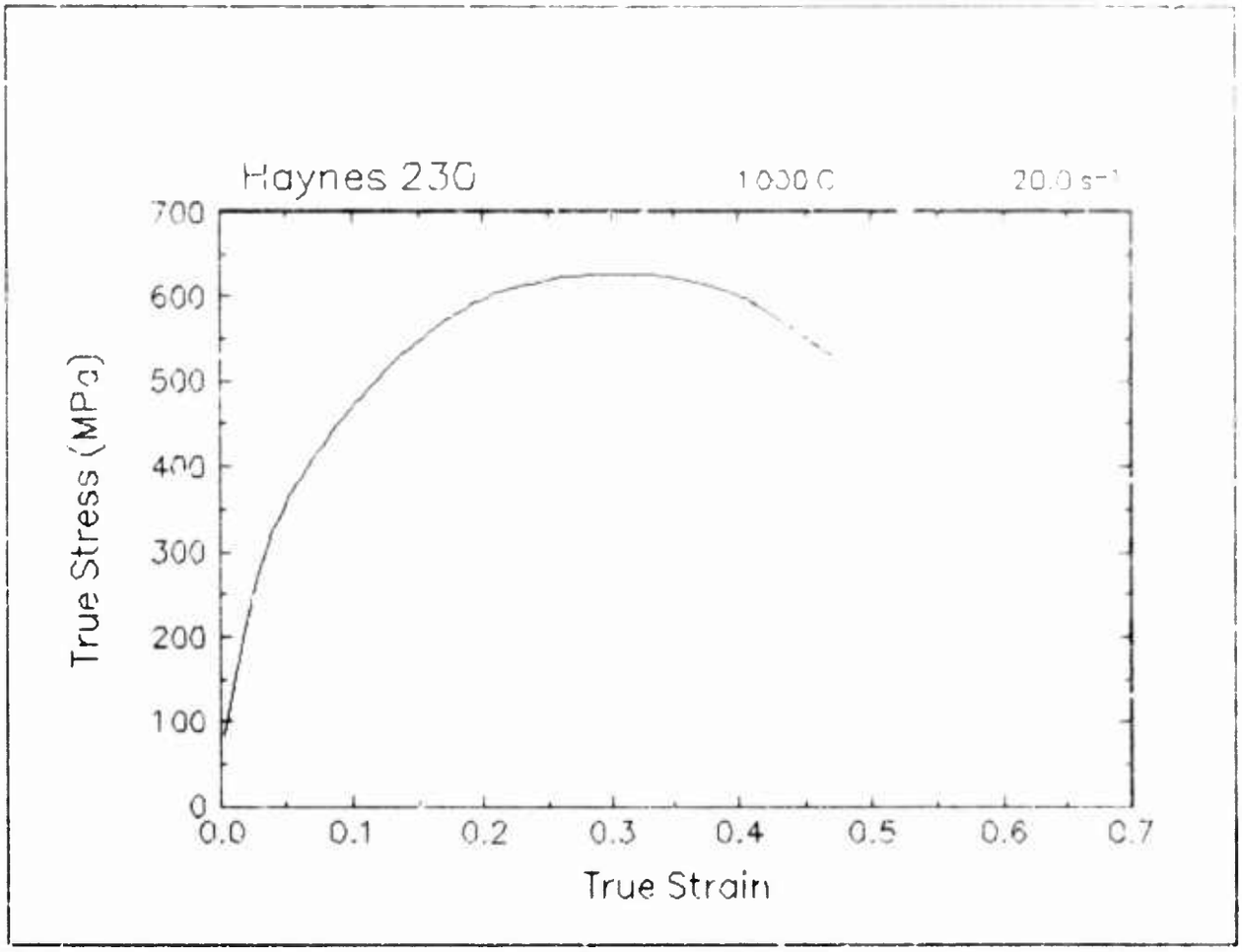

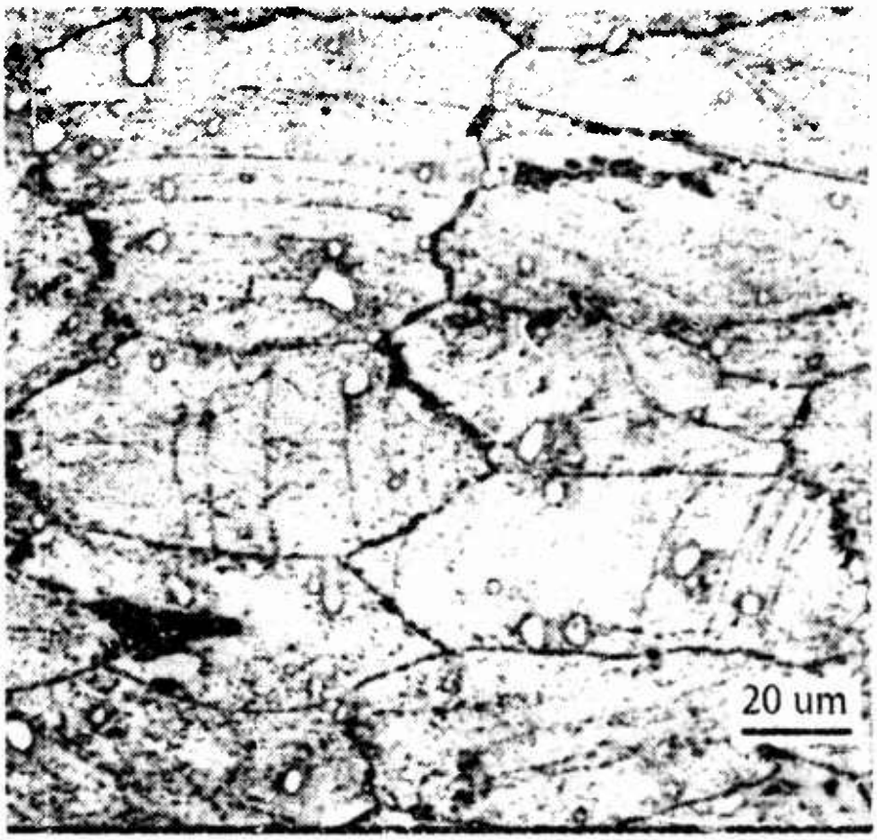

Figure 17. True stress-true strain curve and an optical micrograph from the center of the compressed sample cut through the compression axis, 1000 C and 20 s^{-1}.

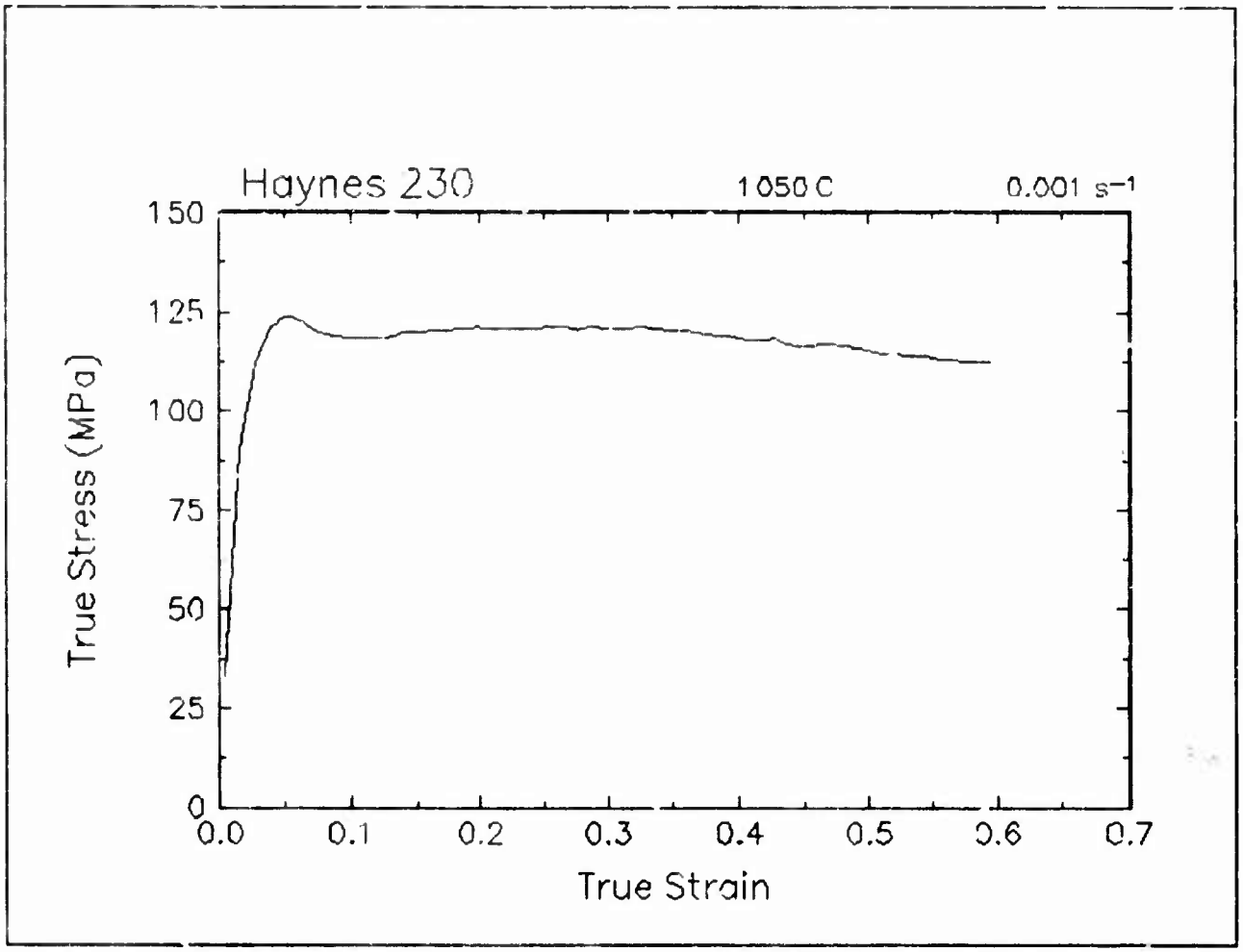

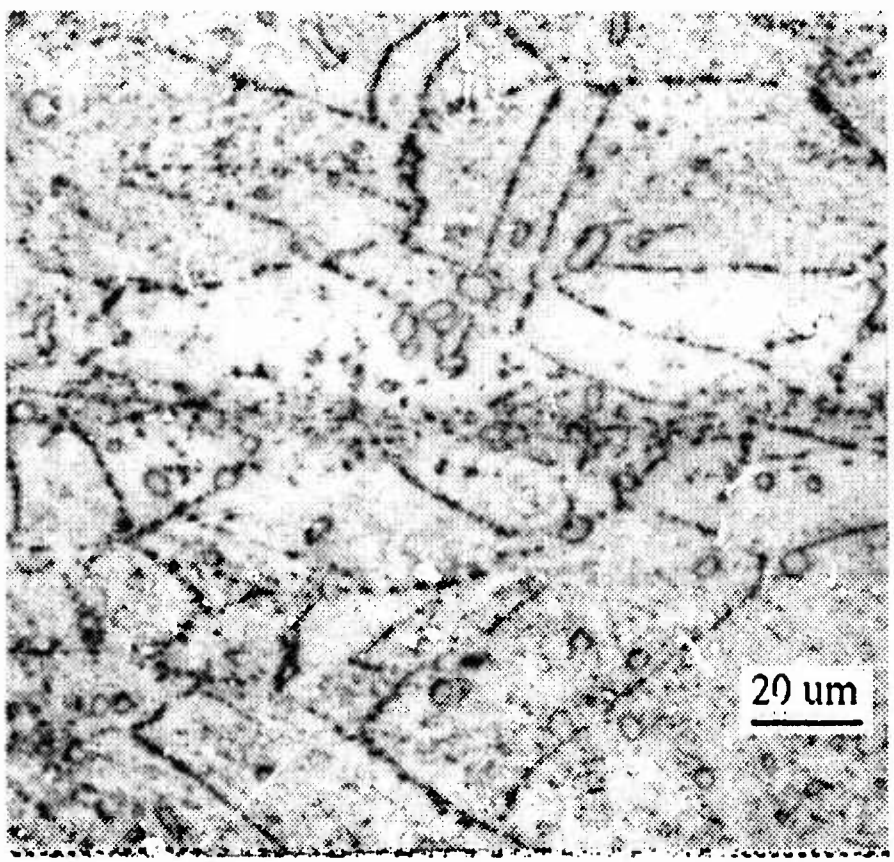

Figure 18. True stress-true strain curve and an optical micrograph from the center of the compressed sample cut through the compression axis, 1050 C and 0.001 s^{-1}.

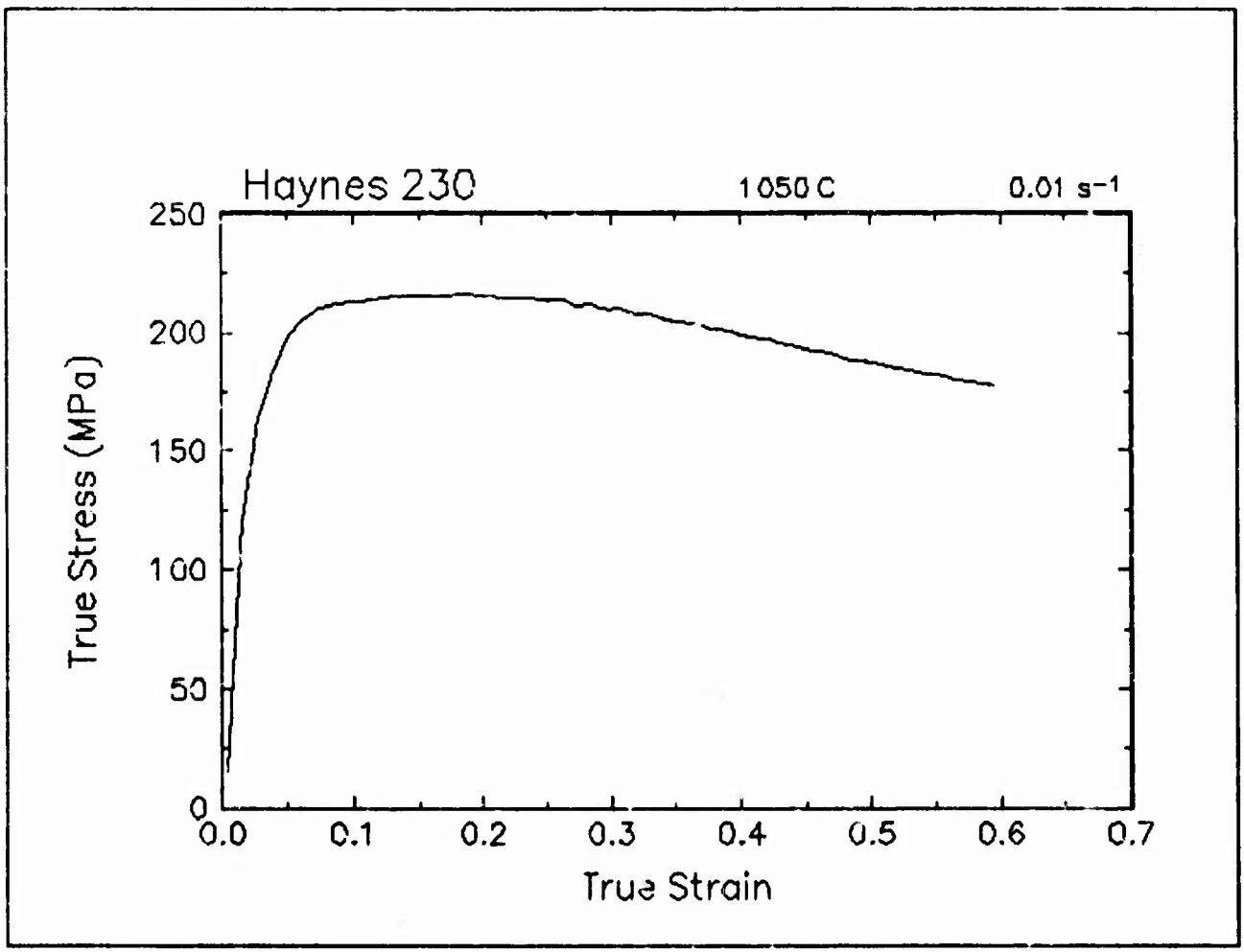

Figure 19. True stress-true strain curve, 1050 C and 0.01 s^{-1}.

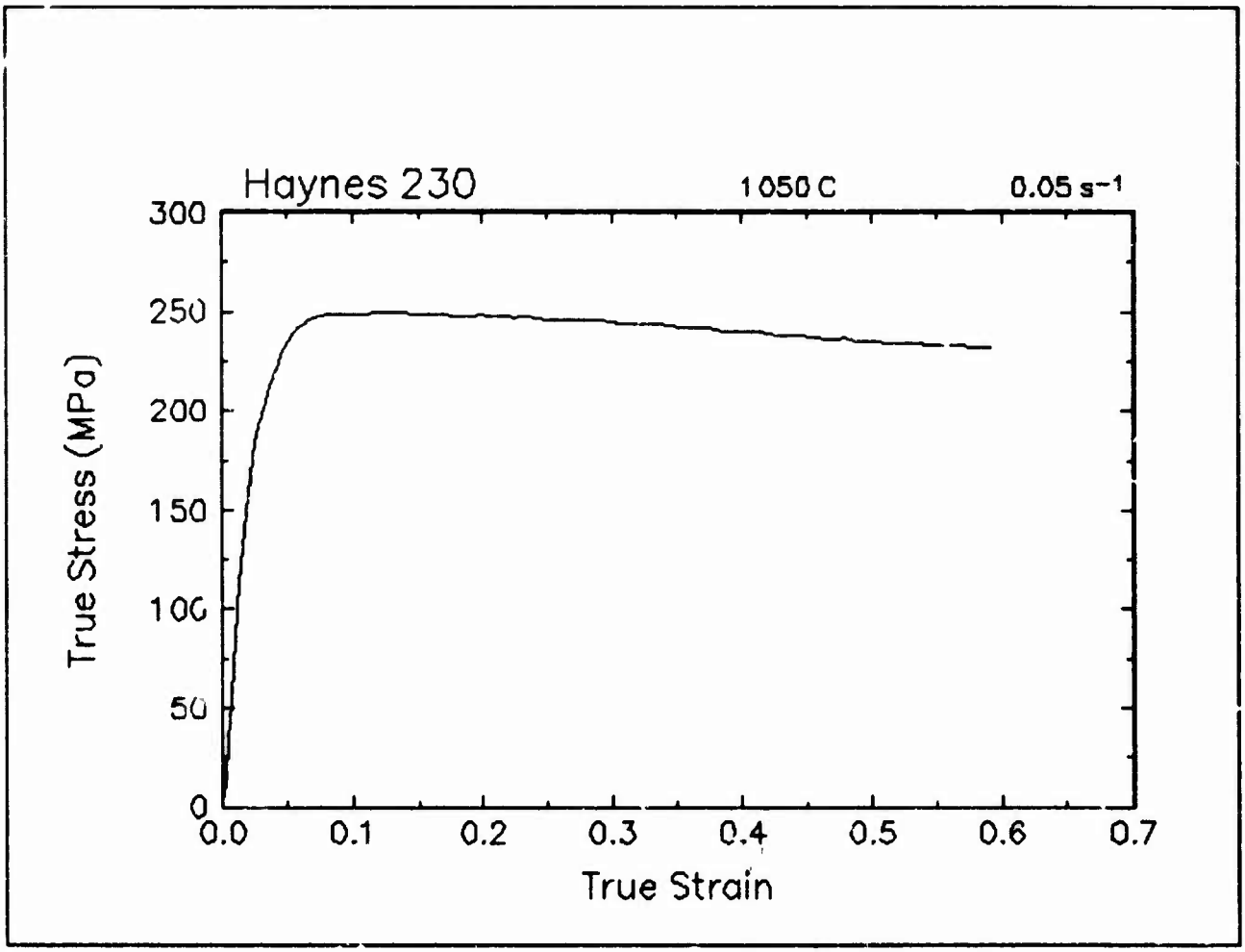

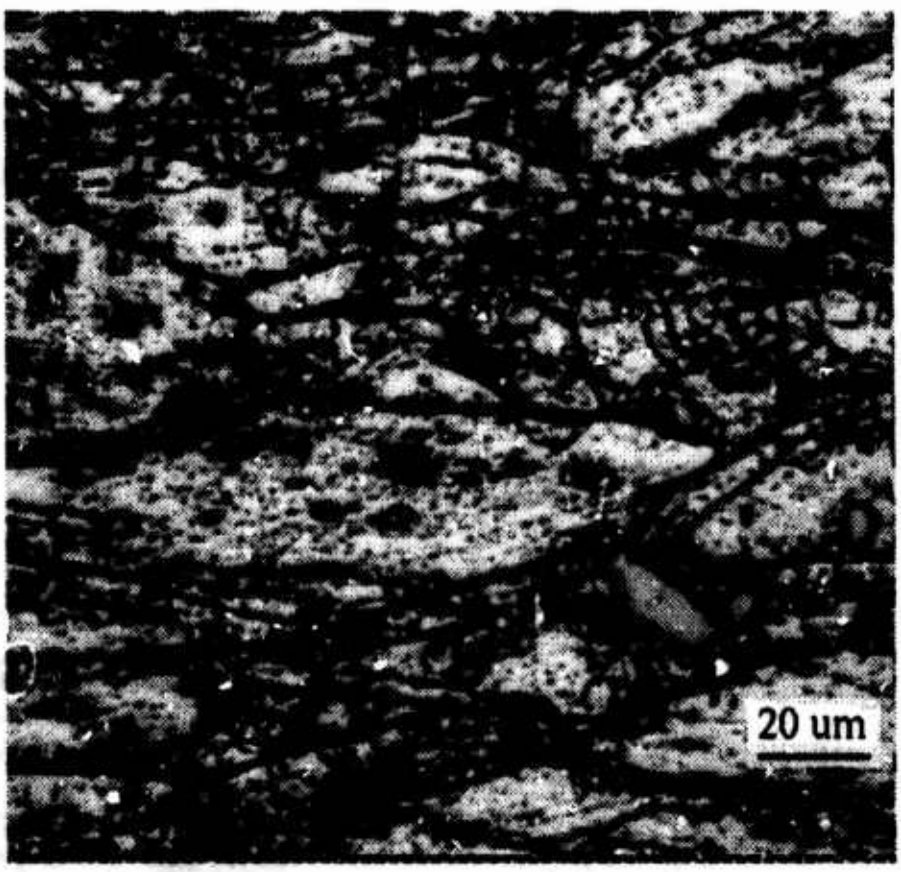

Figure 20. True stress-true strain curve and an optical micrograph from the center of the compressed sample cut through the compression axis, 1050 C and 0.05 s^{-1}.

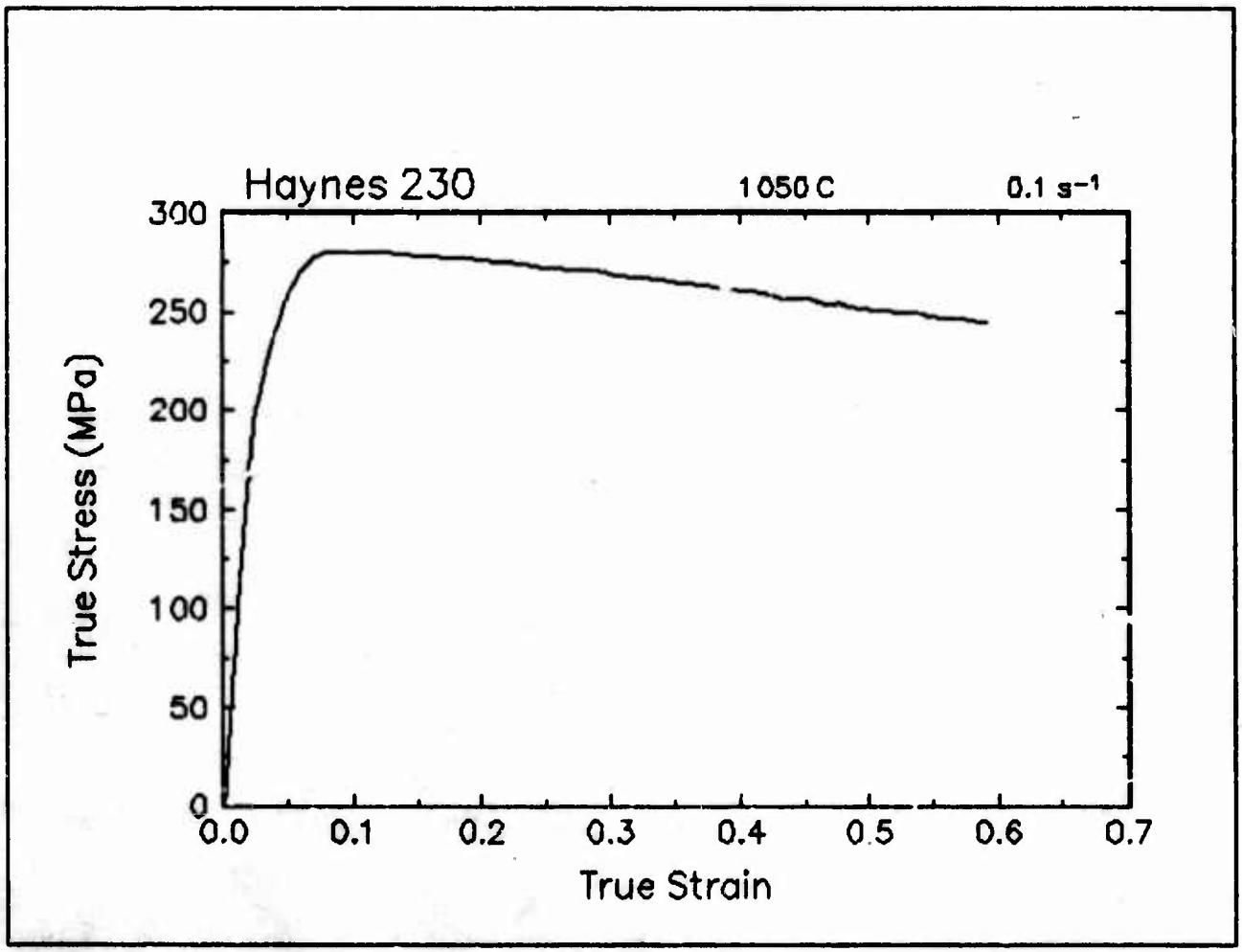

Figure 21. True stress-true strain curve, 1050 C and 0.1 s^{-1}.

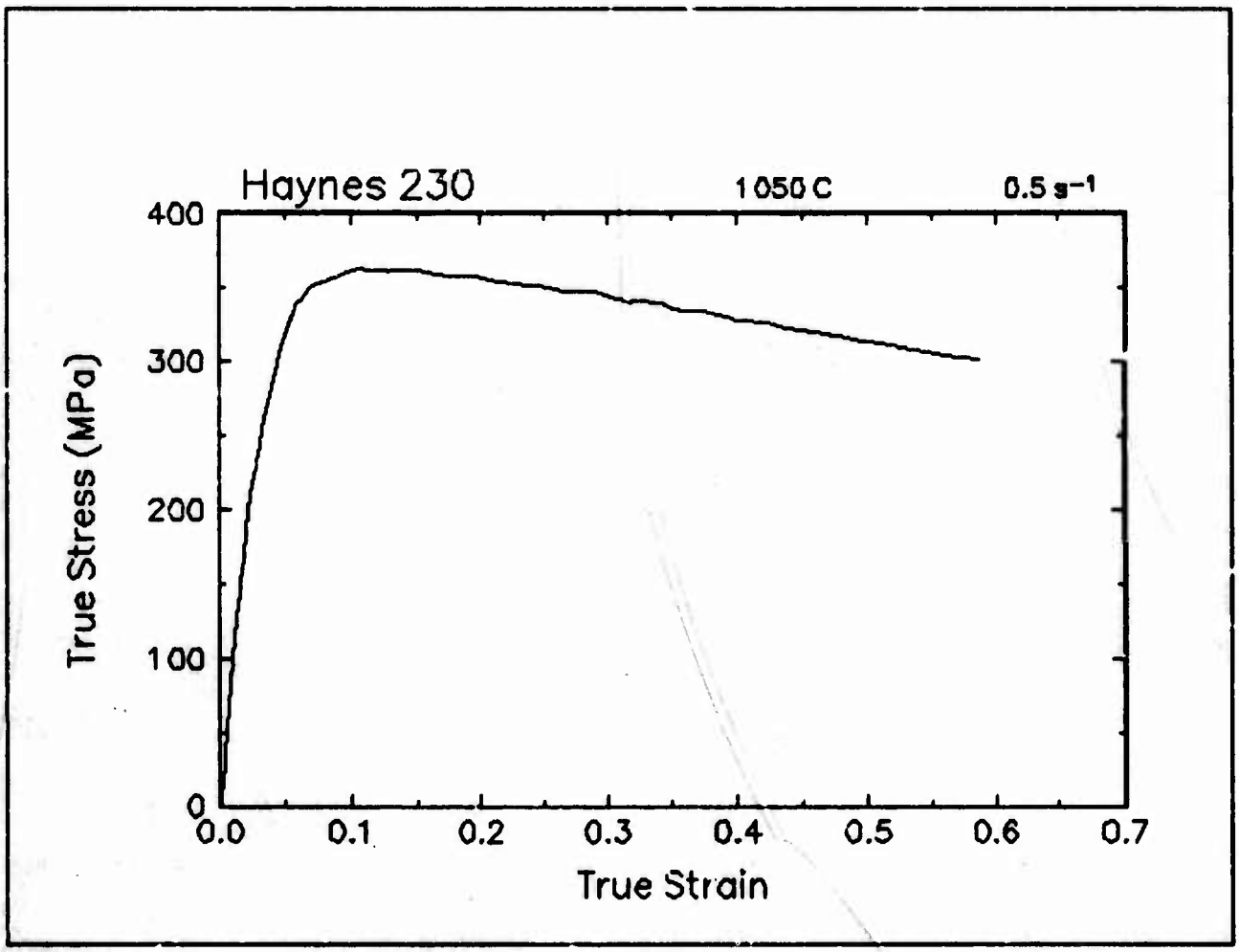

Figure 22. True stress-true strain curve, 1050 C and 0.5 s^{-1}.

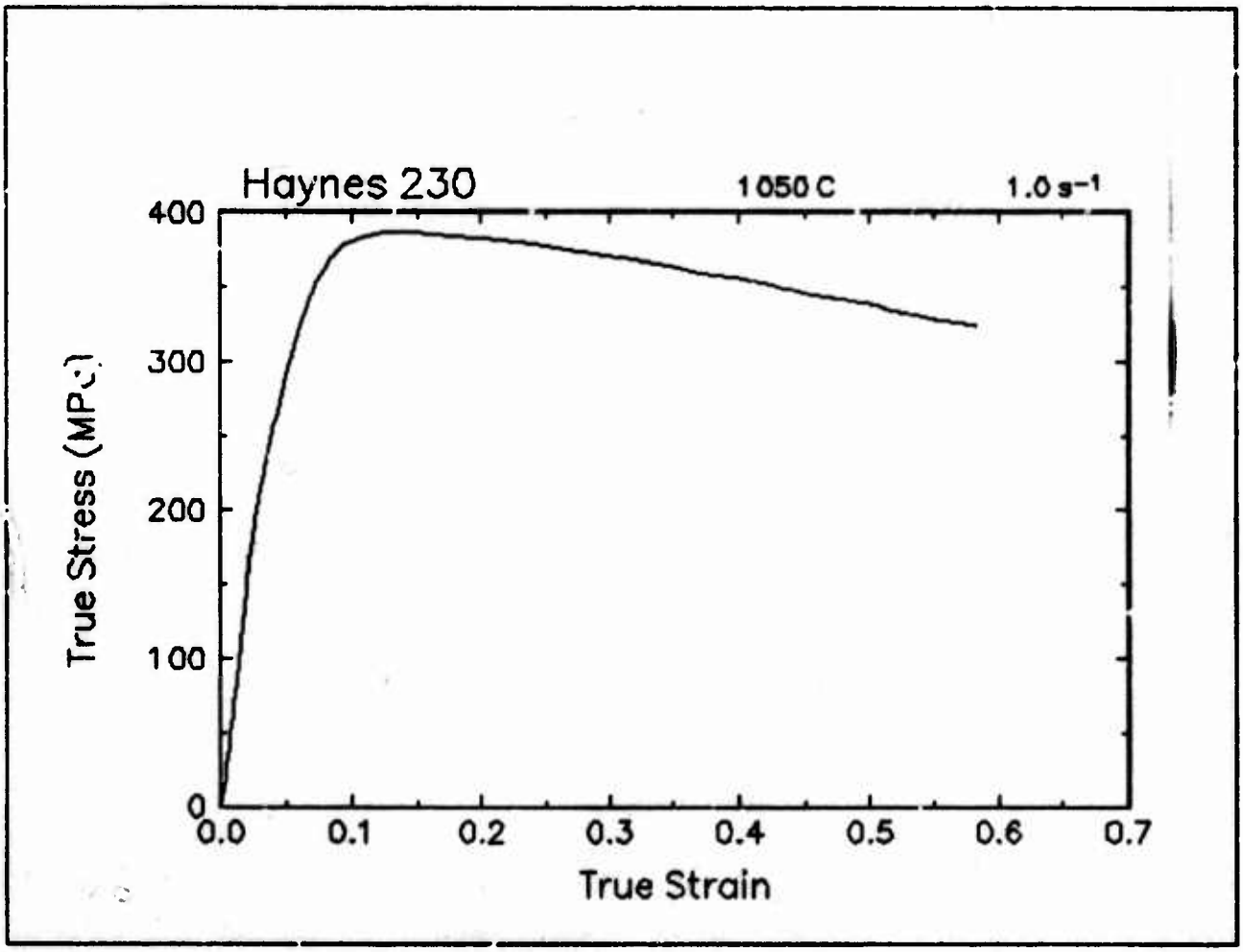

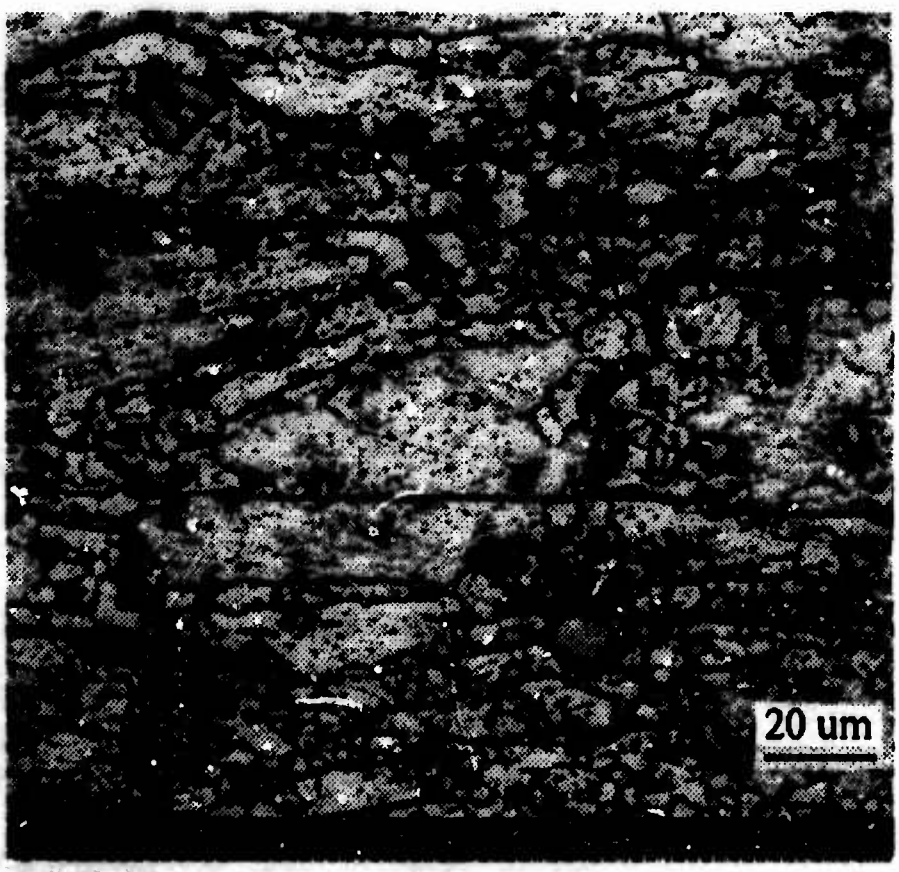

Figure 23. True stress-true strain curve and an optical micrograph from the center of the compressed sample cut through the compression axis, 1050 C and 1.0 s^{-1}.

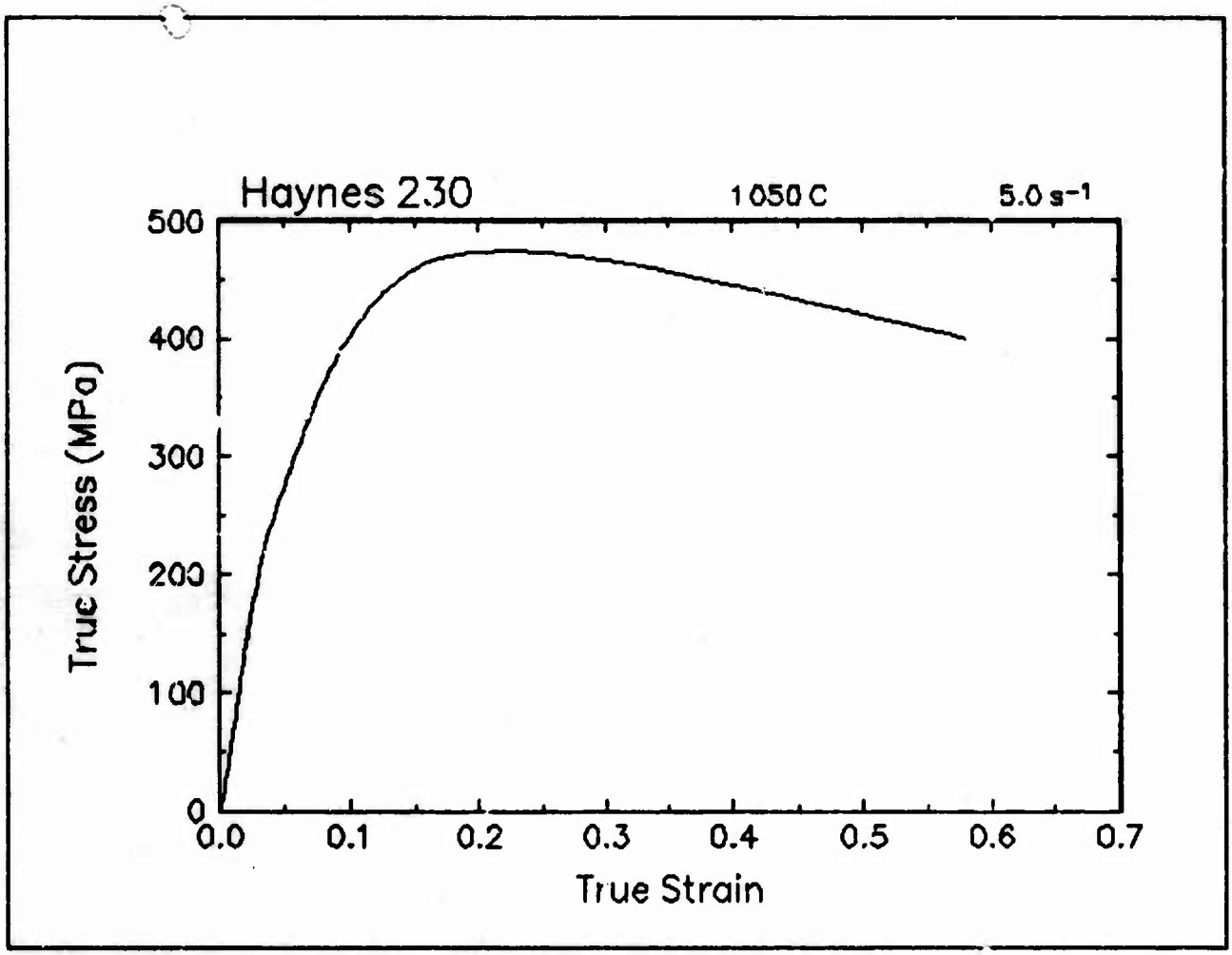

Figure 24. True stress-true strain curve, 1050 C and 5.0 s^{-1}.

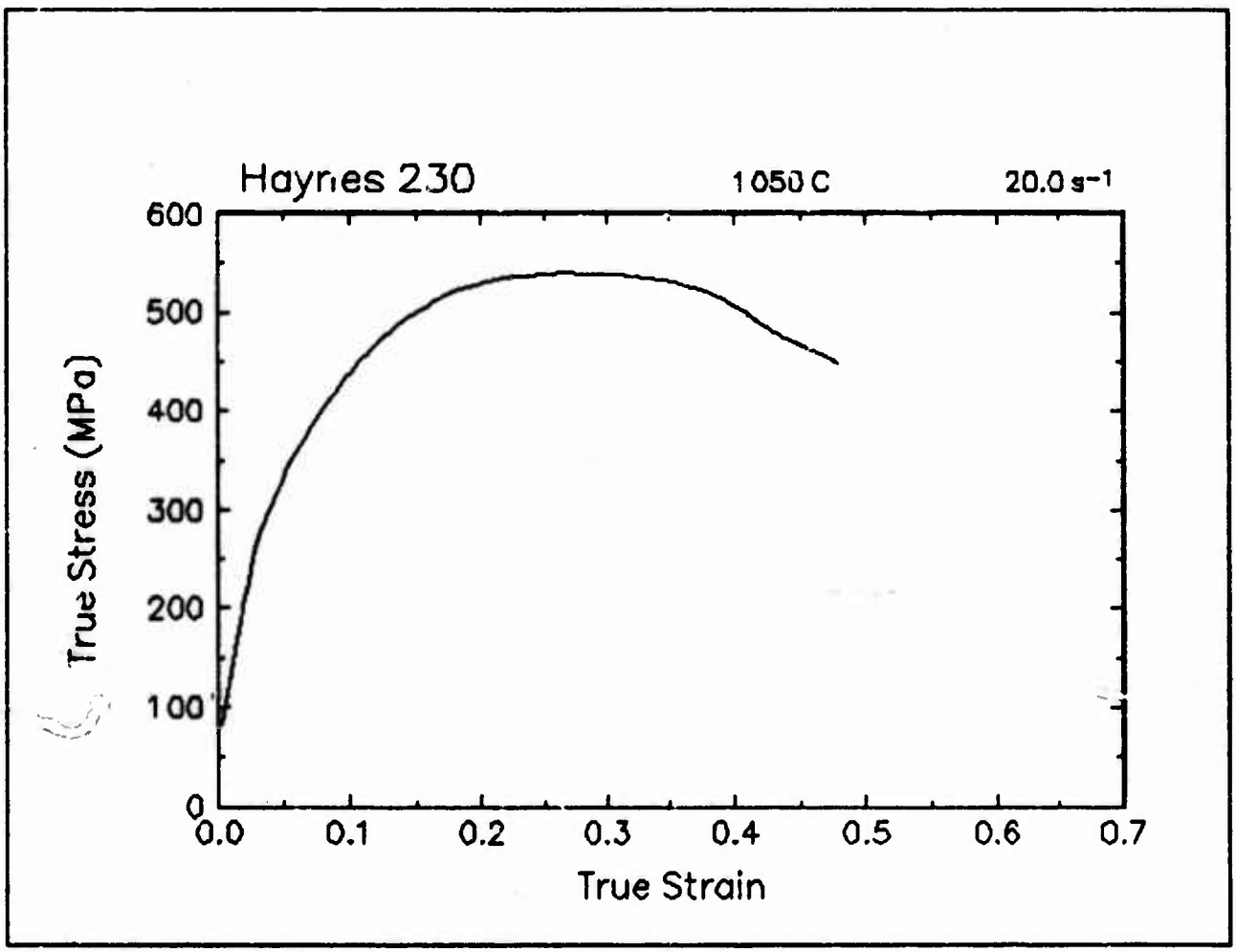

Figure 25. True stress-true strain curve, 1050 C and 20.0 s^{-1}.

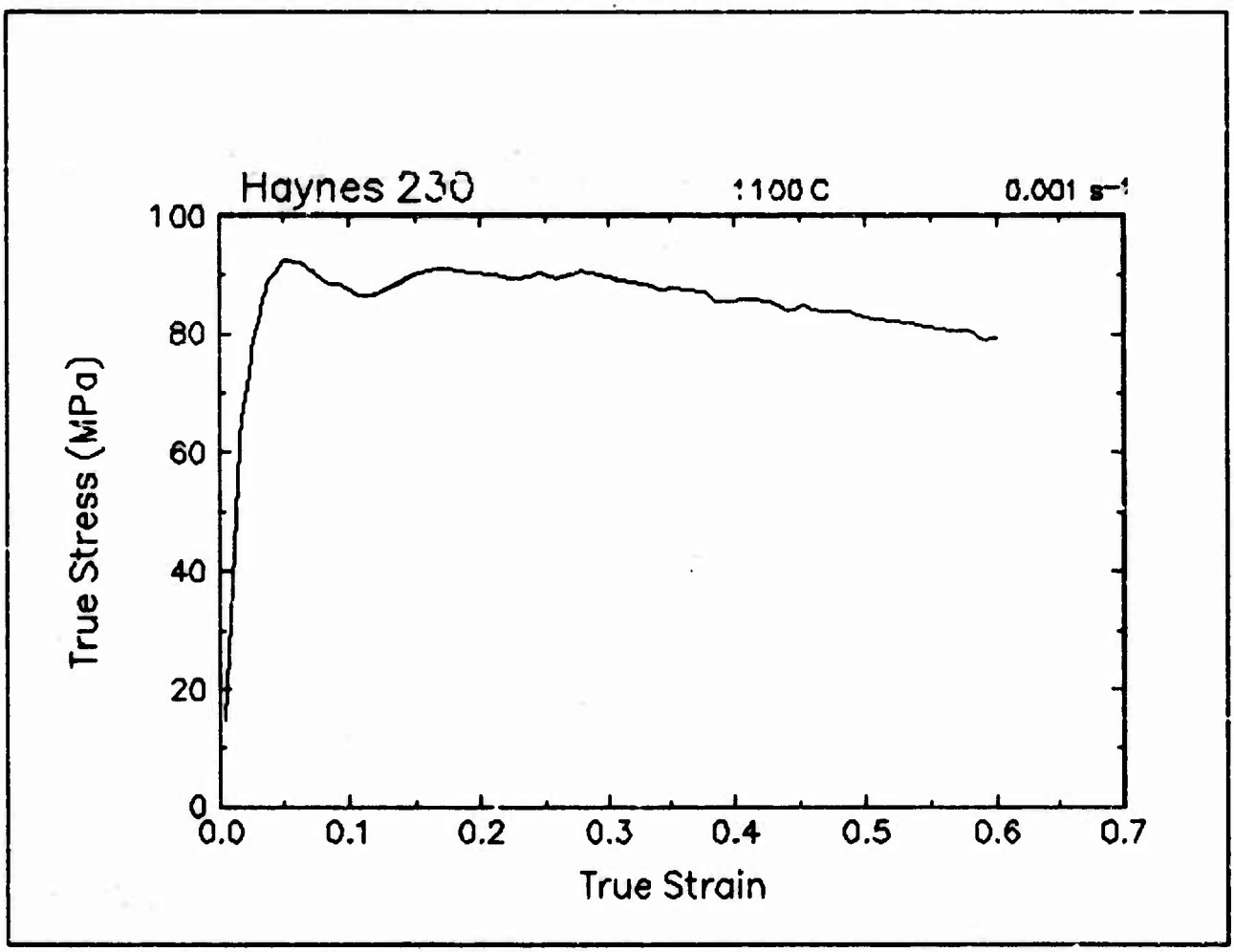

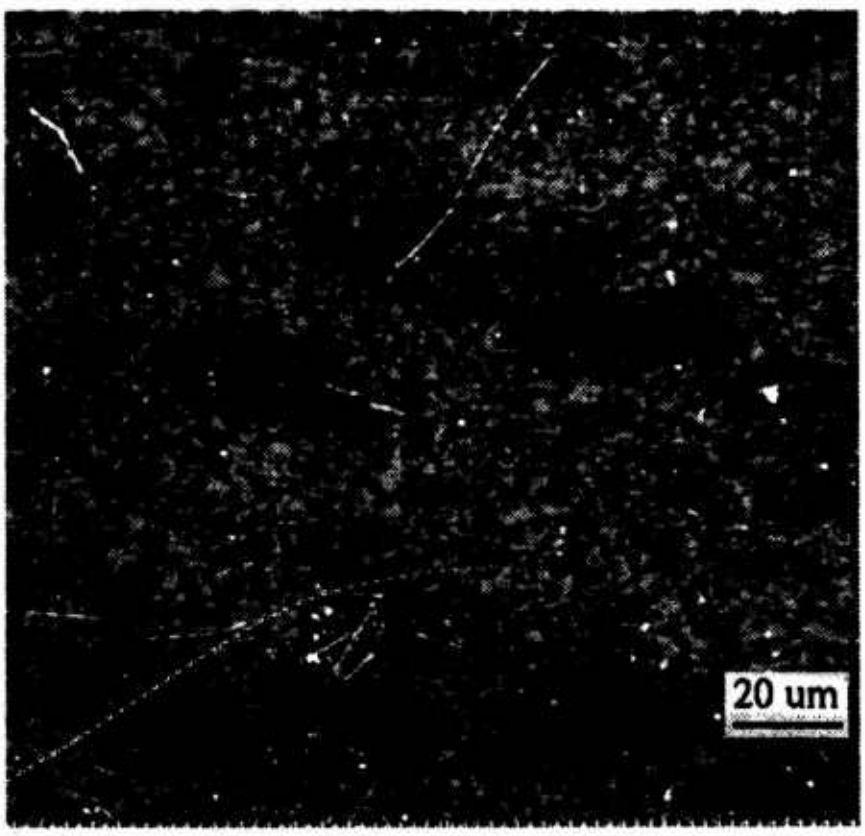

Figure 26. True stress-true strain curve and an optical micrograph from the center of the compressed sample cut through the compression axis, 1100 C and 0.001 s^{-1}.

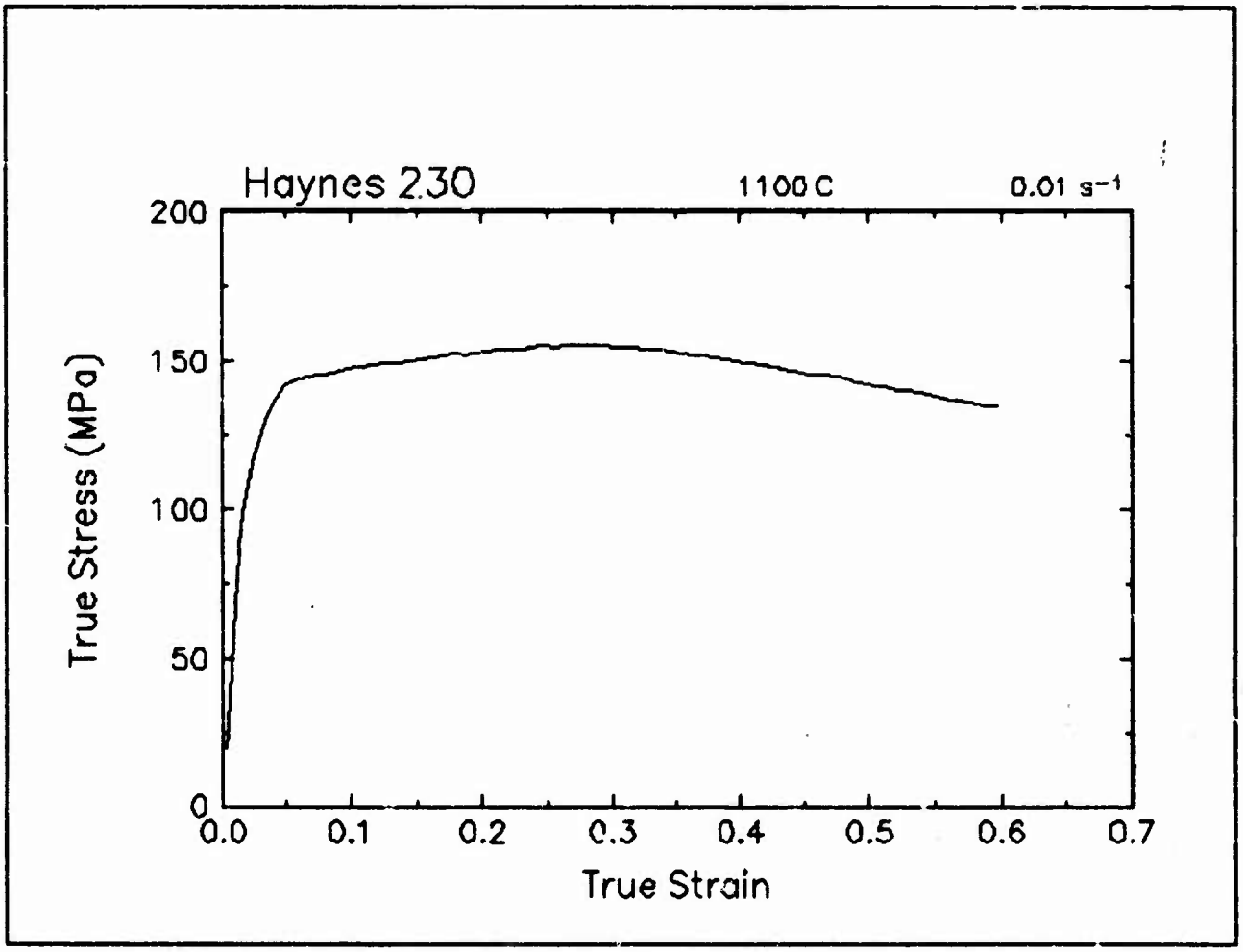

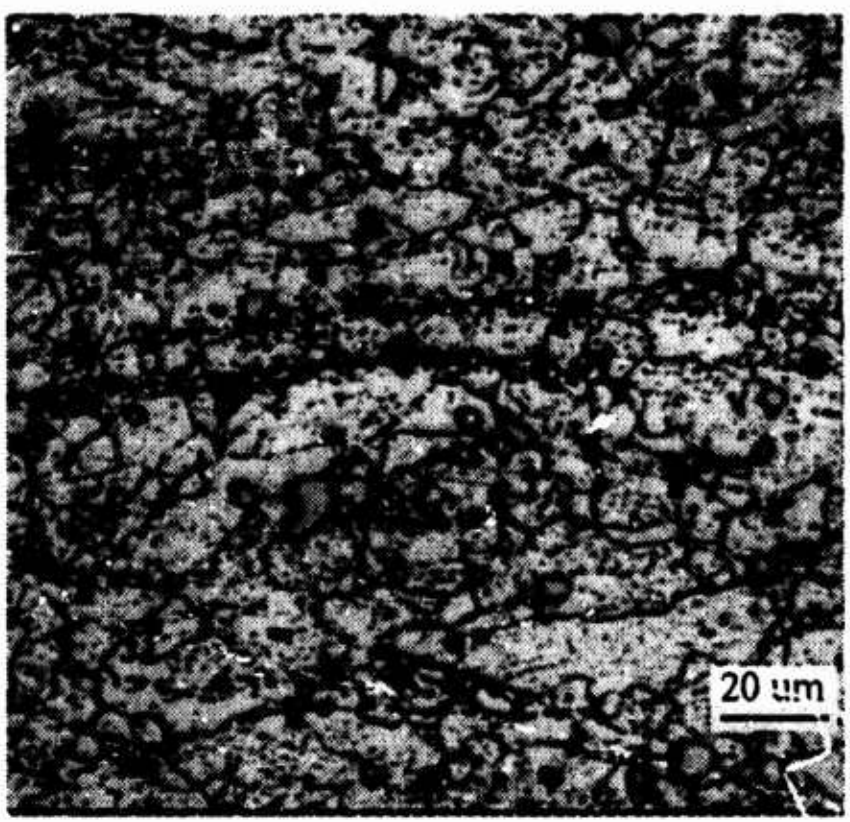

Figure 27. True stress-true strain curve and an optical micrograph from the center of the compressed sample cut through the compression axis, 1100 C and 0.01 s^{-1}.

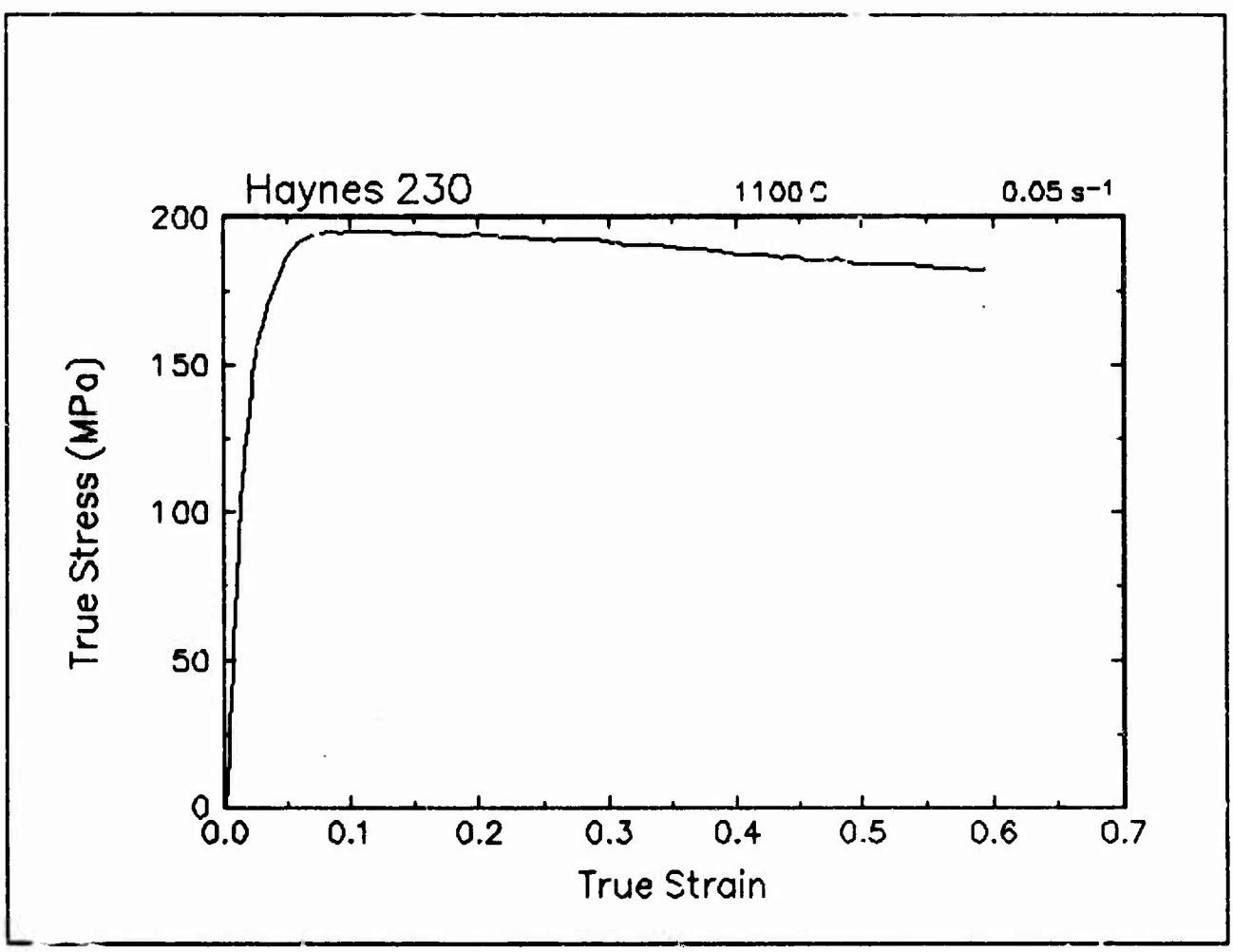

Figure 28. True stress-true strain curve, 1100 C and 0.05 s^{-1}.

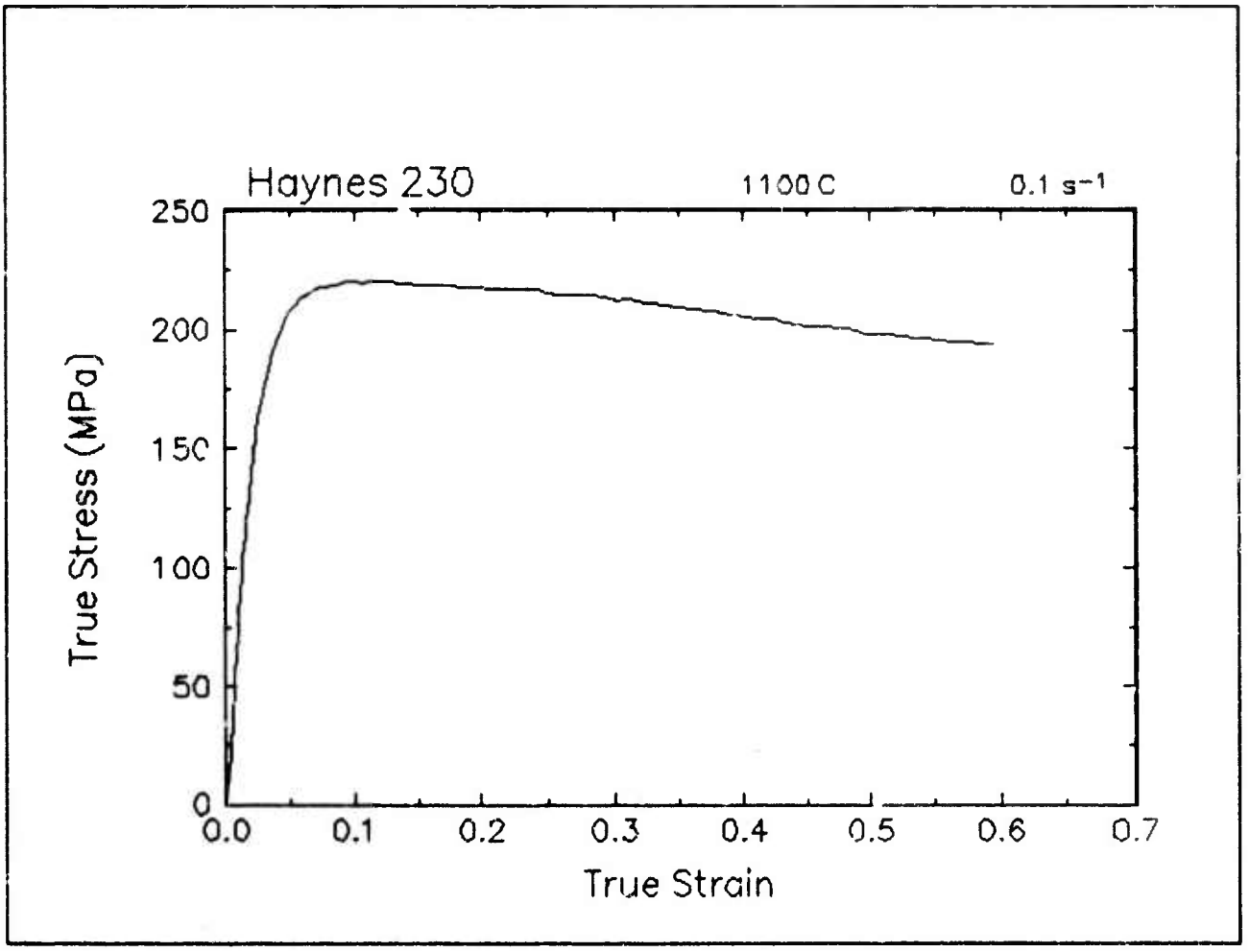

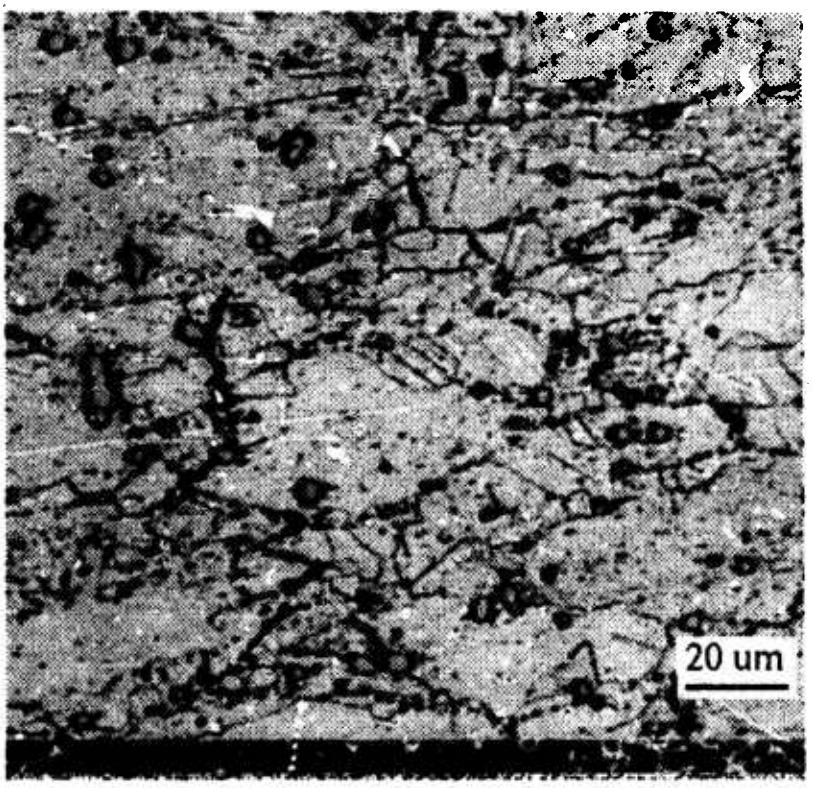

Figure 29. True stress-true strain curve and an optical micrograph from the center of the compressed sample cut through the compression axis, 1100 C and 0.1 s^{-1}.

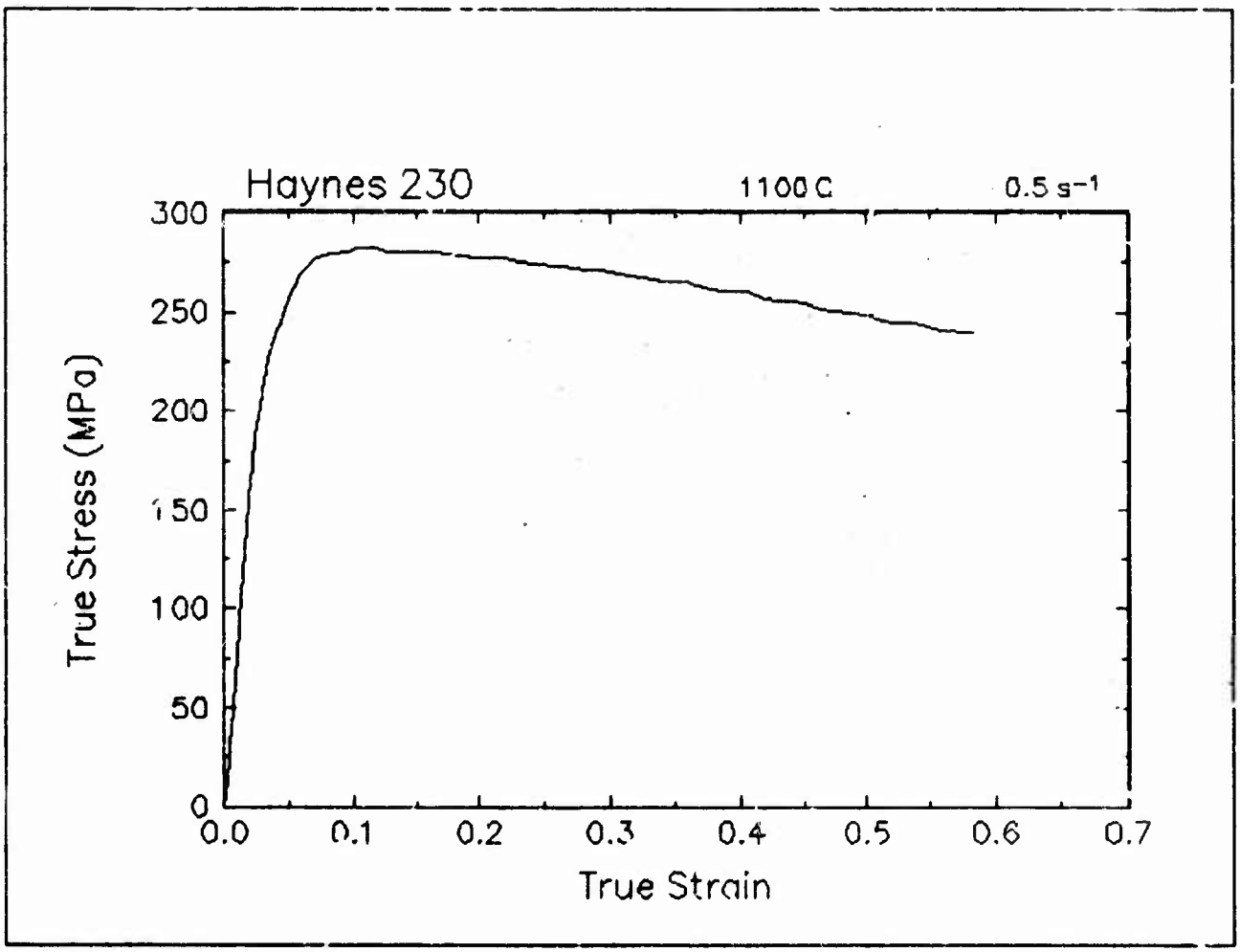

Figure 30. True stress-true strain curve, 1100 C and 0.5 s^{-1}.

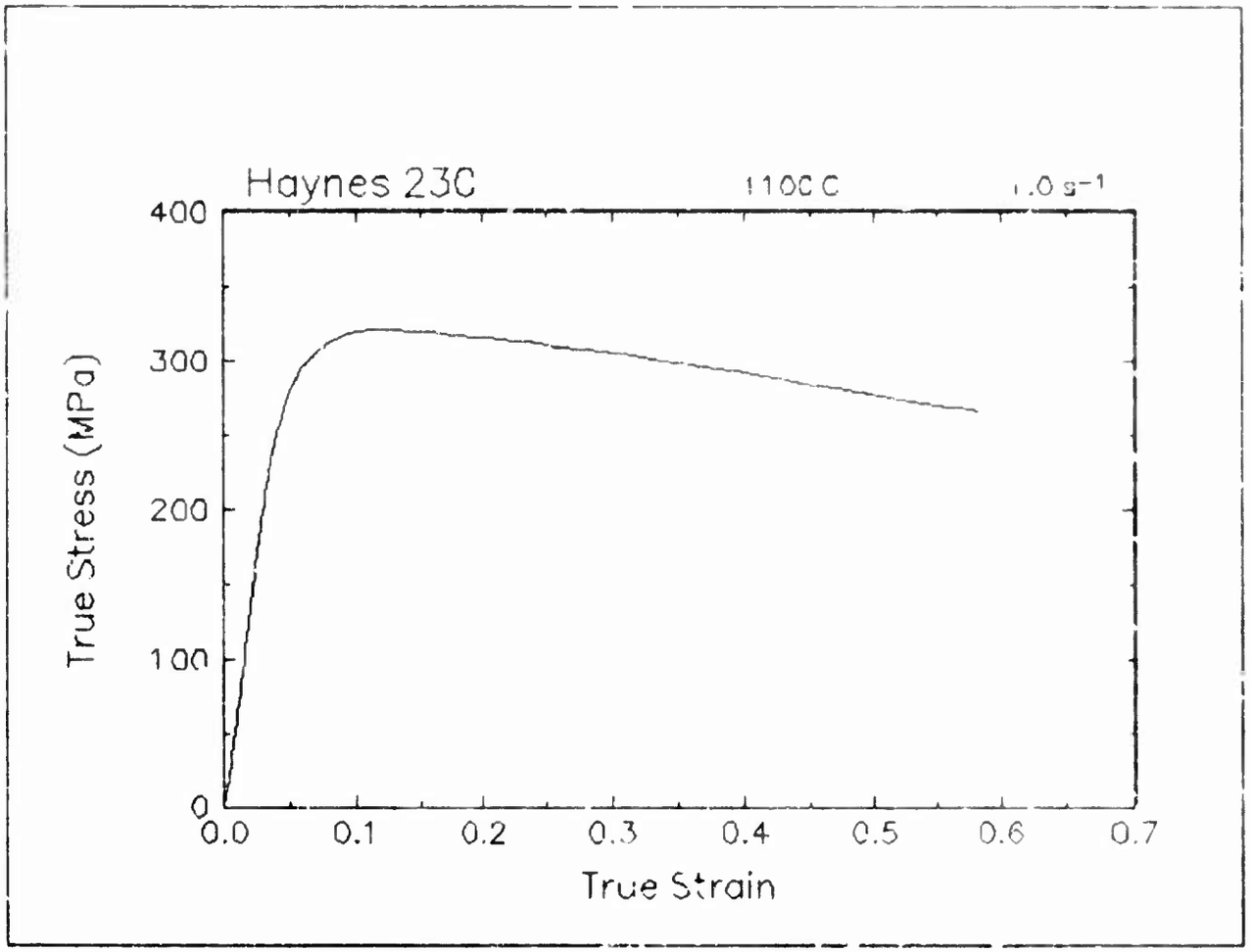

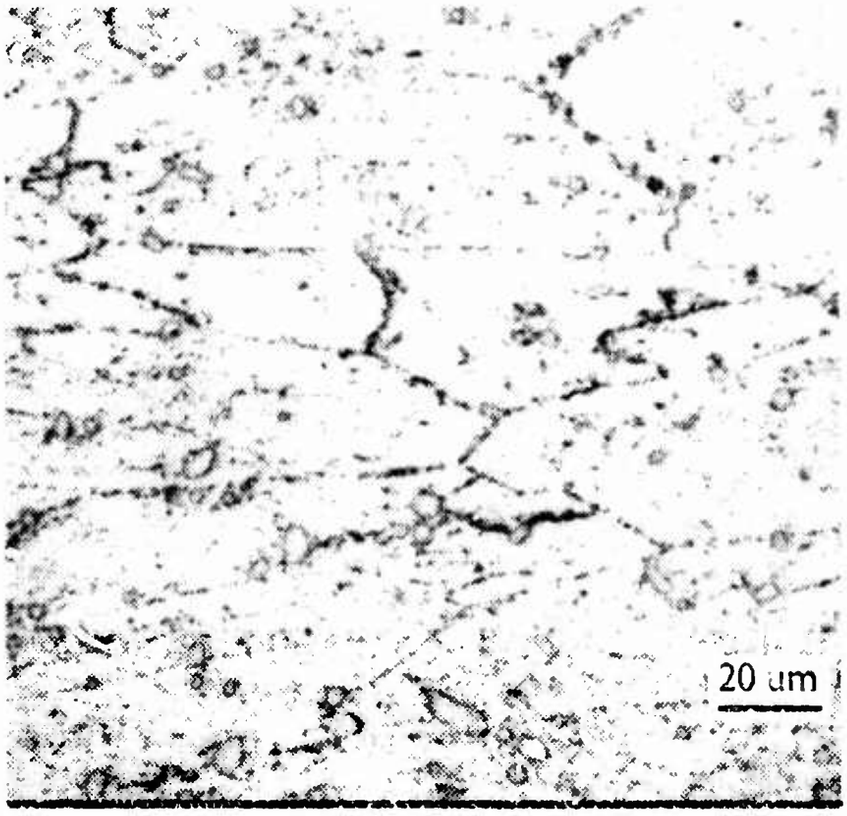

Figure 31. True stress-true strain curve and an optical micrograph from the center of the compressed sample cut through the compression axis, 1100 C and 1.0 s^{-1}.

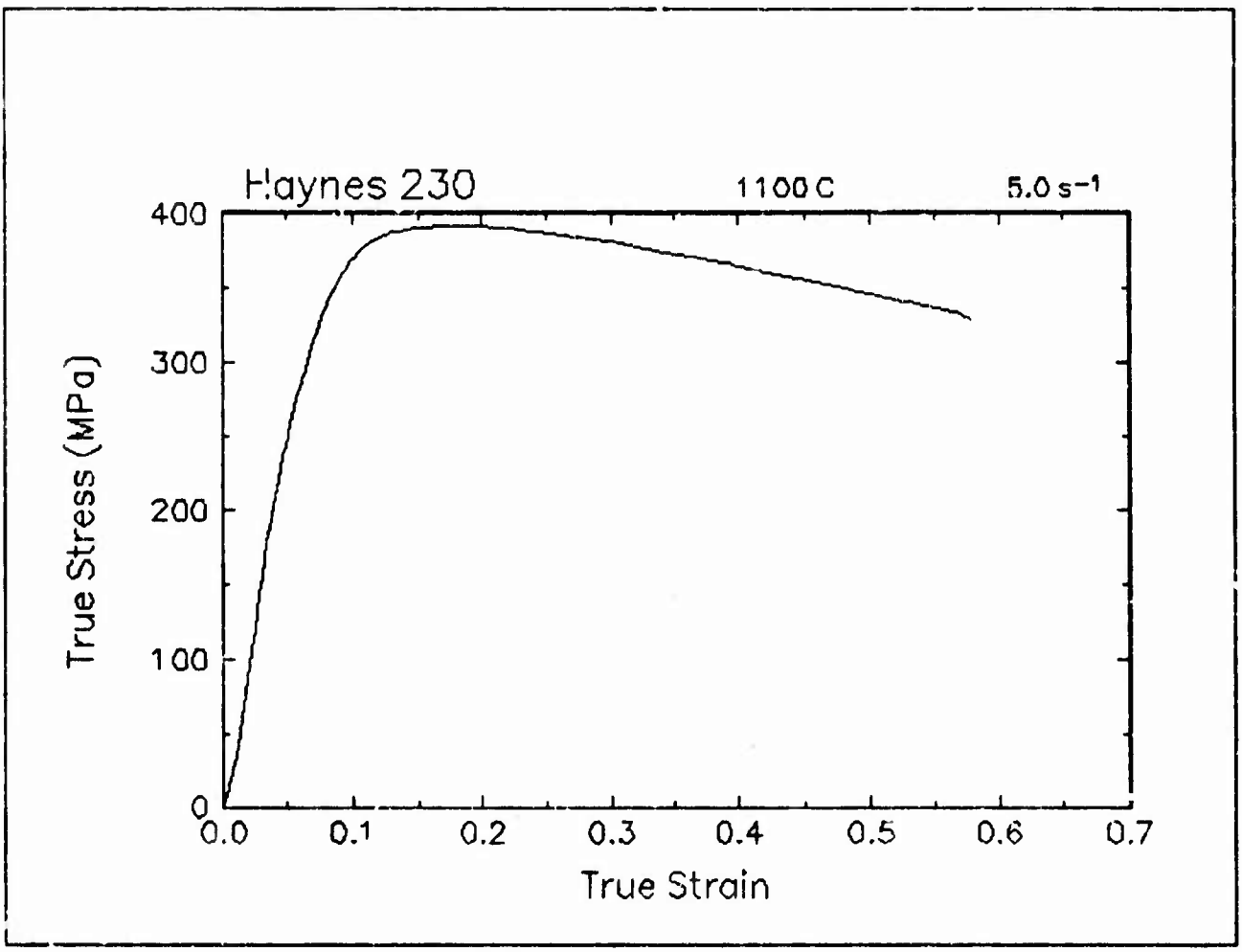

Figure 32. True stress-true strain curve, 1100 C and 5.0 s^{-1}.

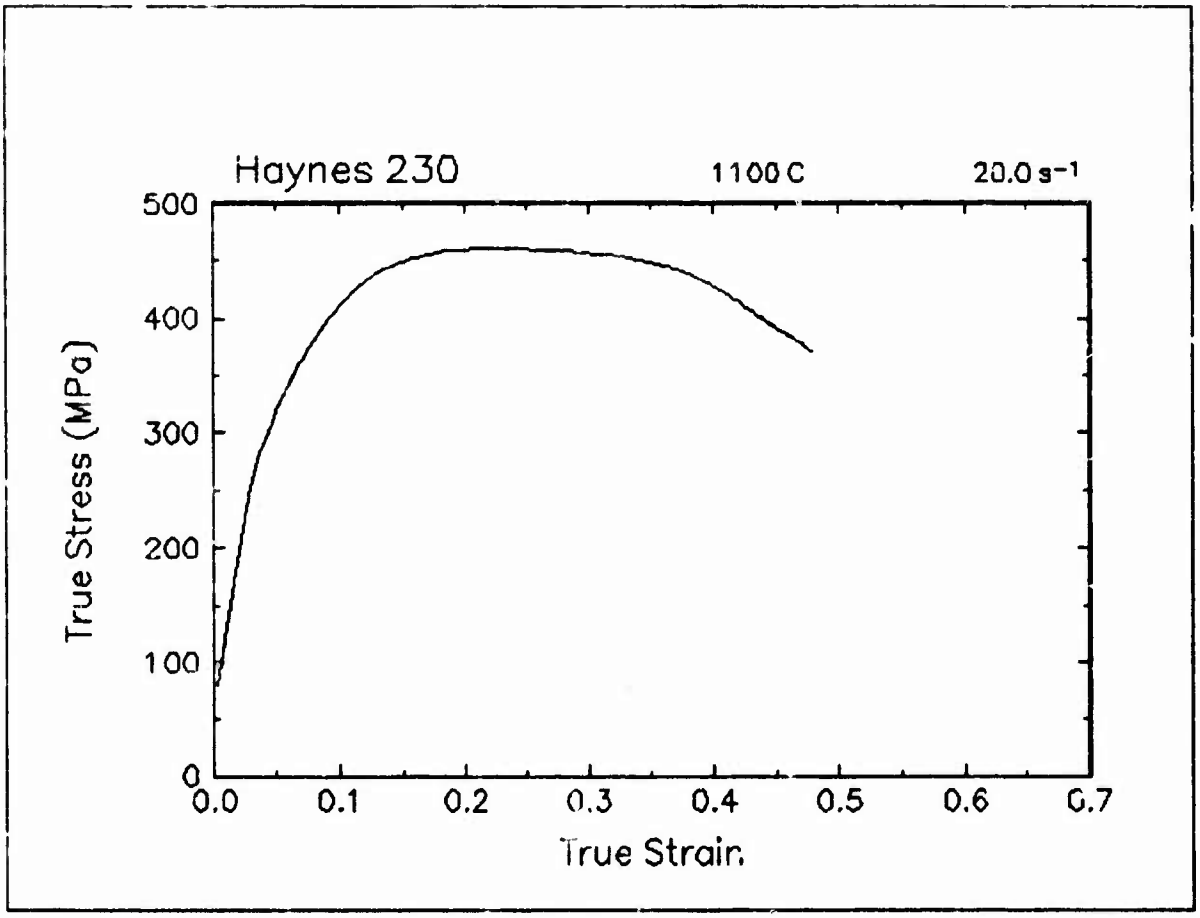

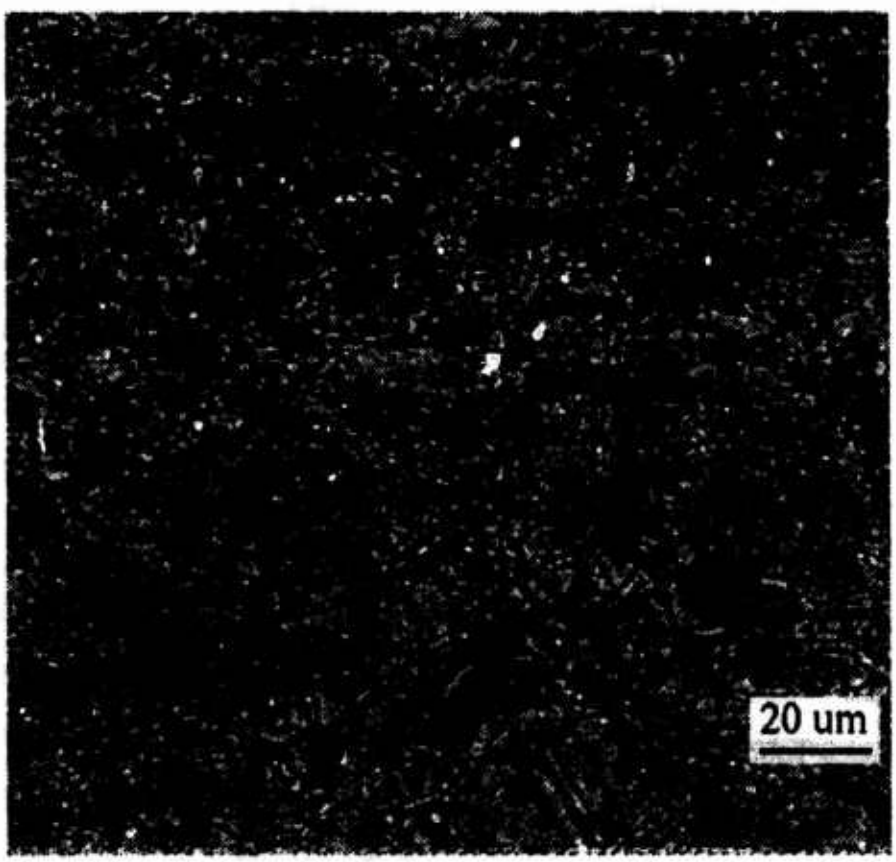

Figure 33. True stress-true strain curve and an optical micrograph from the center of the compressed sample cut through the compression axis, 1100 C and 20 s^{-1}.

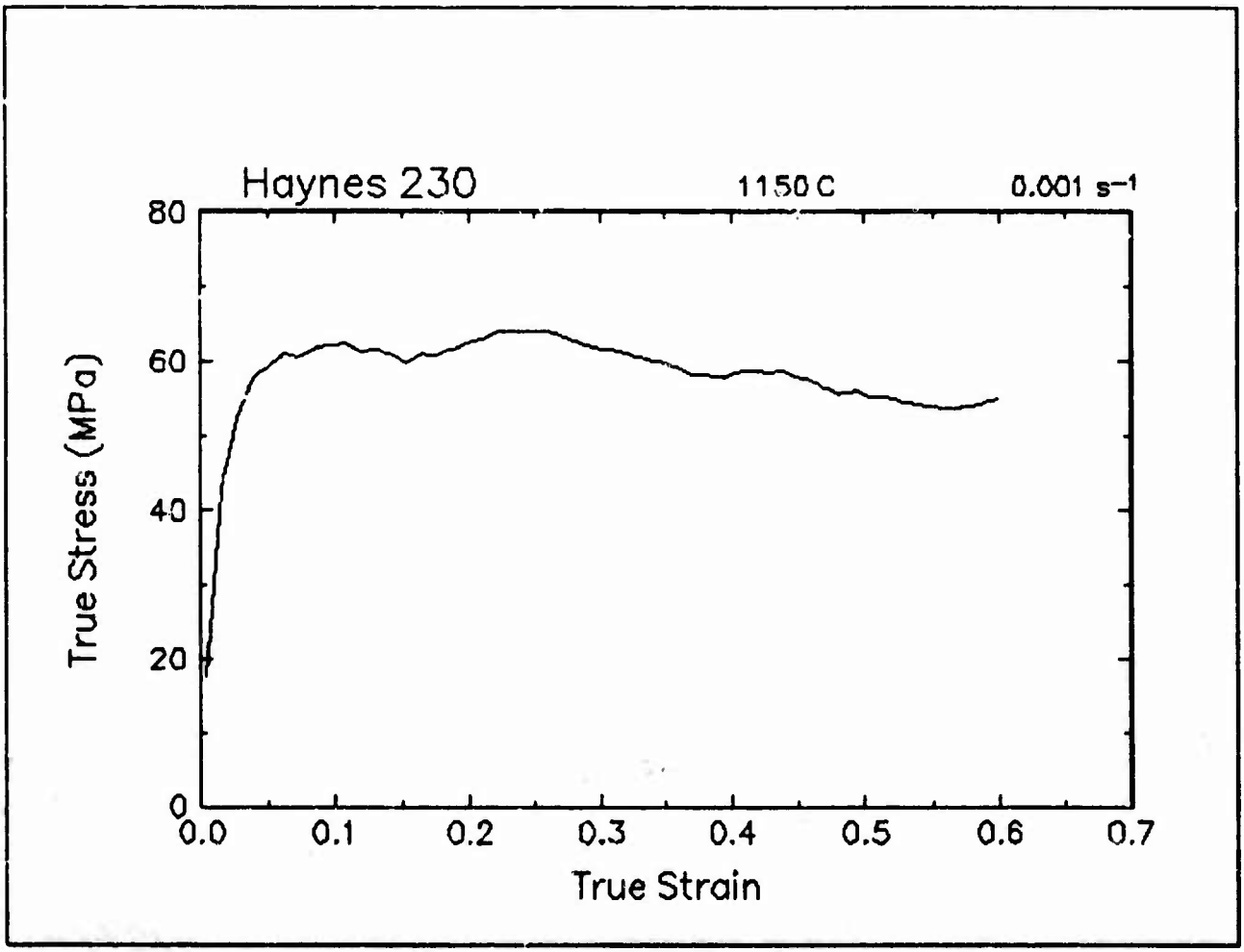

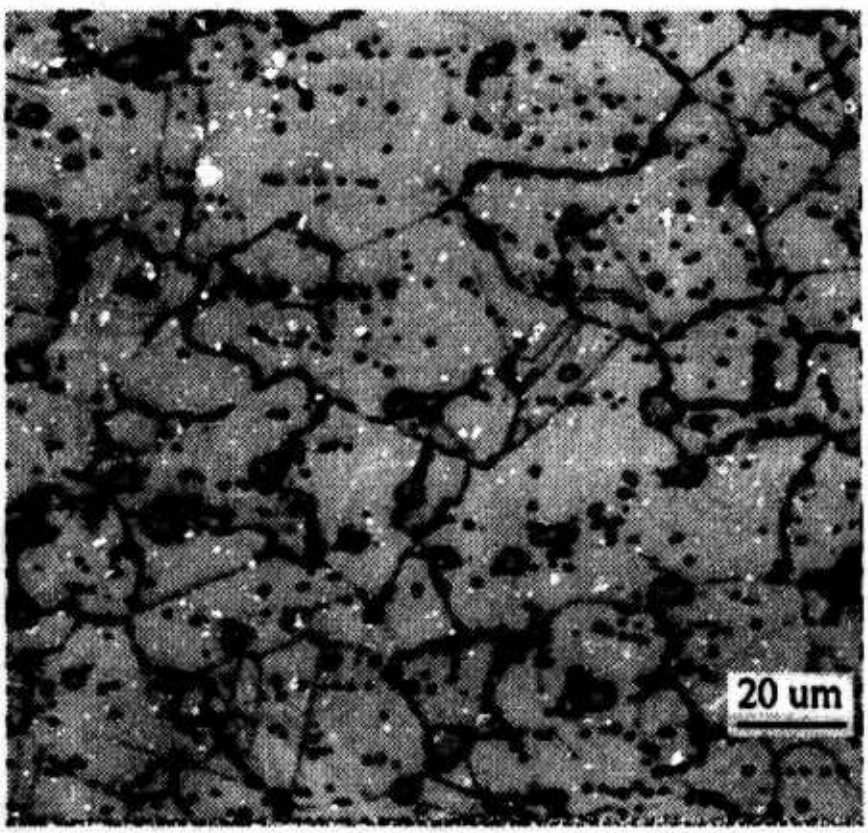

Figure 34. True stress-true strain curve and an optical micrograph from the center of the compressed sample cut through the compression axis, 1150 C and $0.001s^{-1}$.

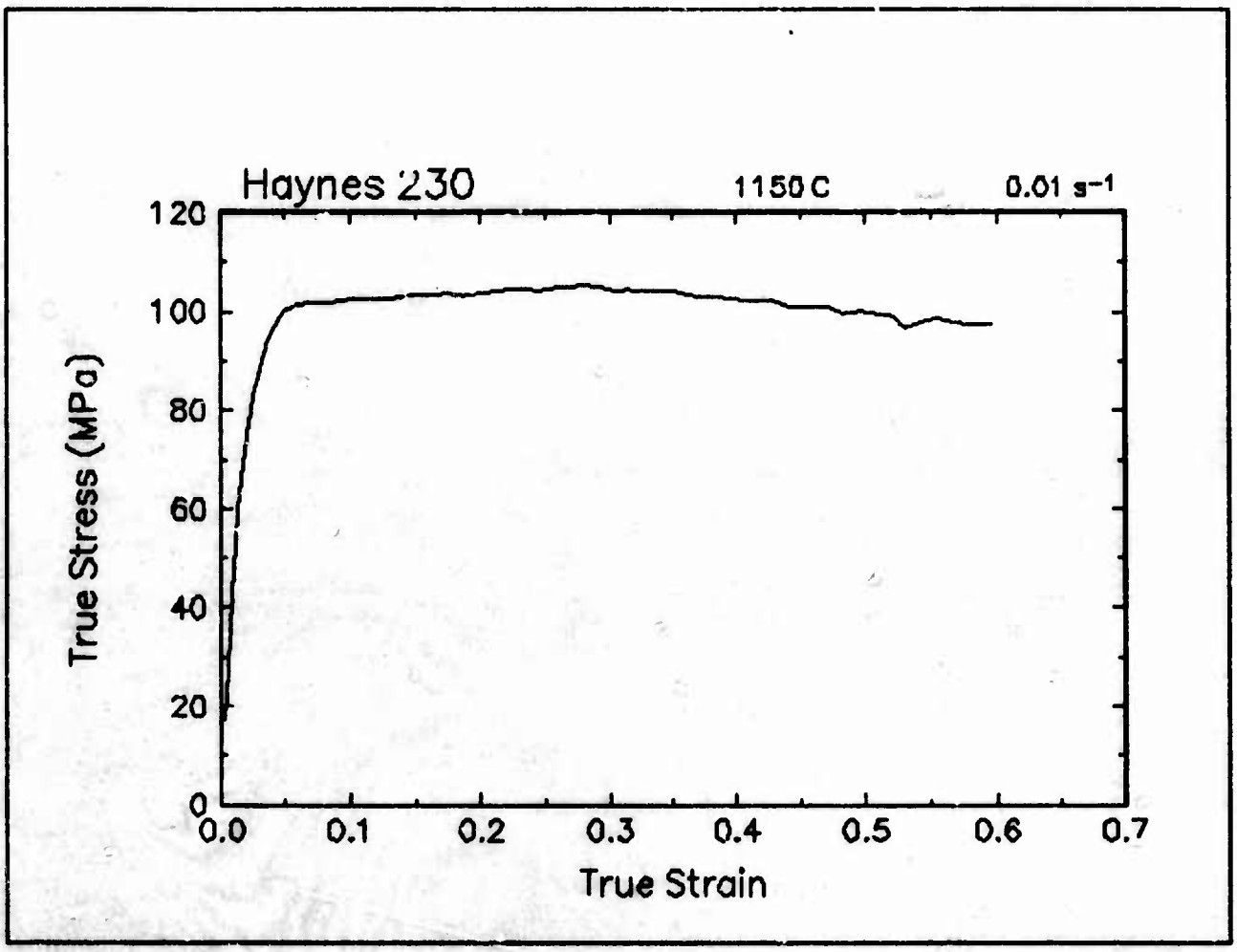

Figure 35. True stress-true strain curve, 1150 C and 0.01 s^{-1}.

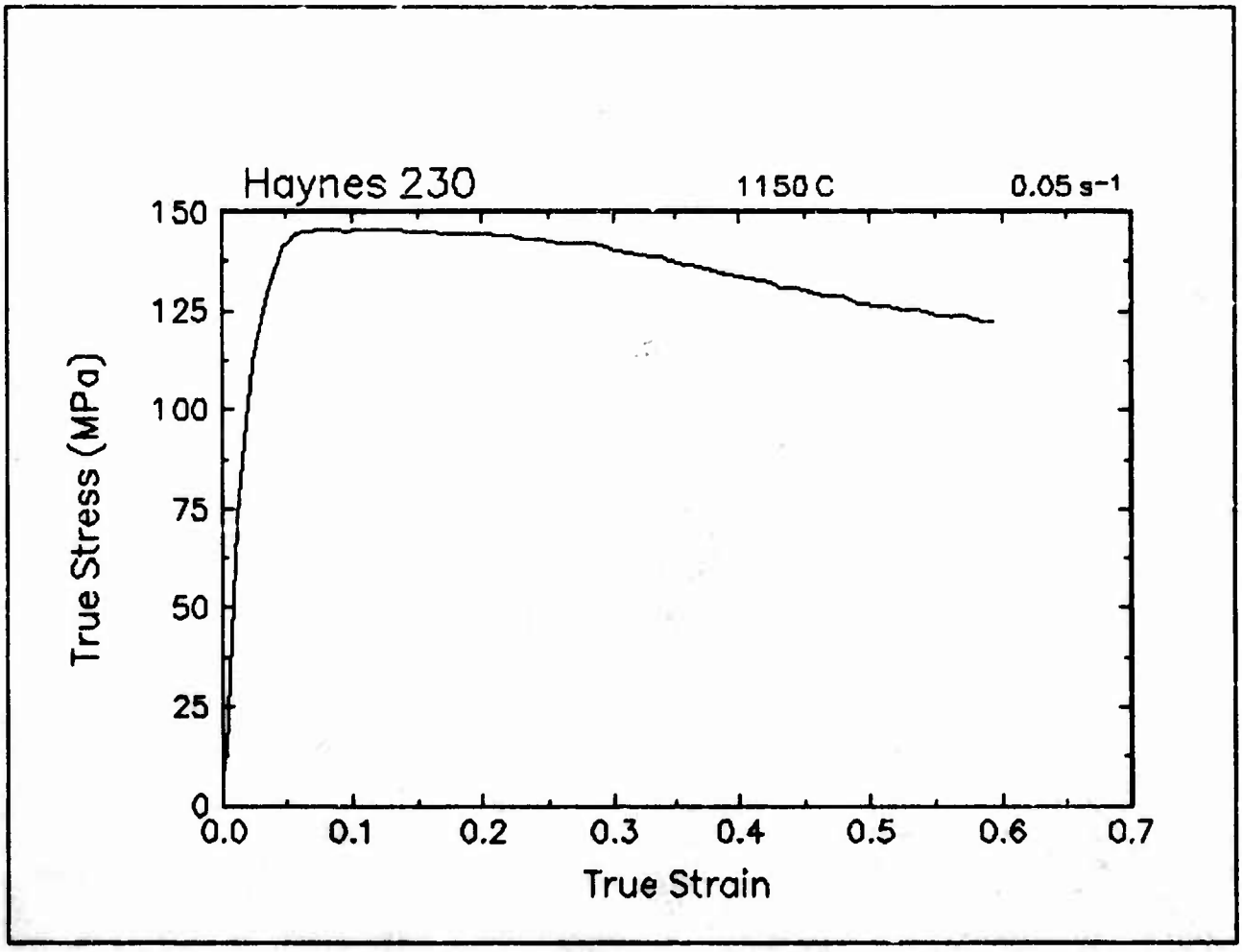

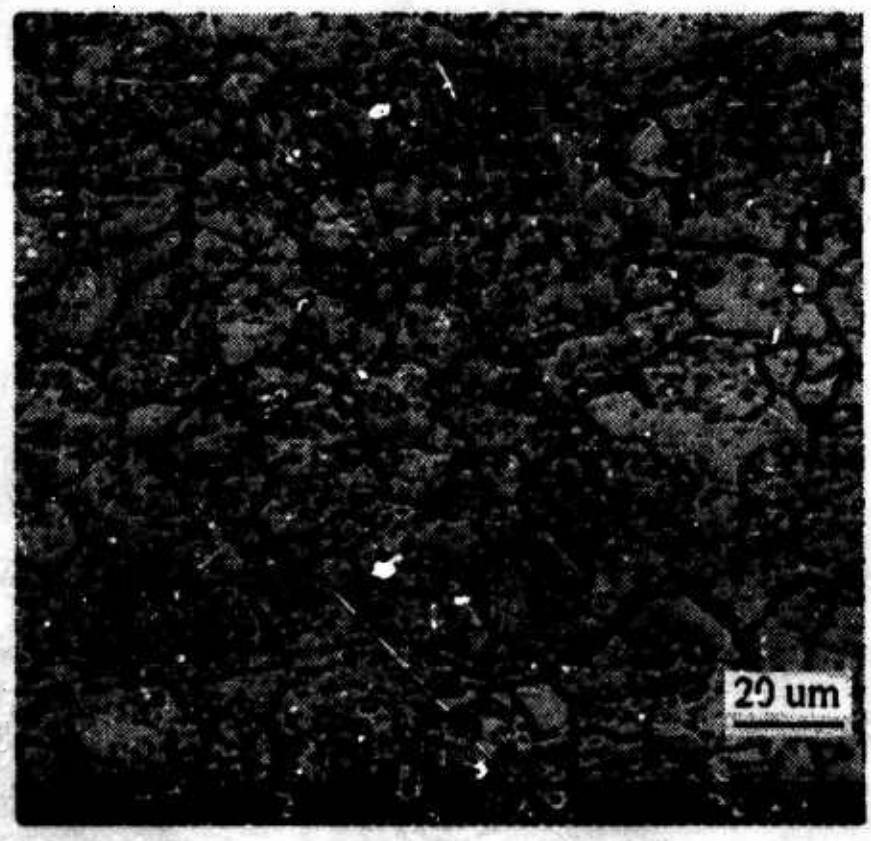

Figure 36. True stress-true strain curve and an optical micrograph from the center of the compressed sample cut through the compression axis, 1150 C and 0.05 s^{-1}.

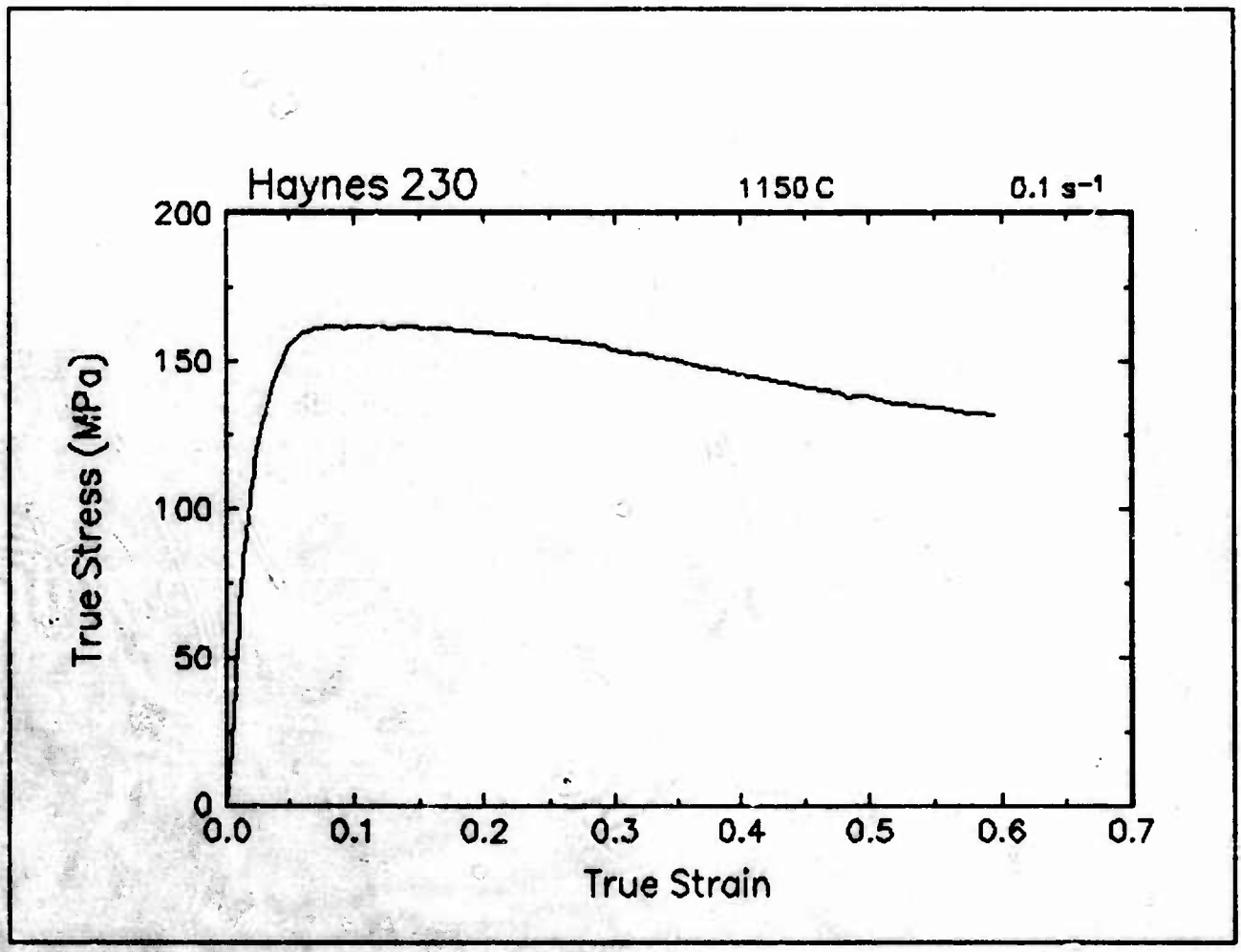

Figure 37. True stress-true strain curve, 1150 C and 0.1 s^{-1}.

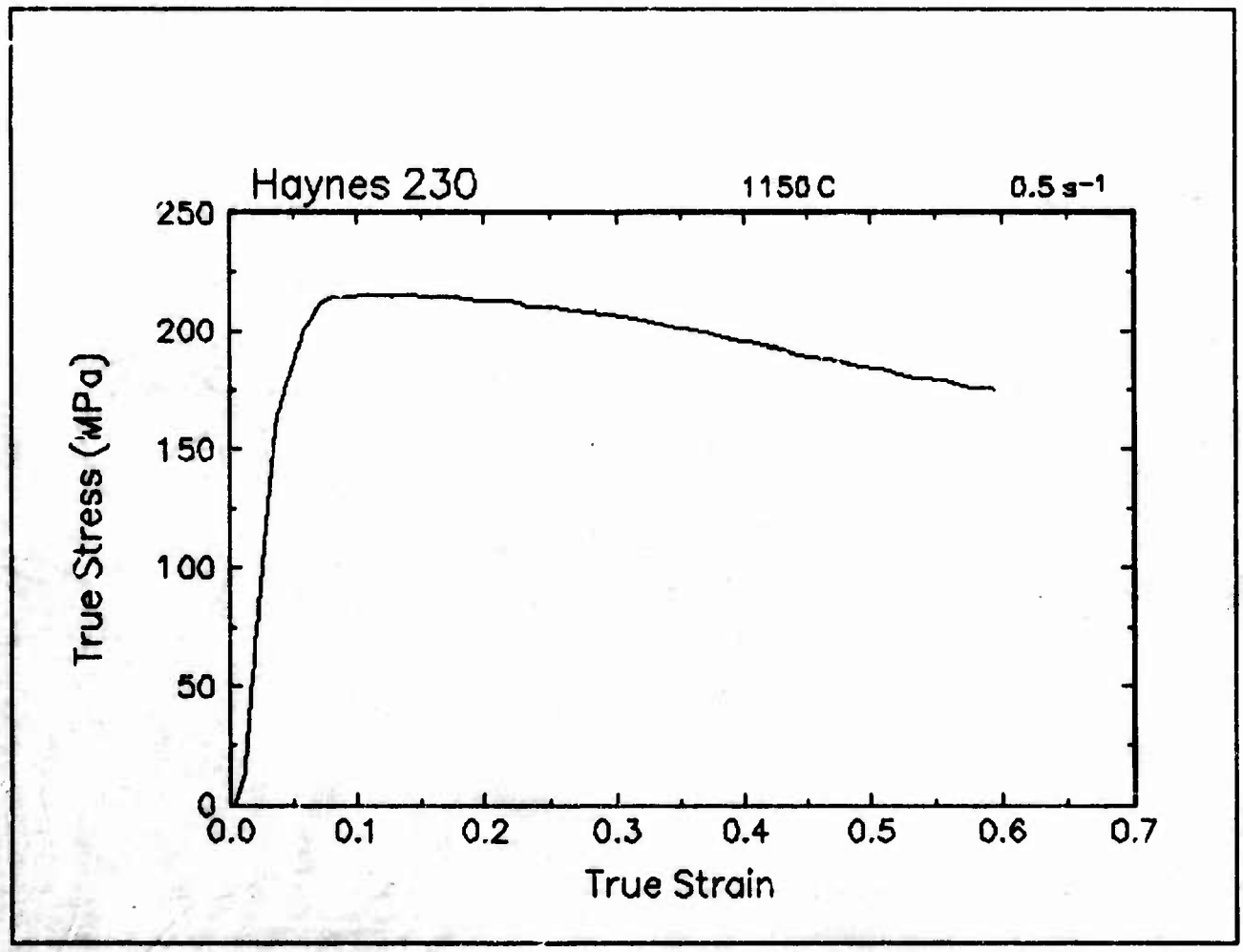

Figure 38. True stress-true strain curve, 1150 C and 0.5 s^{-1}.

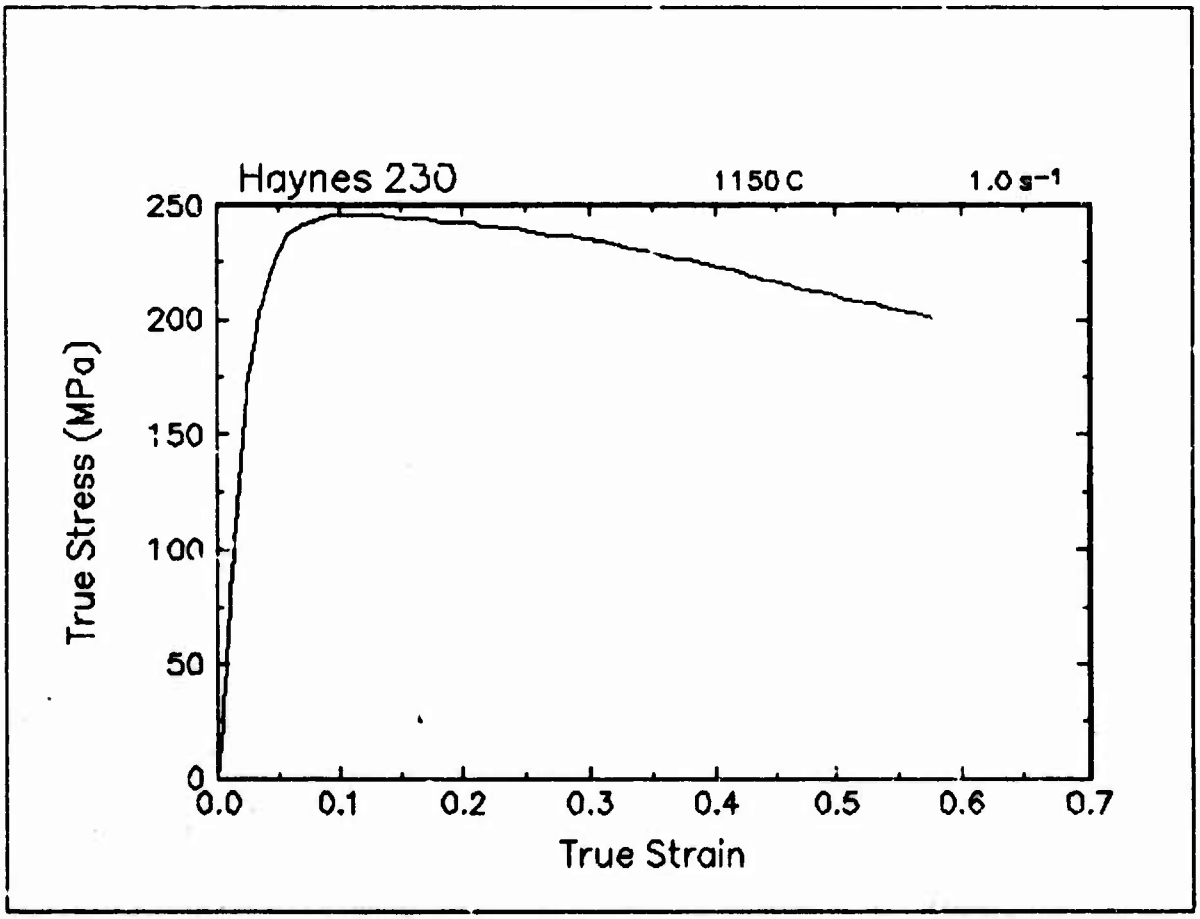

Figure 39. True stress-true strain curve and an optical micrograph from the center of the compressed sample cut through the compression axis, 1150 C and 1 s^{-1}.

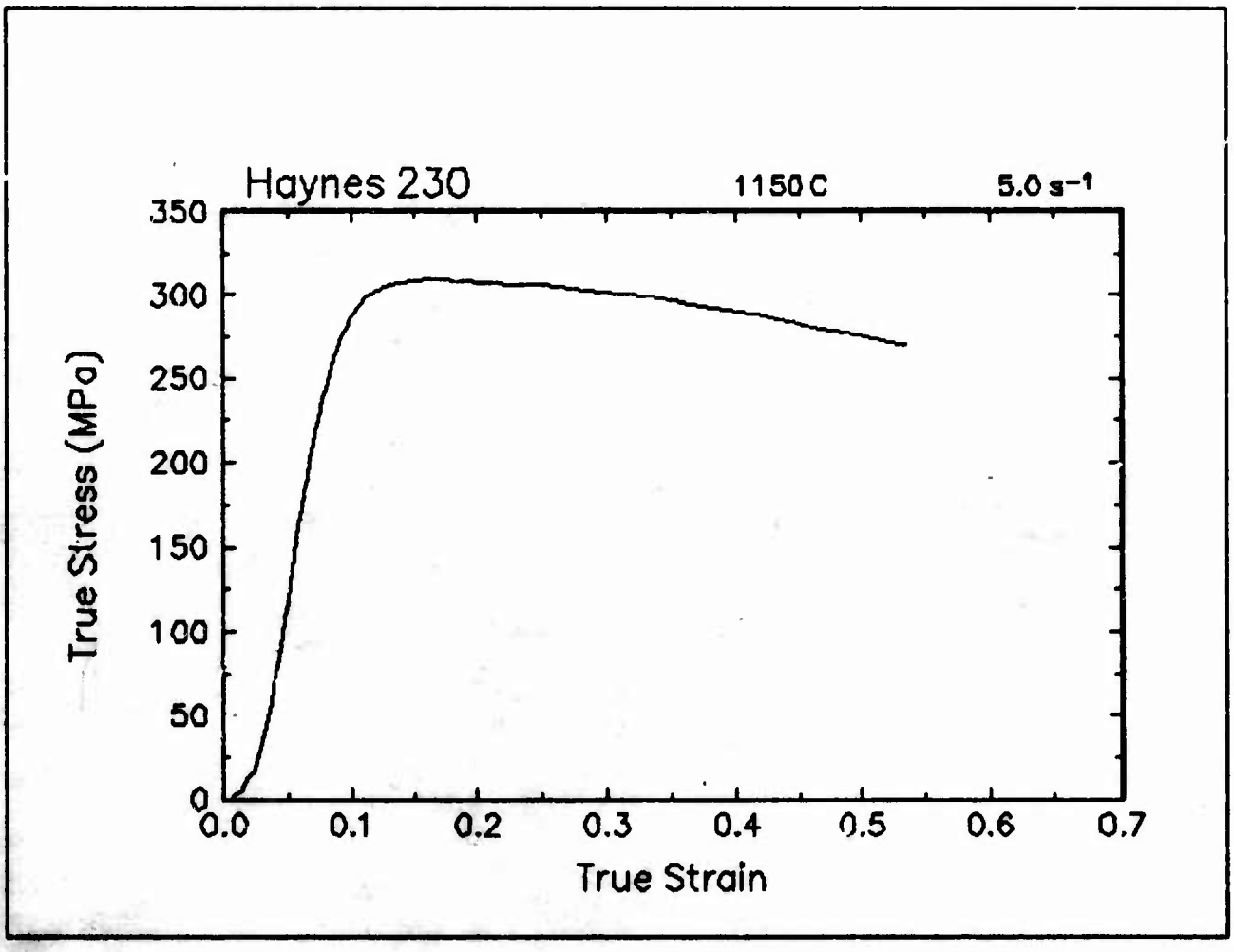

Figure 40. True stress-true strain curve, 1150 C and 5 s^{-1}.

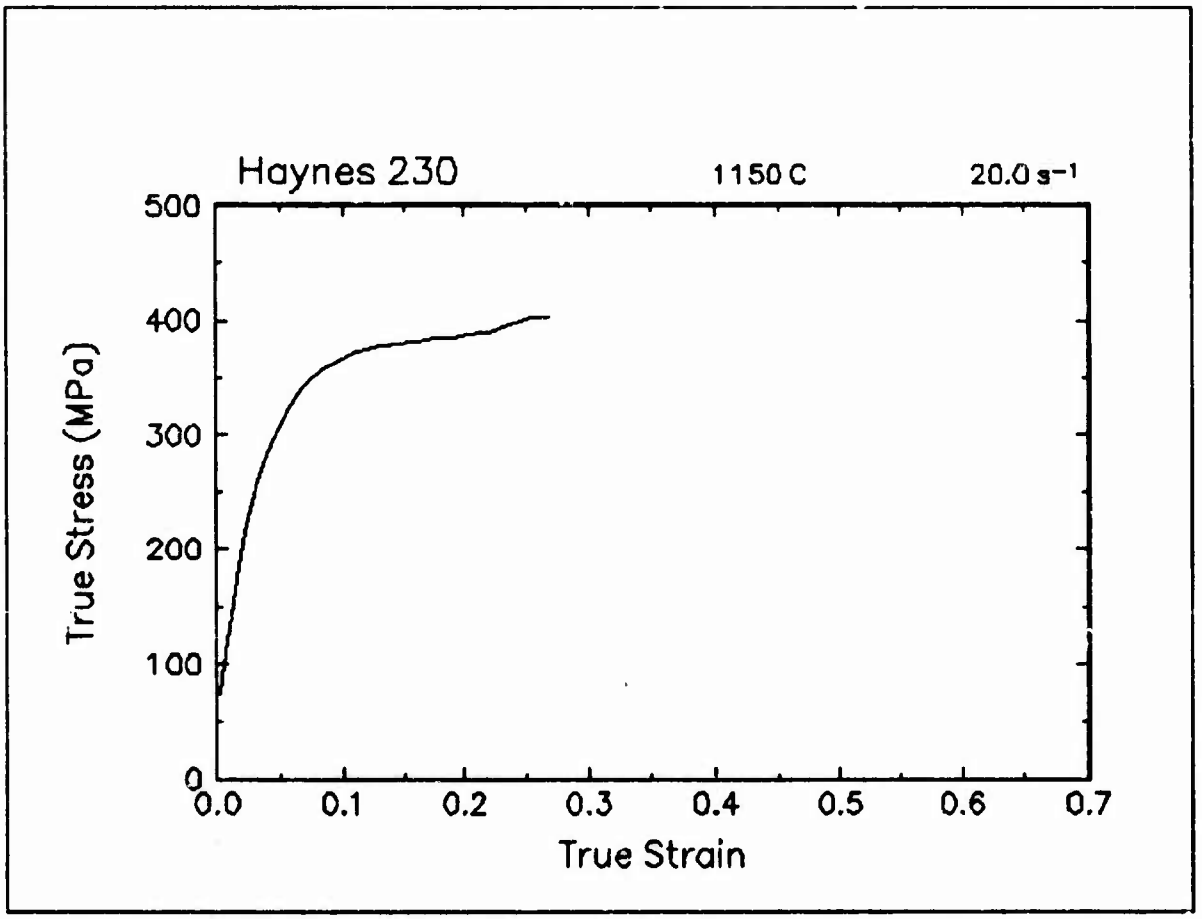

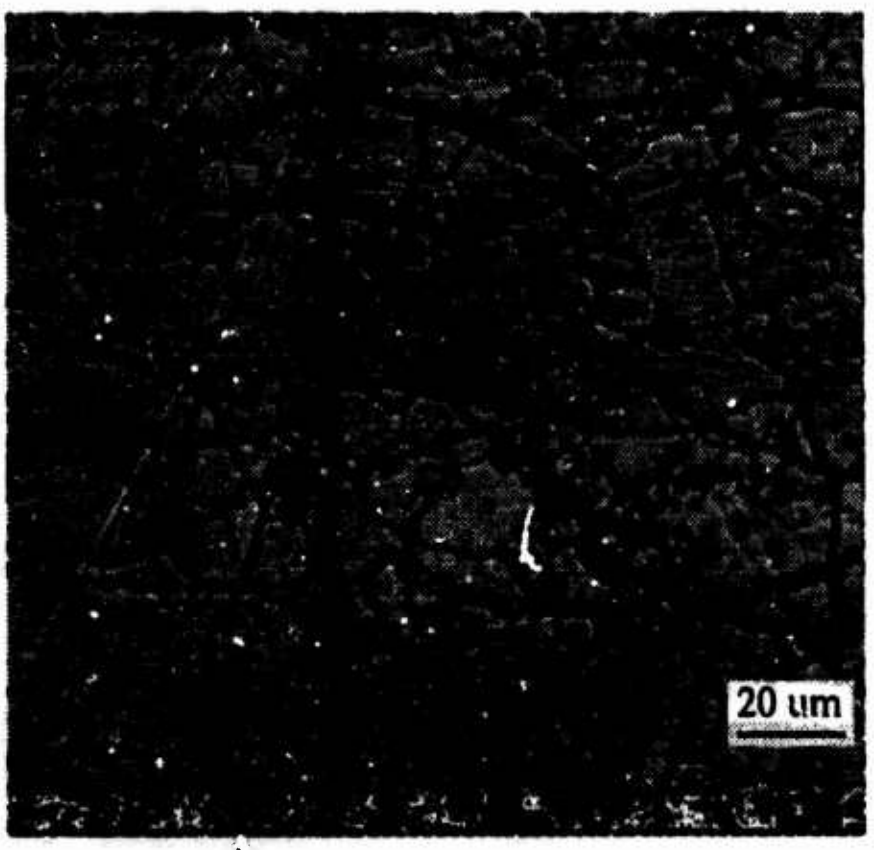

Figure 41. True stress-true strain curve and an optical micrograph from the center of the compressed sample cut through the compression axis, 1150 C and 20.0 s^{-1}.

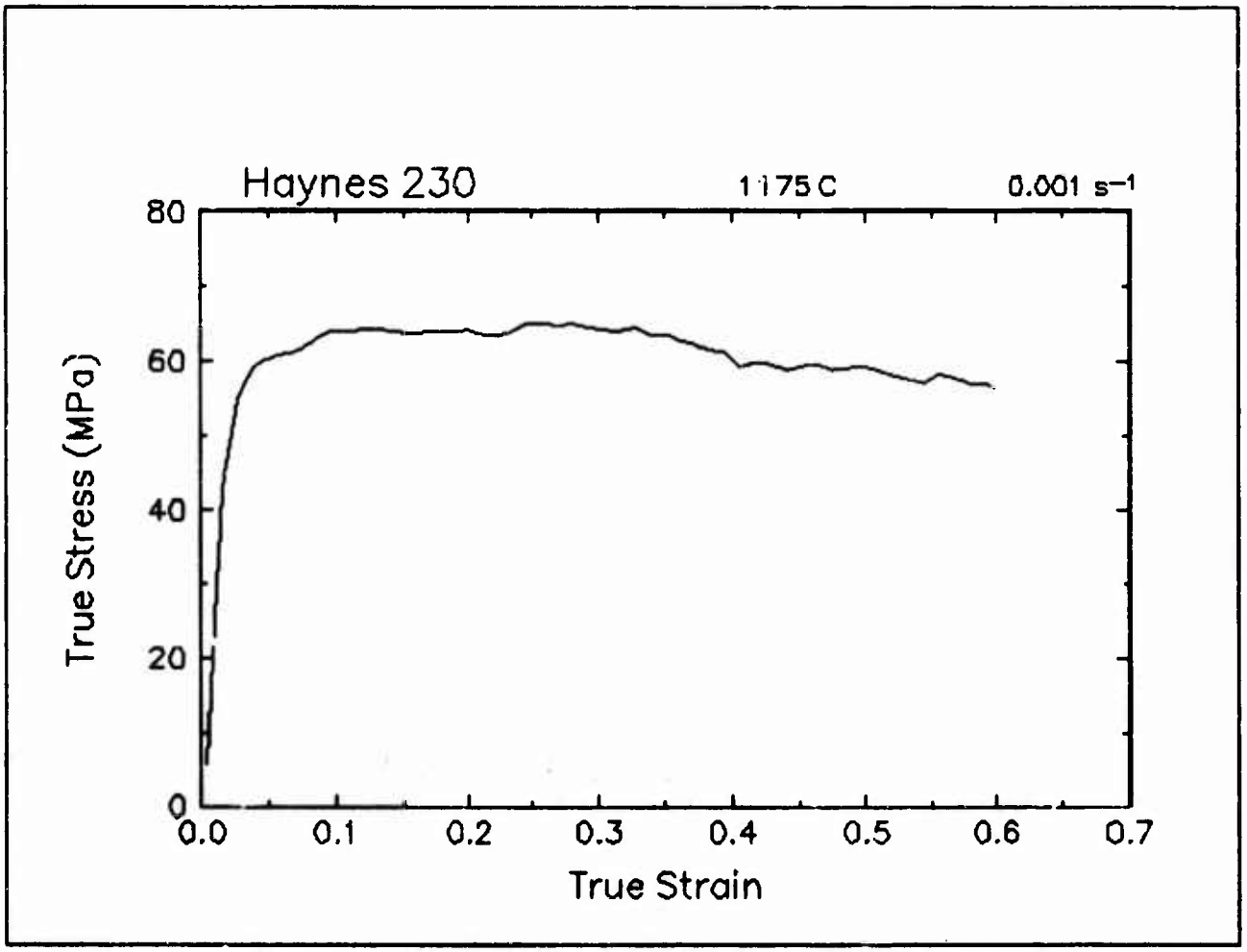

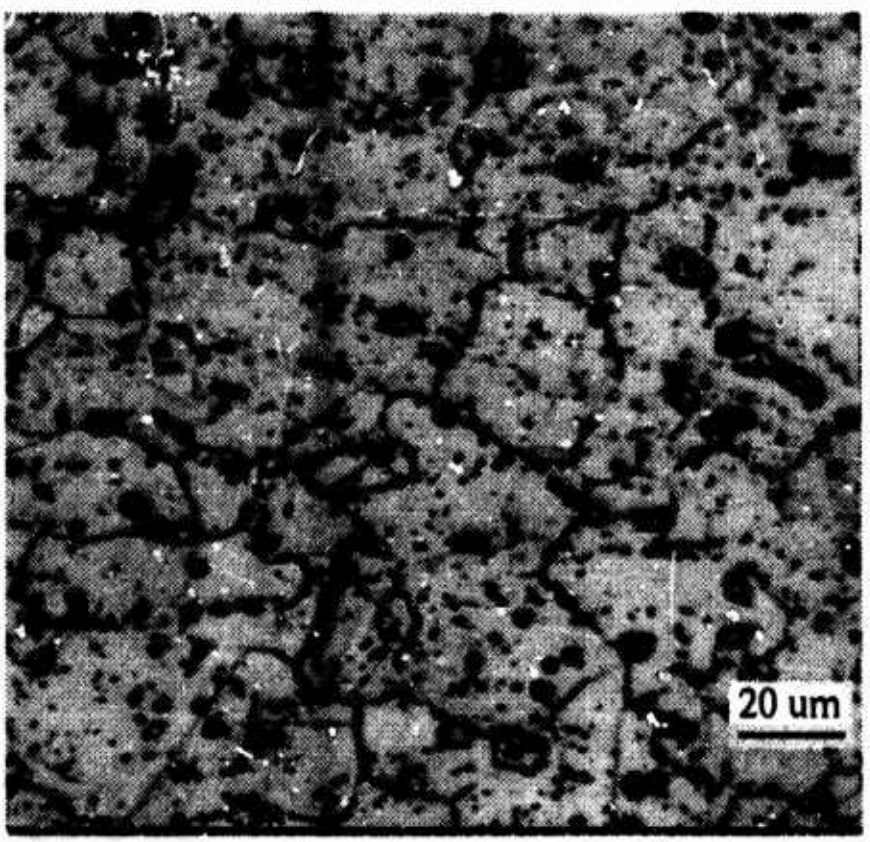

Figure 42. True stress-true strain curve and an optical micrograph from the center of the compressed sample cut through the compression axis; 1175 C and 0.001 s^{-1}.

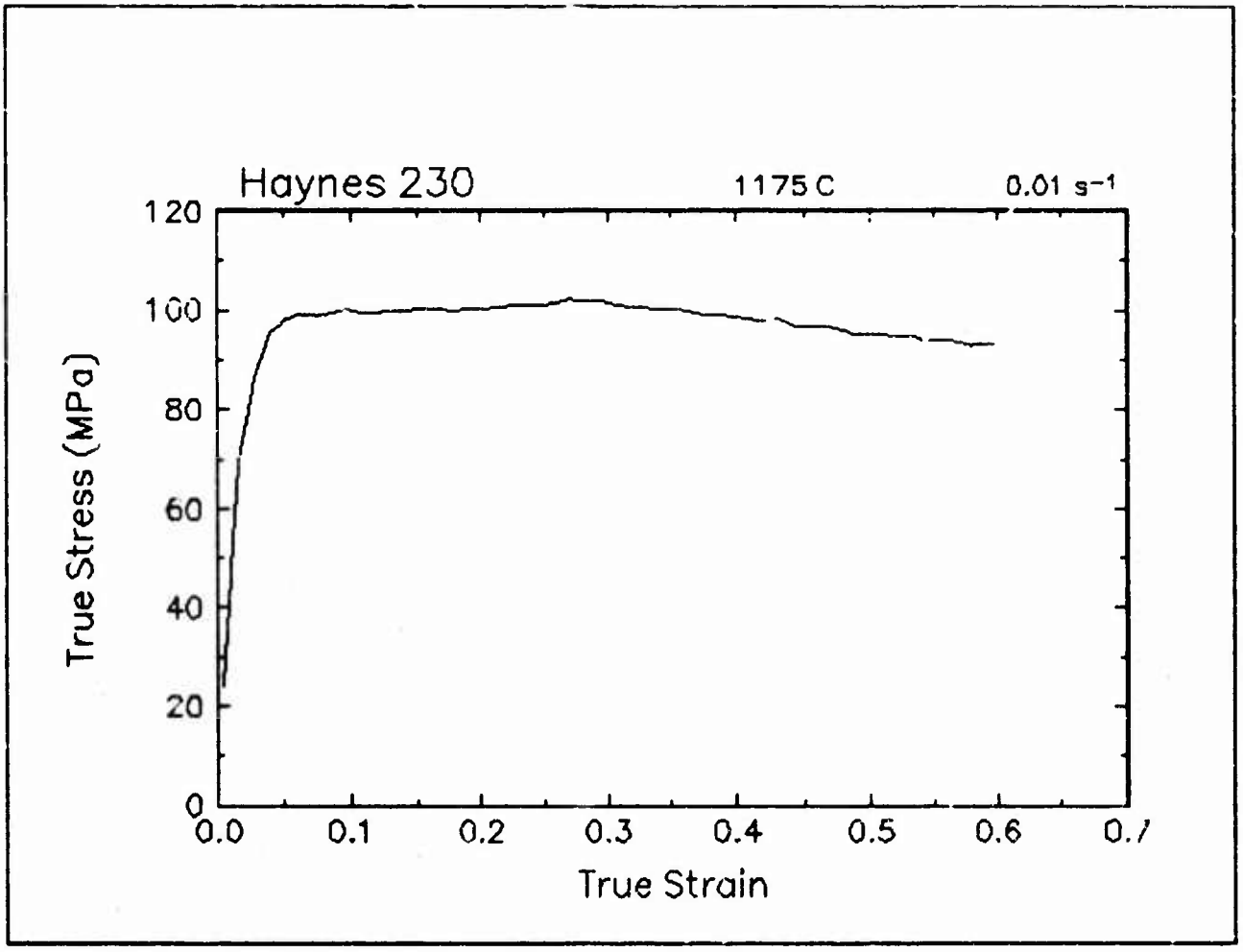

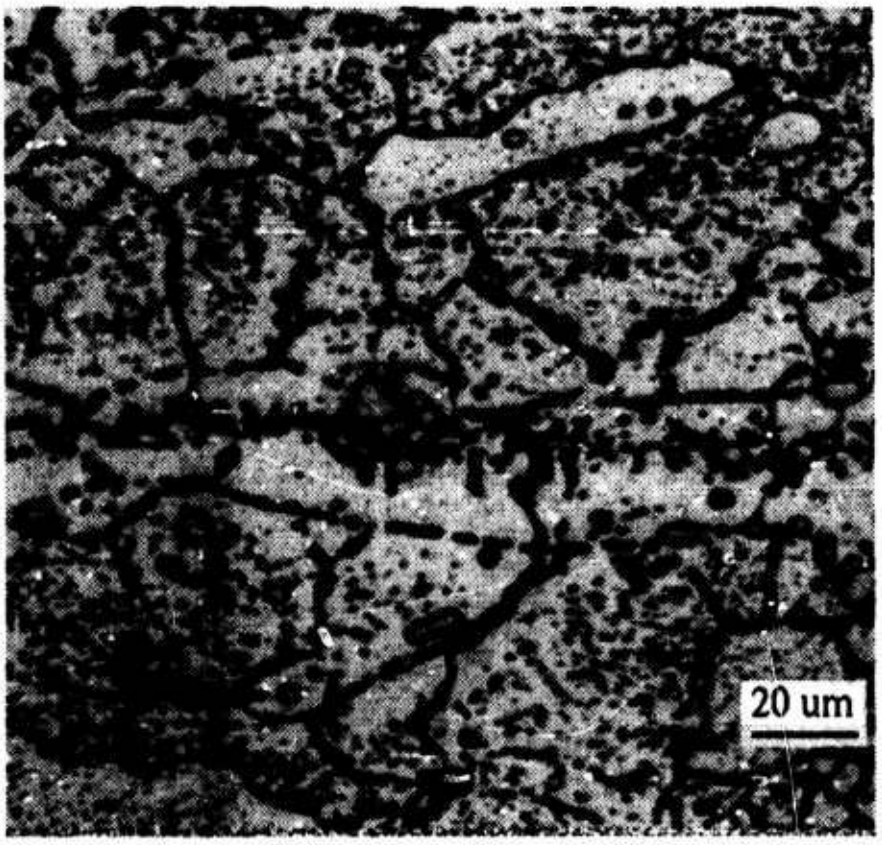

Figure 43. True stress-true strain curve and an optical micrograph from the center of the compressed sample cut through the compression axis, 1175 C and 0.01 s^{-1}.

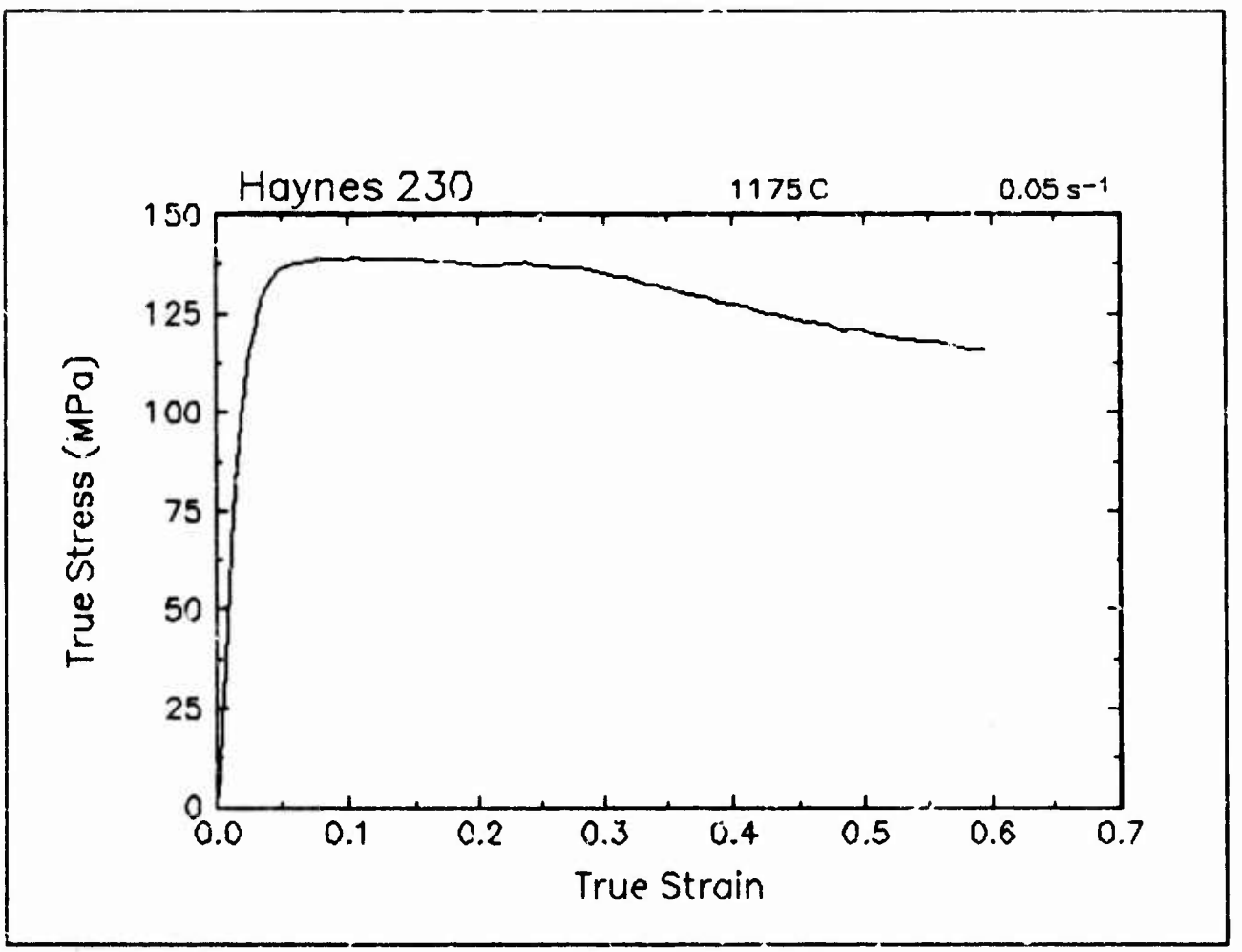

Figure 44. True stress-true strain curve, 1175 C and 0.05 s^{-1}.

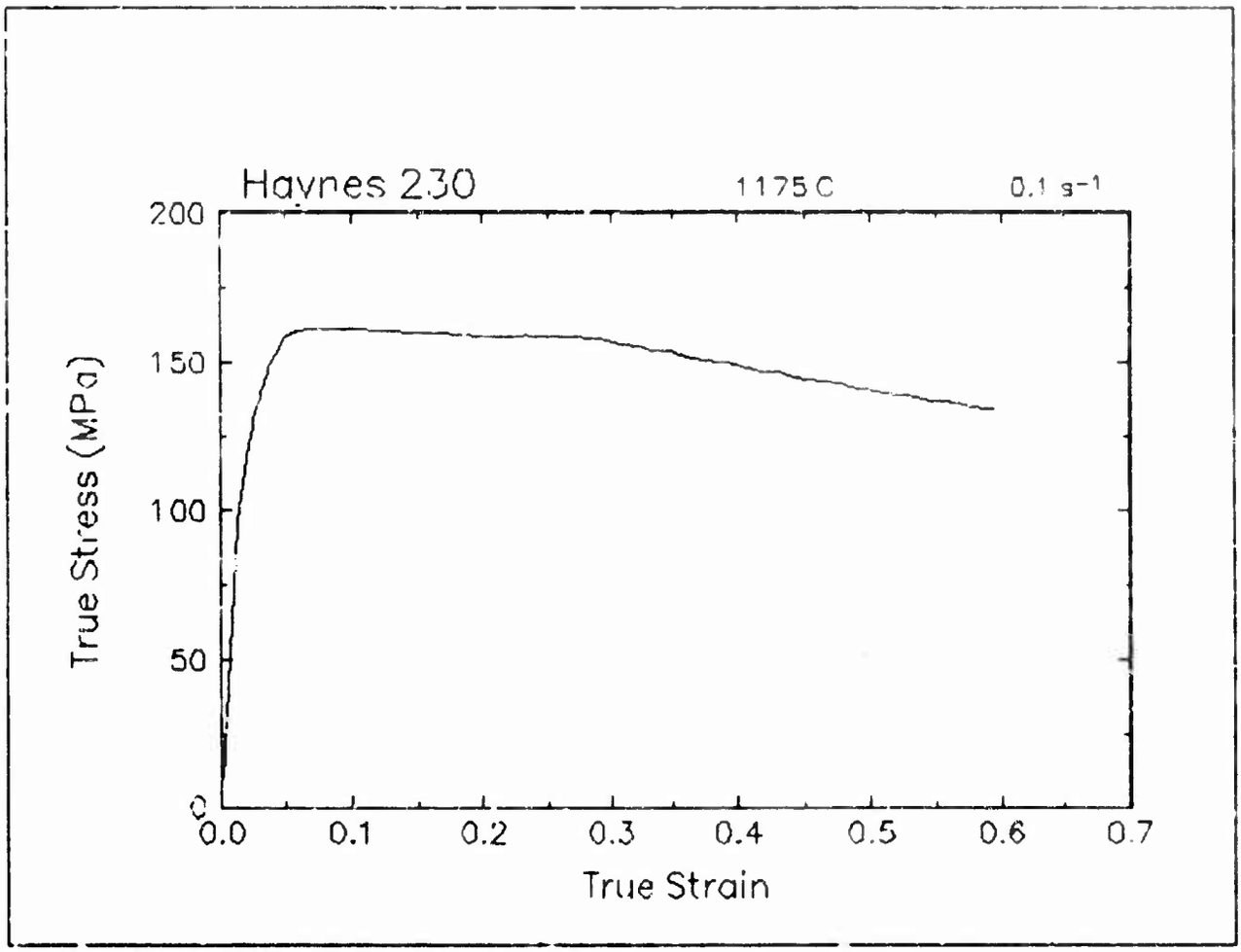

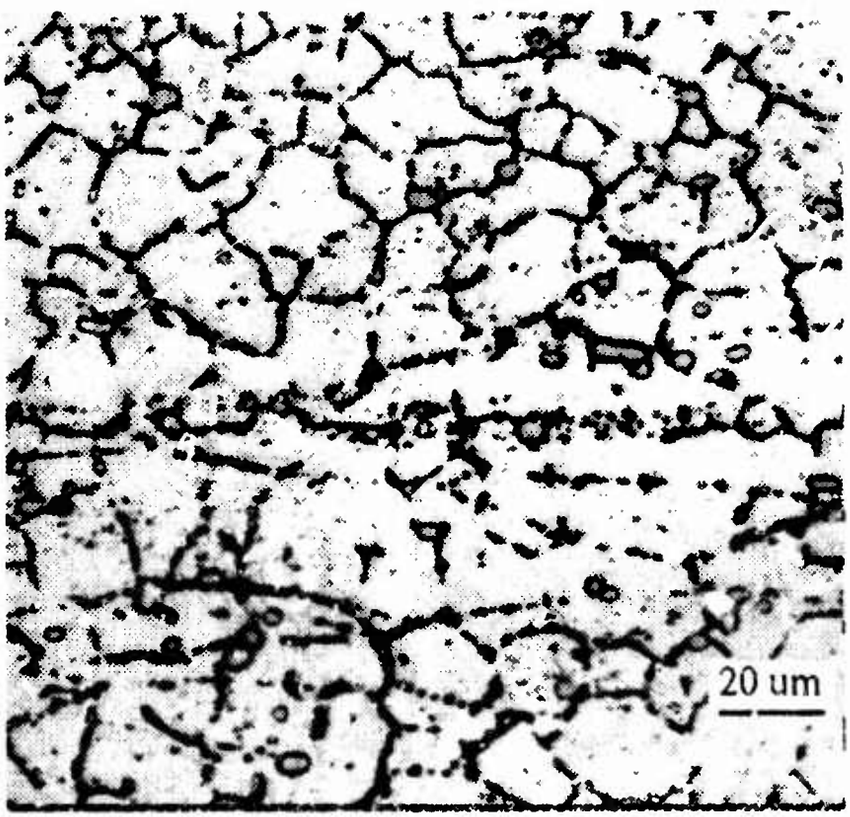

Figure 45. True stress-true strain curve and an optical micrograph from the center of the compressed sample cut through the compression axis, 1175 C and 0.1 s^{-1}.

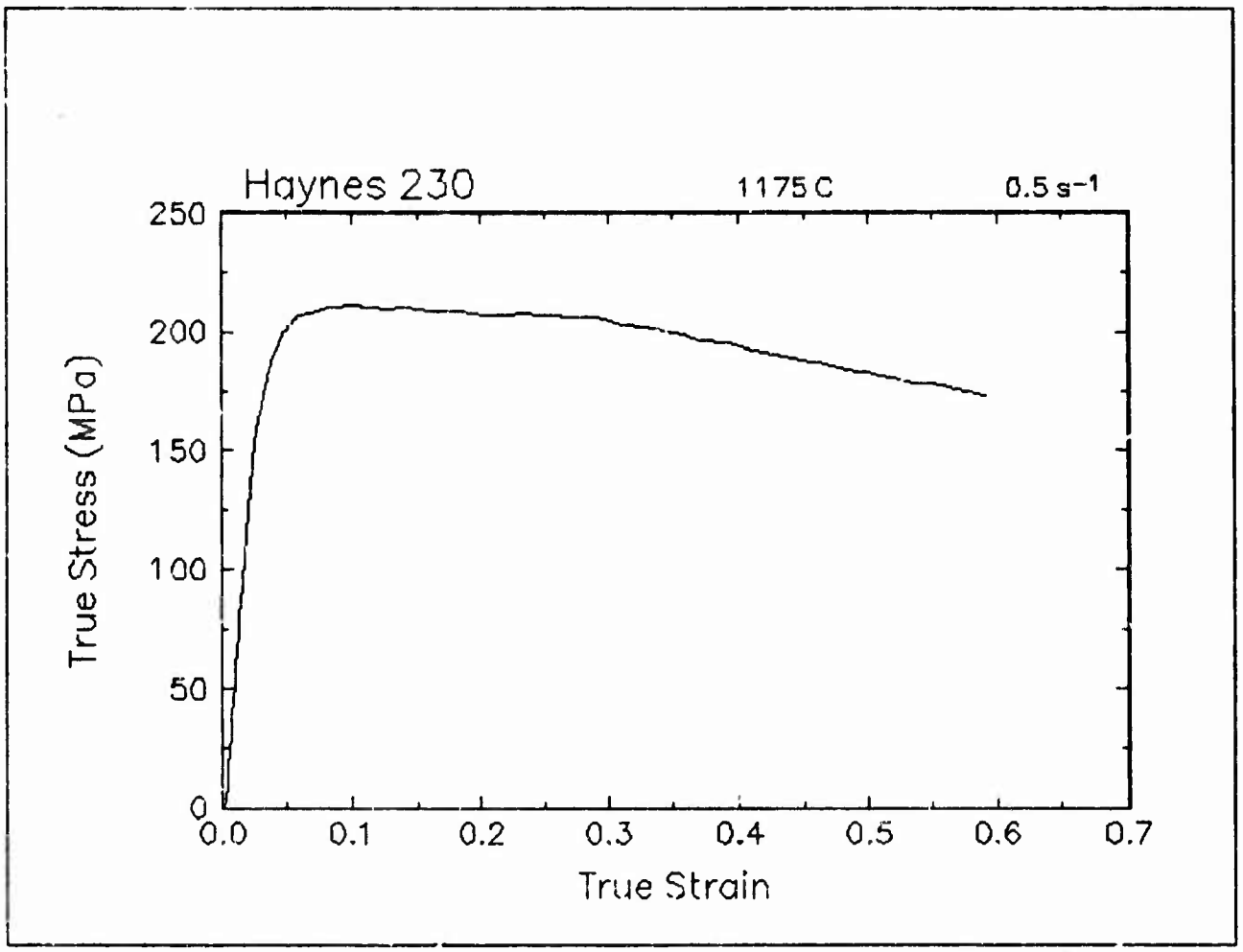

Figure 46. True stress-true strain curve, 1175 C and 0.5 s^{-1}.

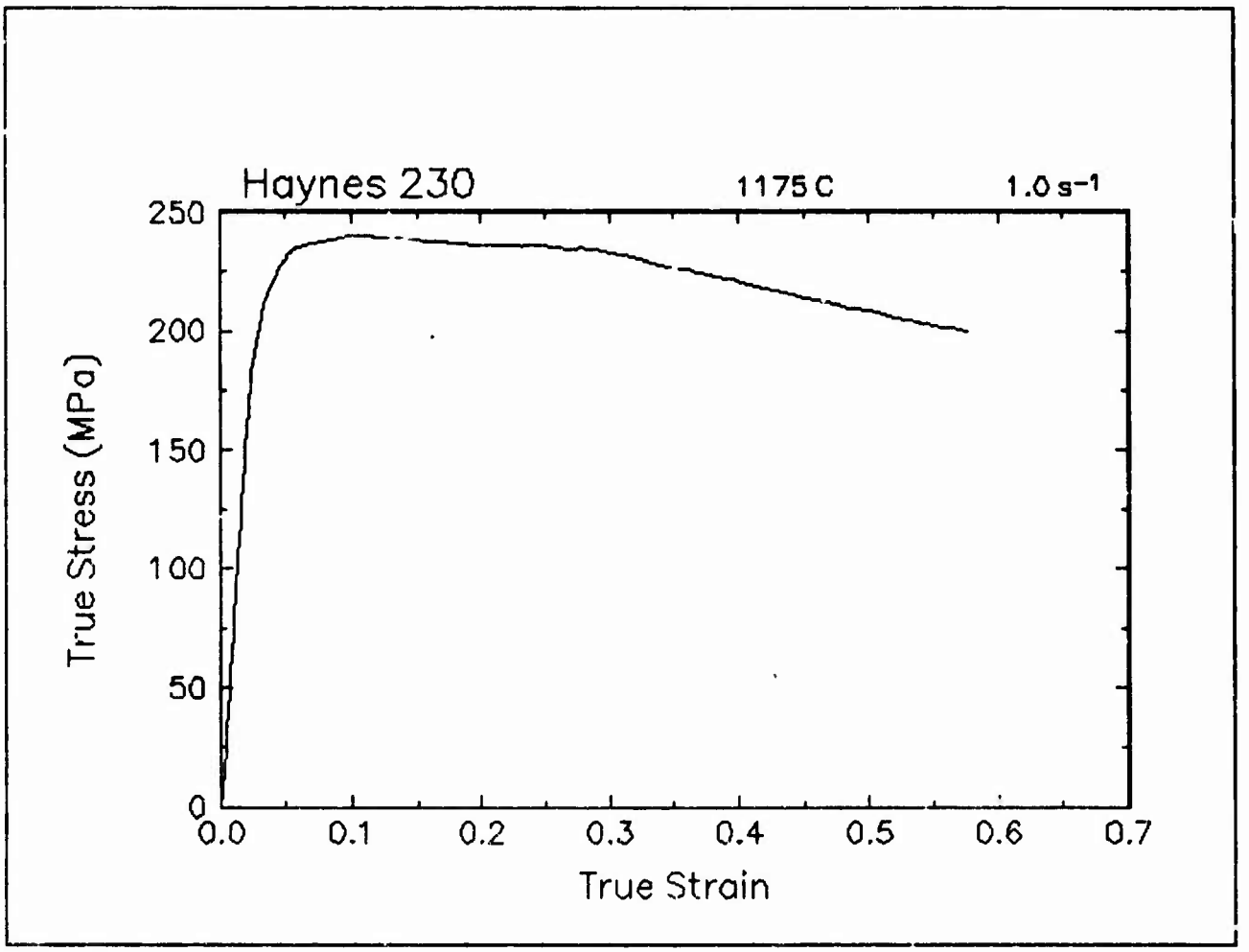

Figure 47. True stress-true strain curve, 1175 C and 1 s^{-1}.

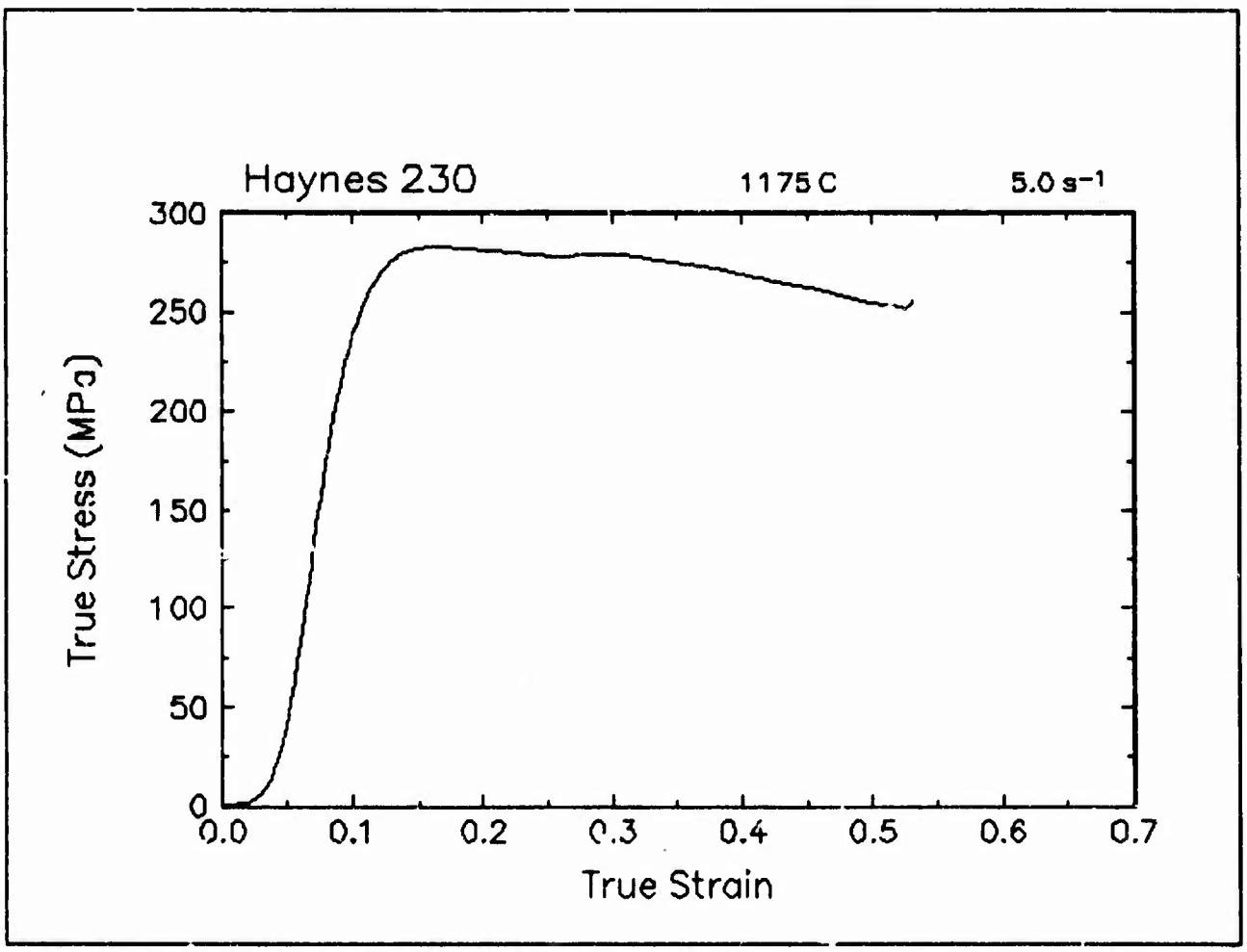

Figure 48. True stress-true strain curve, 1175 C and 5 s^{-1}.

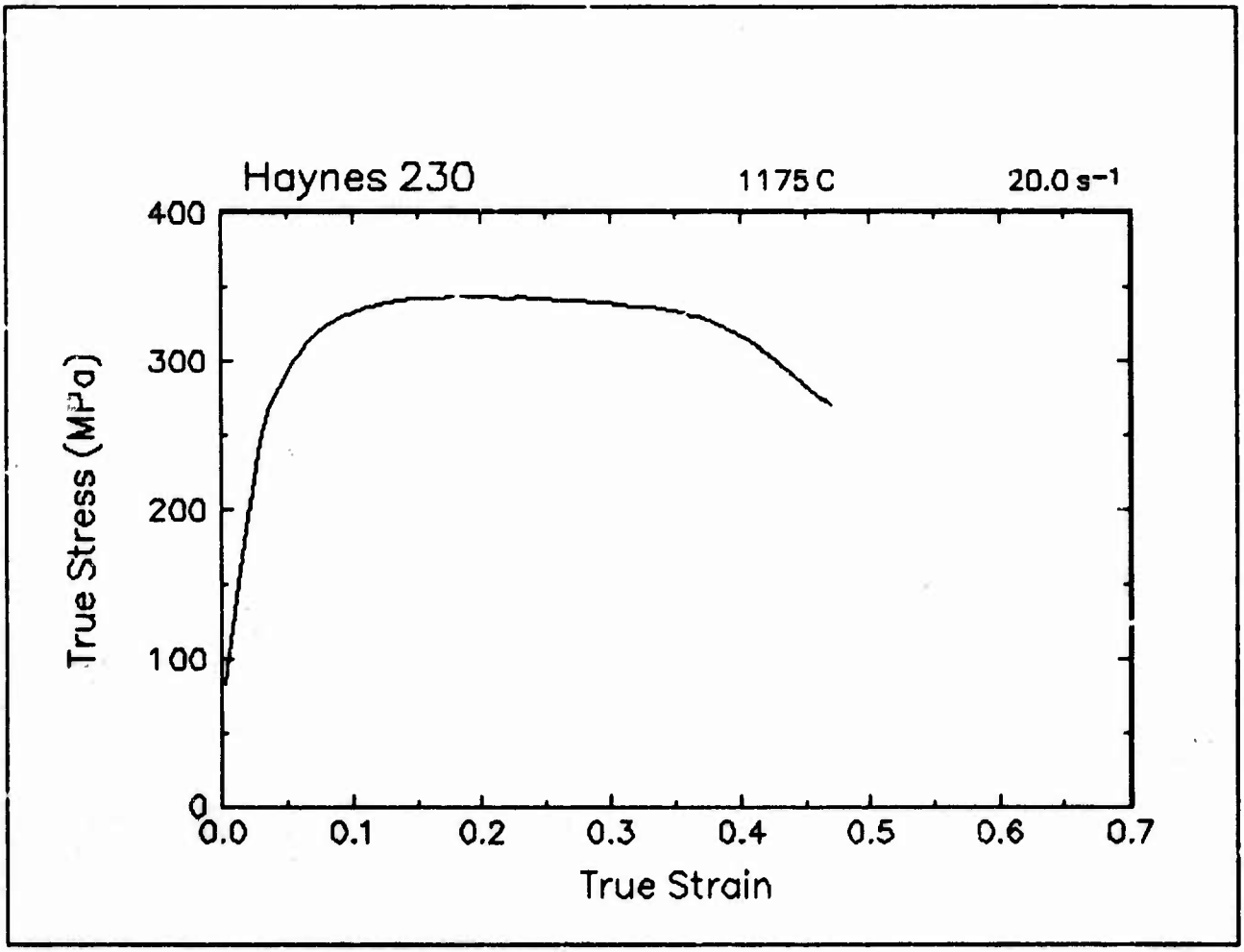

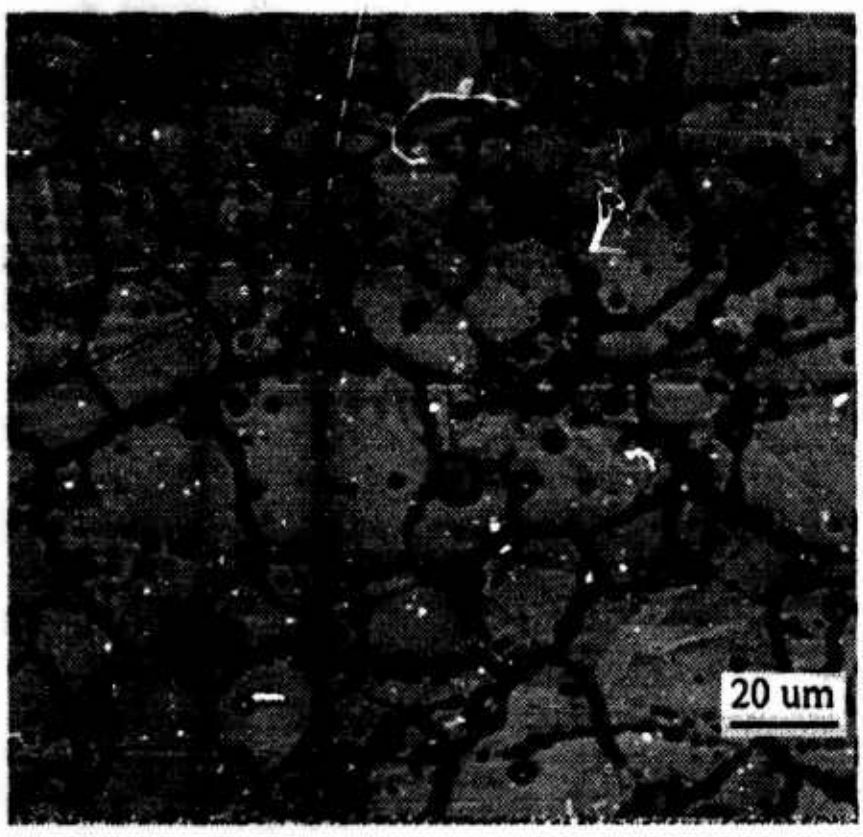

Figure 49. True stress-true strain curve and an optical micrograph from the center of the compressed sample cut through the compression axis, 1175 C and 20 s^{-1}.

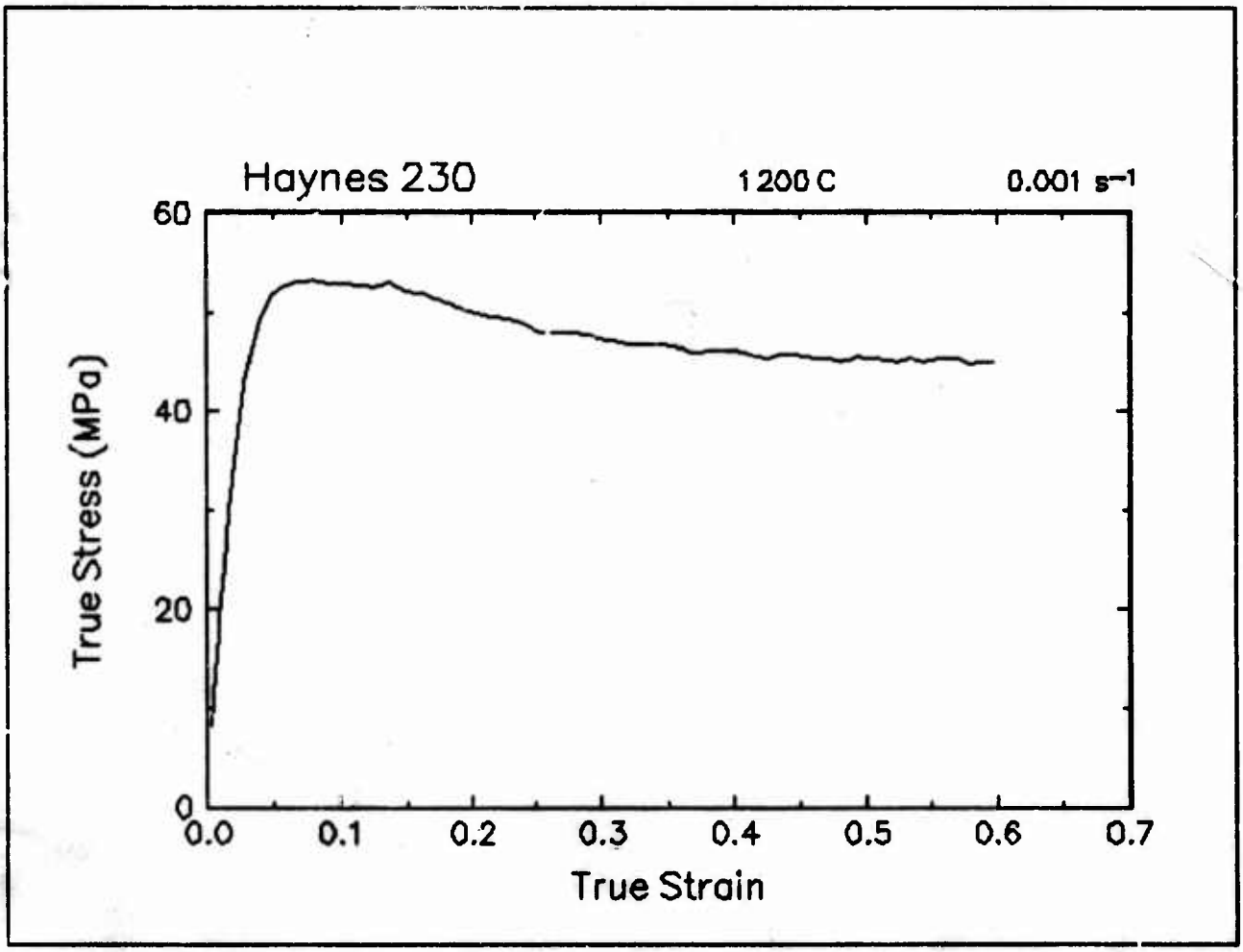

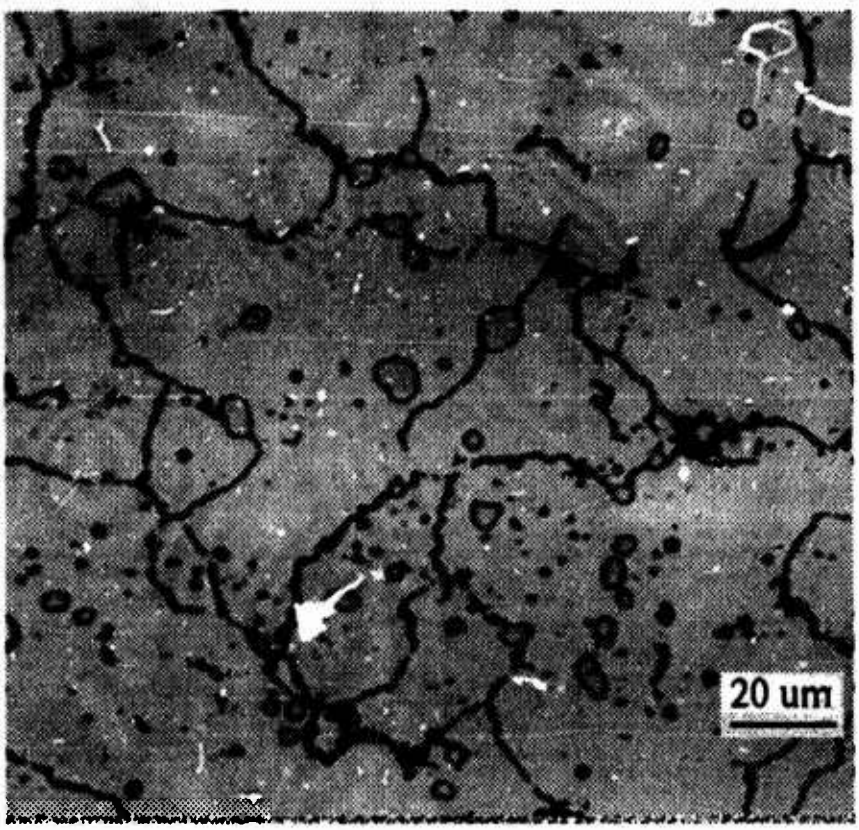

Figure 50. True stress-true strain curve and an optical micrograph from the center of the compressed sample cut through the compression axis, 1200 C and 0.001 s^{-1}.

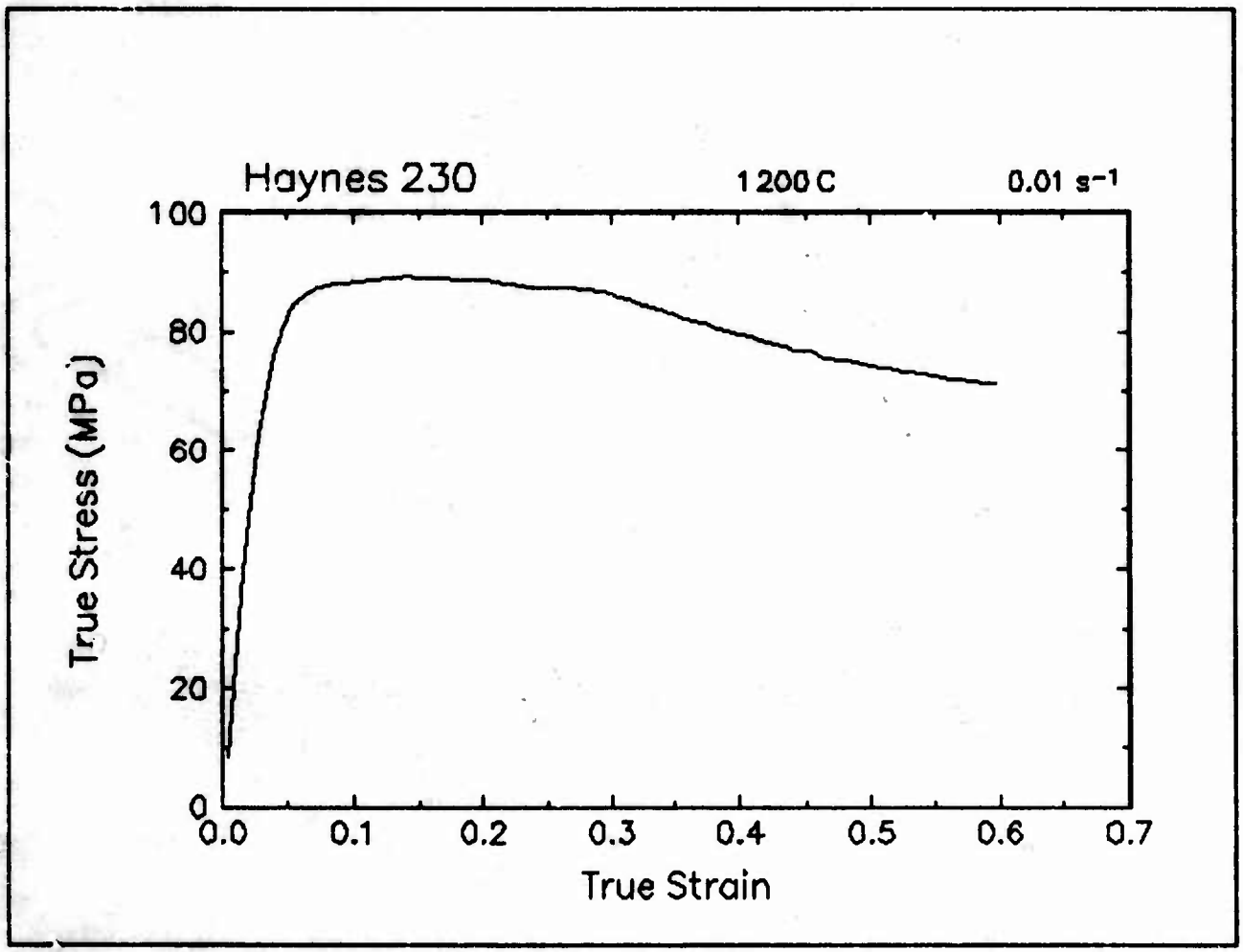

Figure 51. True stress-true strain curve, 1200 C and 0.01 s^{-1}.

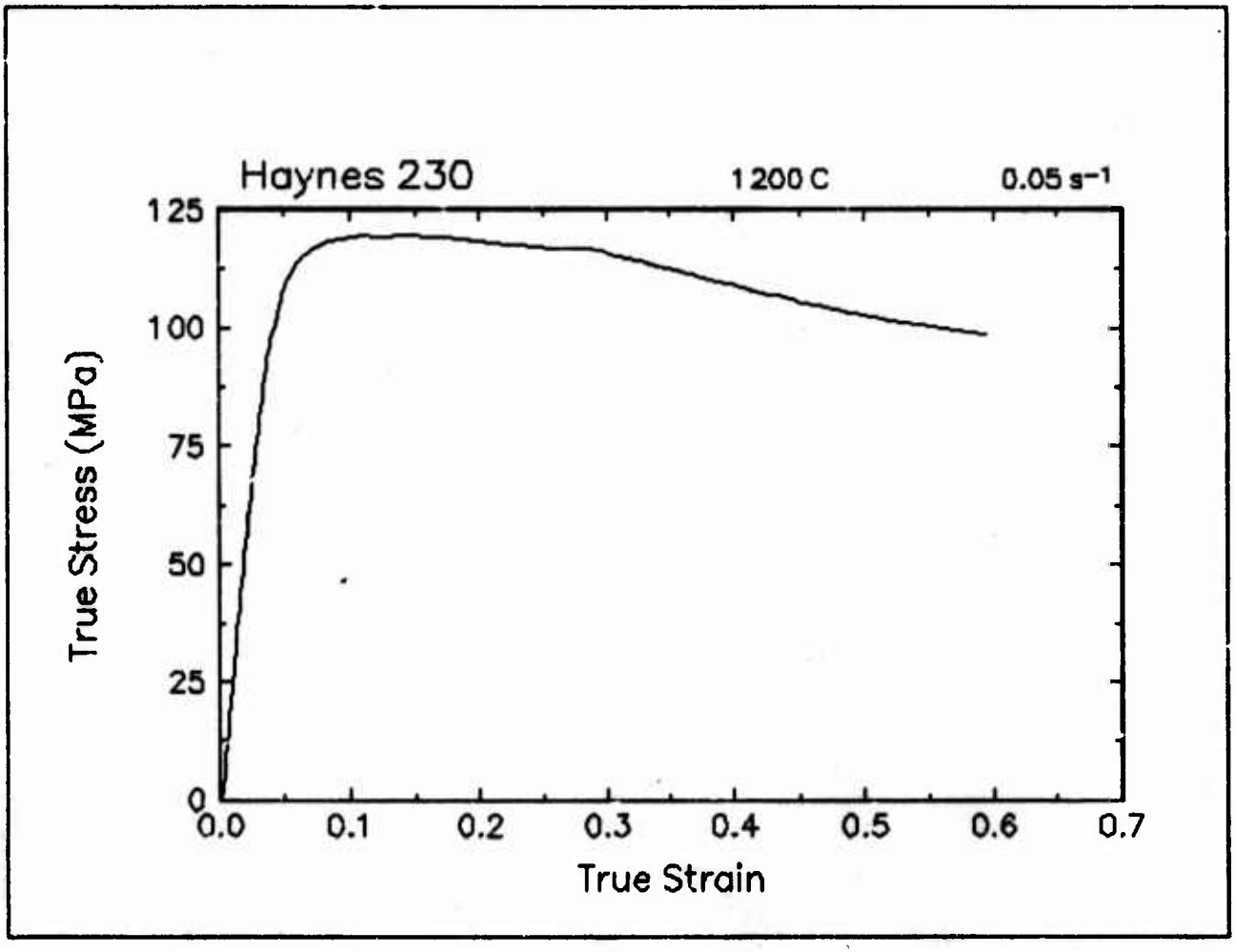

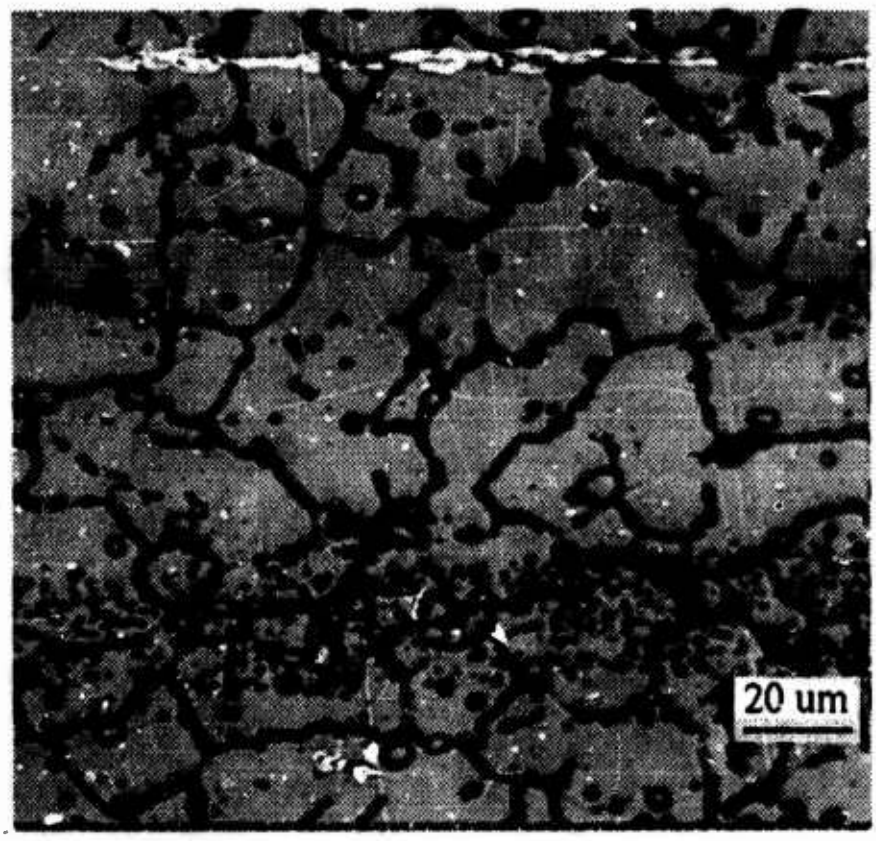

Figure 52. True stress-true strain curve and an optical micrograph from the center of the compressed sample cut through the compression axis, 1200 C and 0.05 s^{-1}.

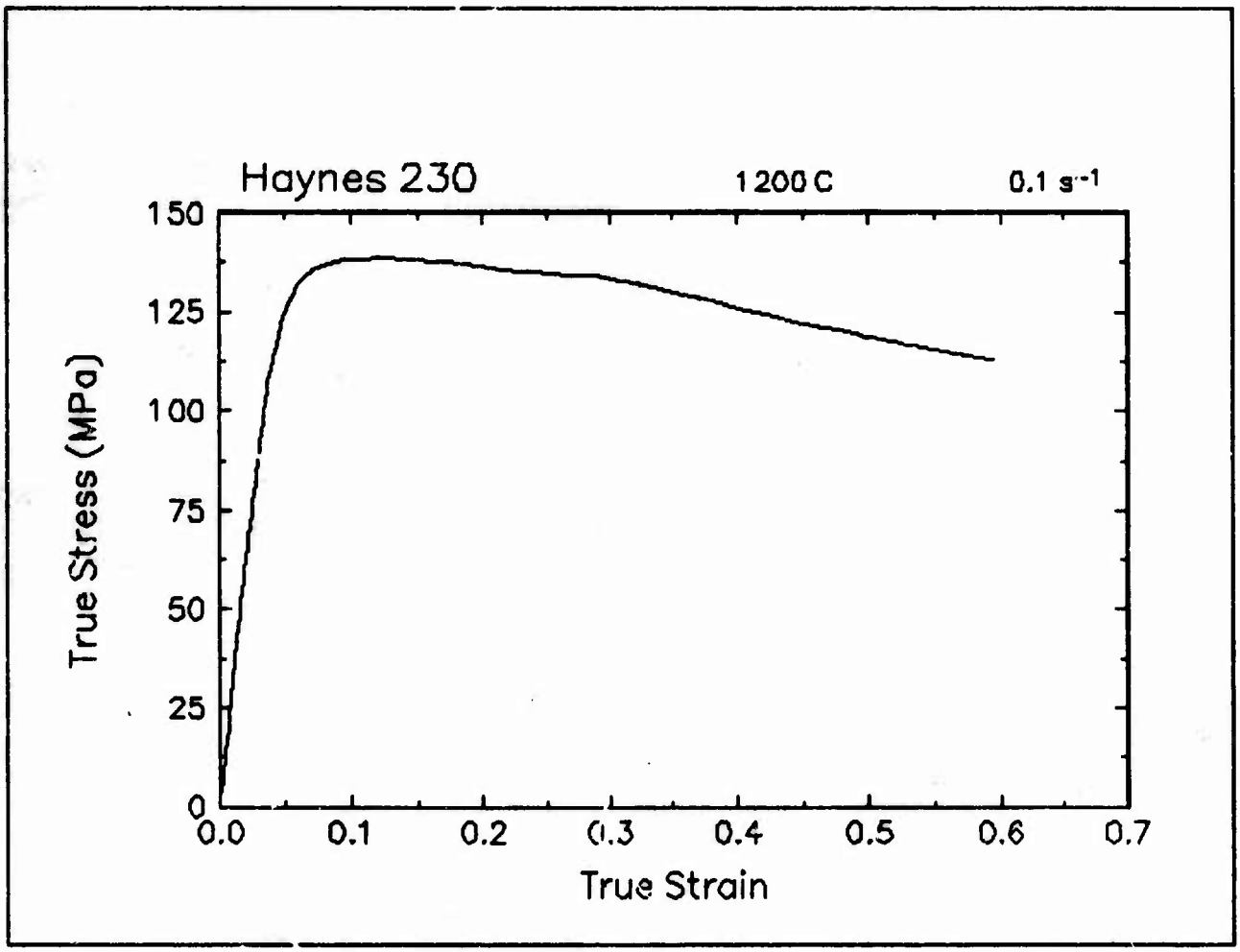

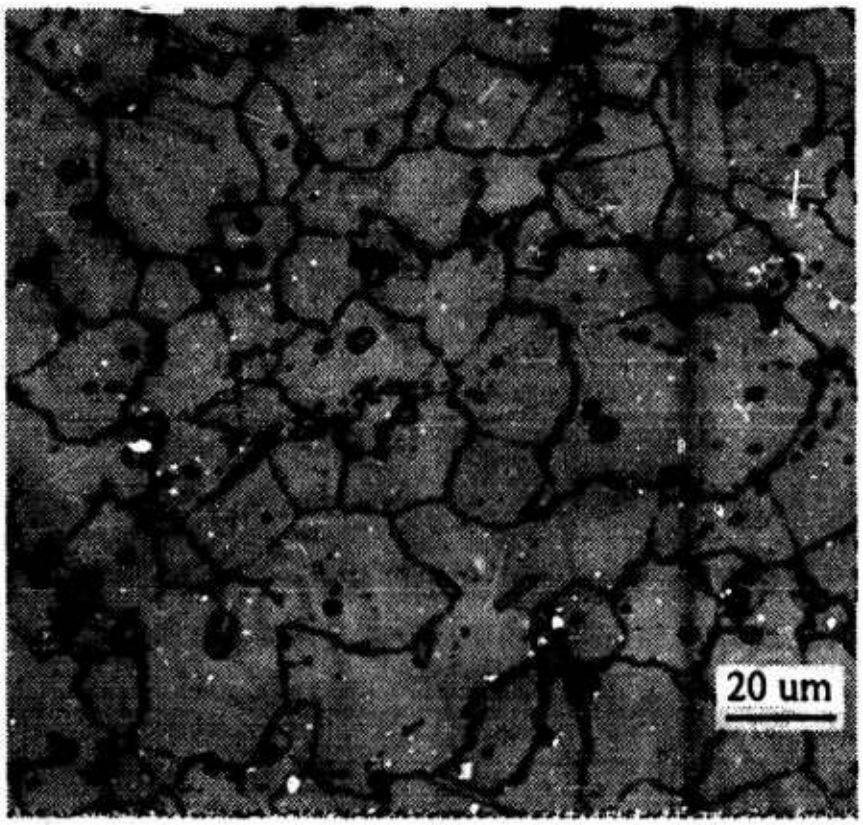

Figure 53. True stress-true strain curve and an optical micrograph from the center of the compressed sample cut through the compression axis, 1200 C and 0.1 s^{-1}.

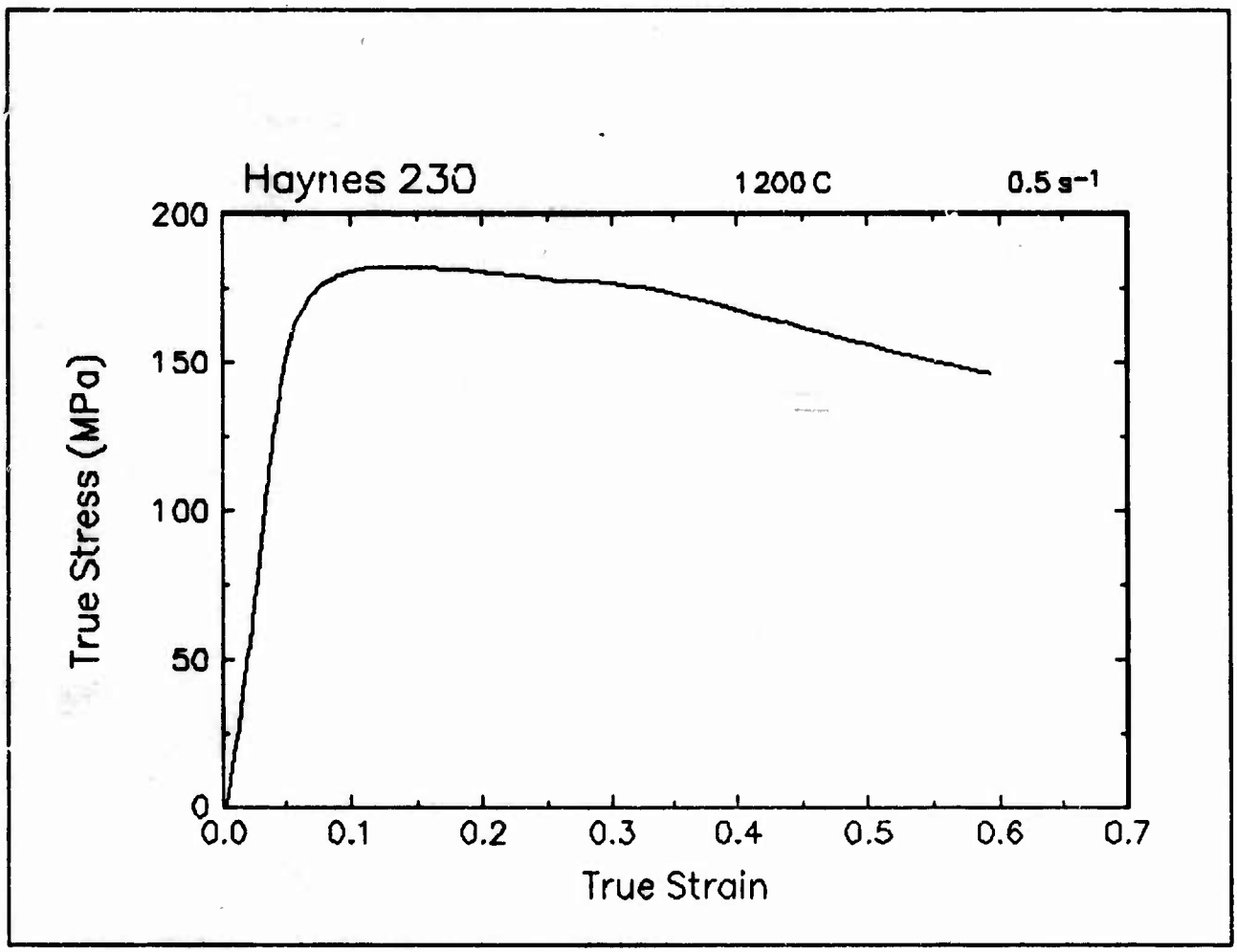

Figure 54. True stress-true strain curve, 1200 C and 0.5 s^{-1}.

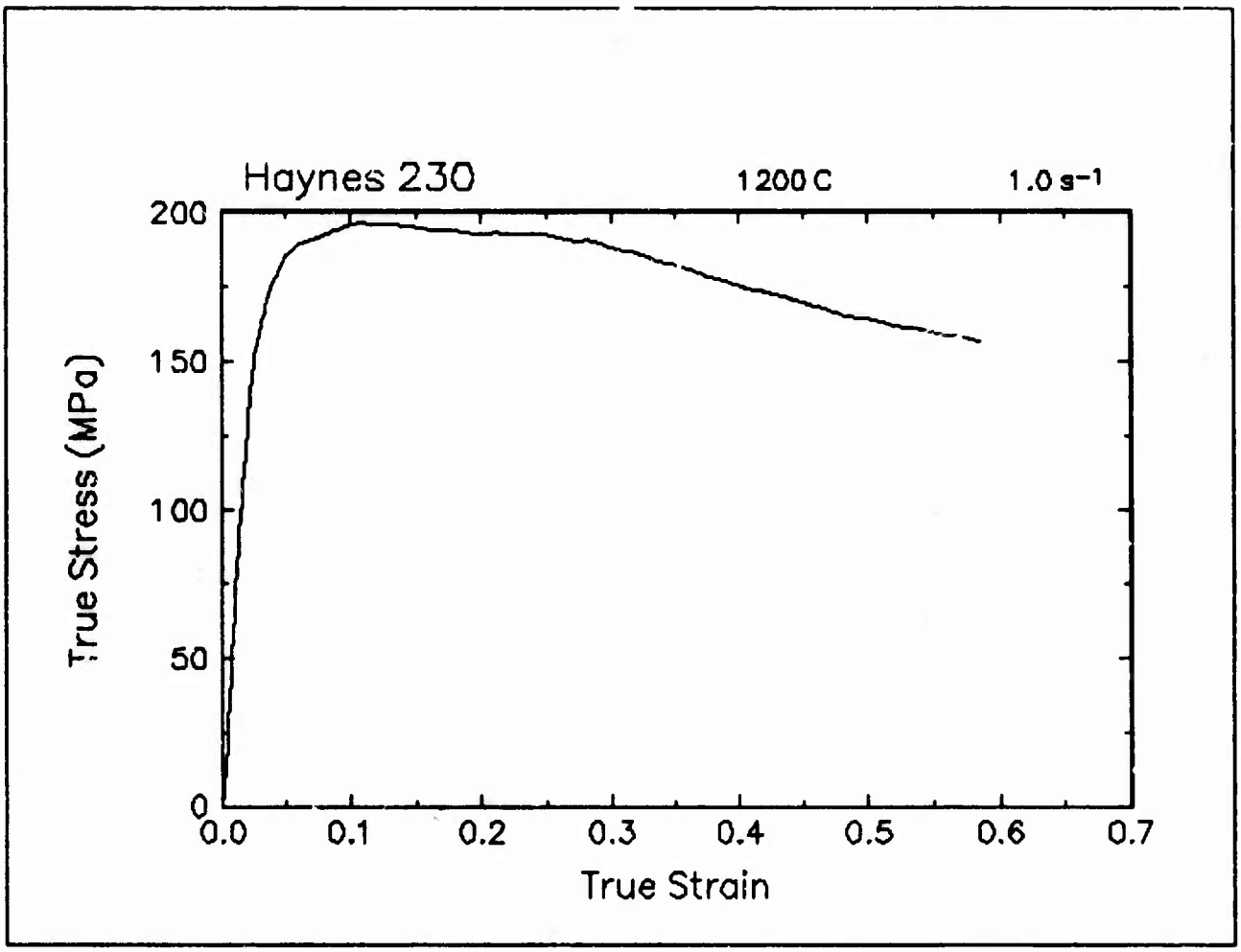

Figure 55. True stress-true strain curve, 1200 C and 1 s^{-1}.

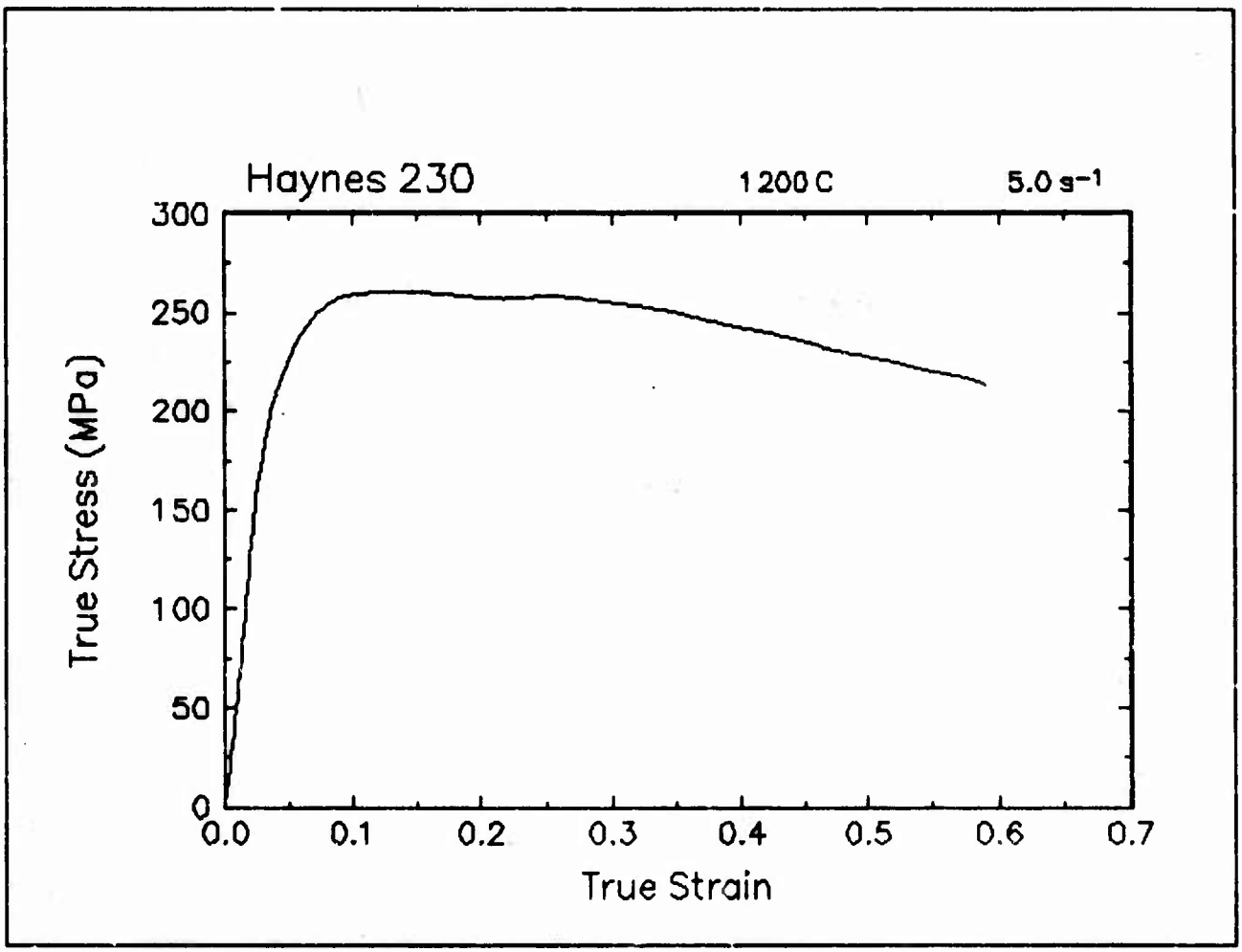

Figure 56. True stress-true strain curve, 1200 C and 5 s^{-1}.

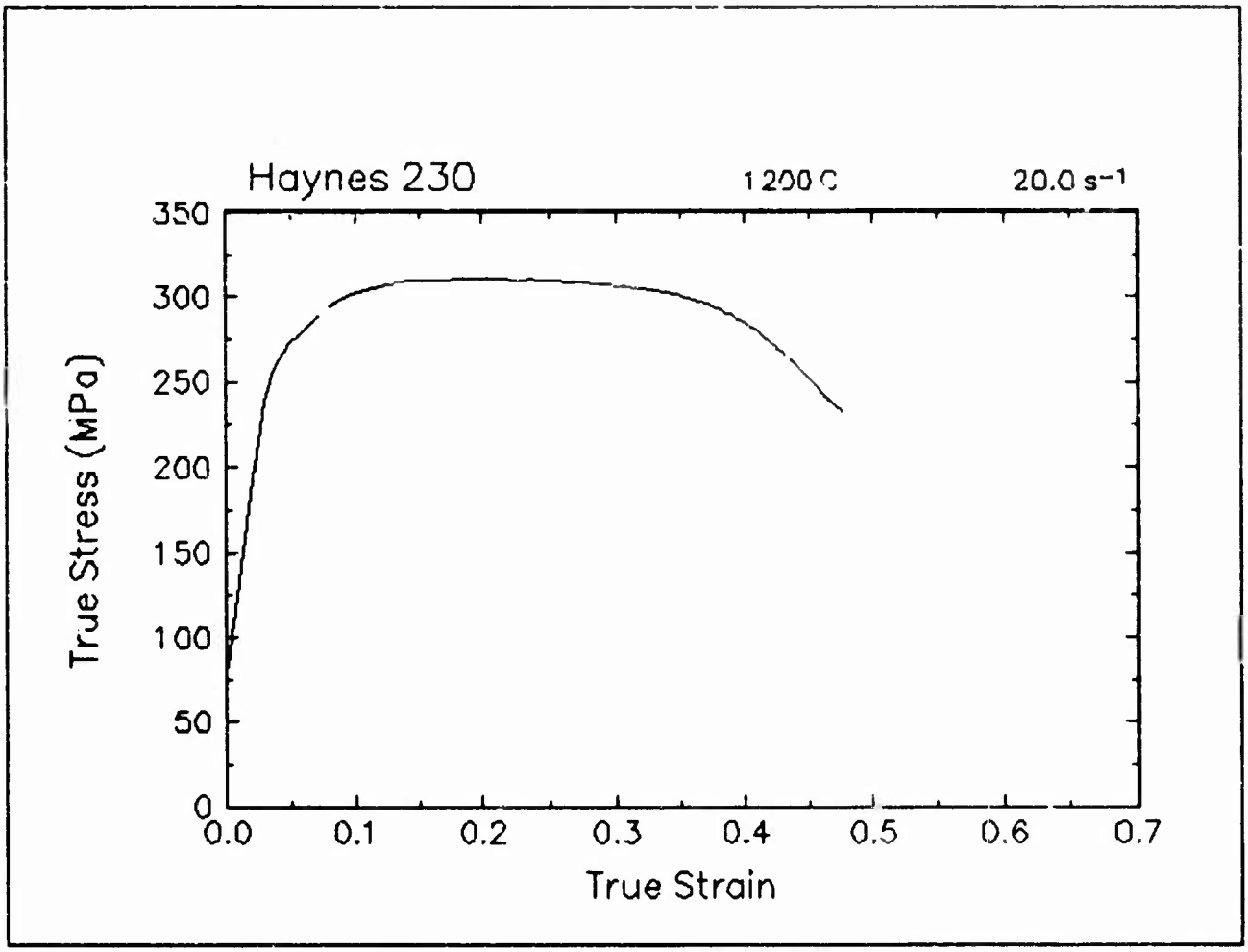

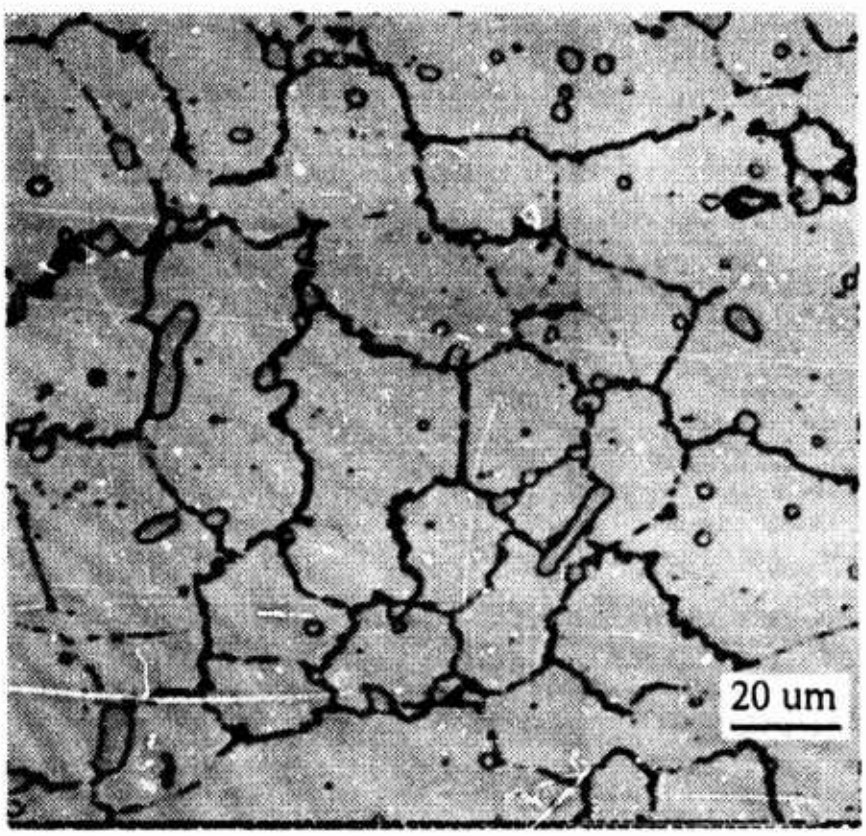

Figure 57. True stress-true strain curve and an optical micrograph from the center of the compressed sample cut through the compression axis, 1200 C and 20 s^{-1}.

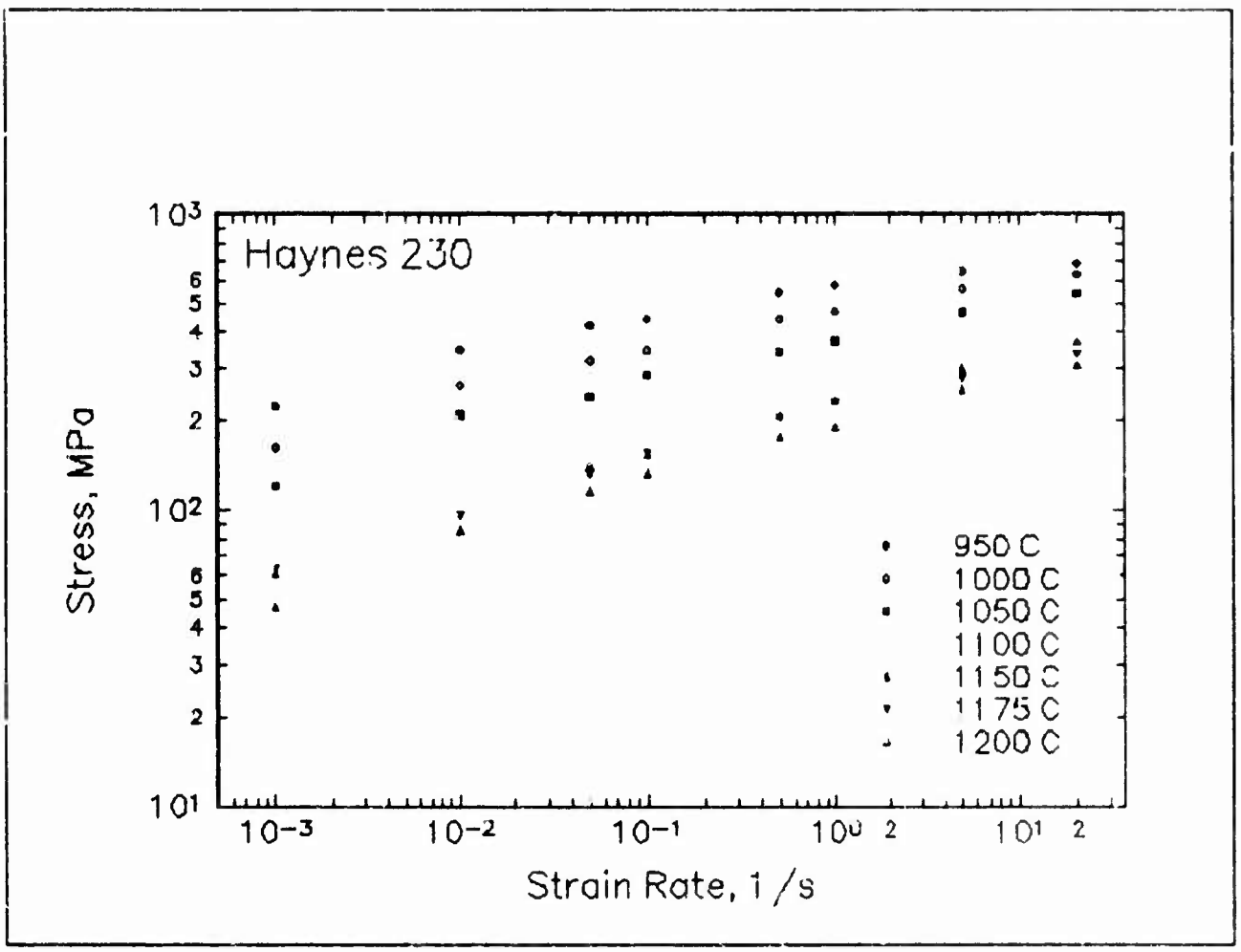

Figure 58. Effect of strain rate on stress in log-log scale at a true strain of 0.3 for Haynes 230.

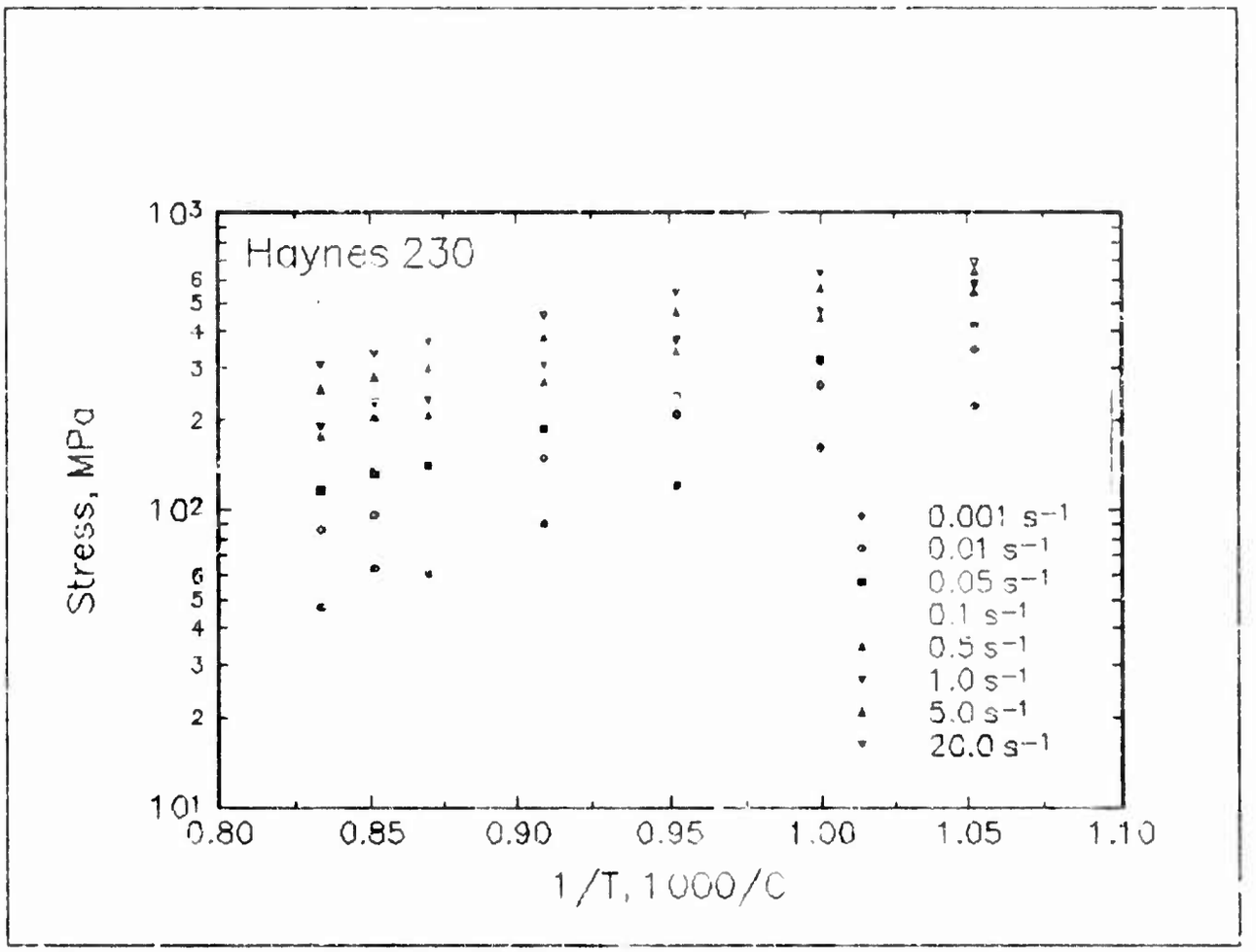

Figure 59. Effect of temperature on stress at a true strain of 0.3 for Haynes 230

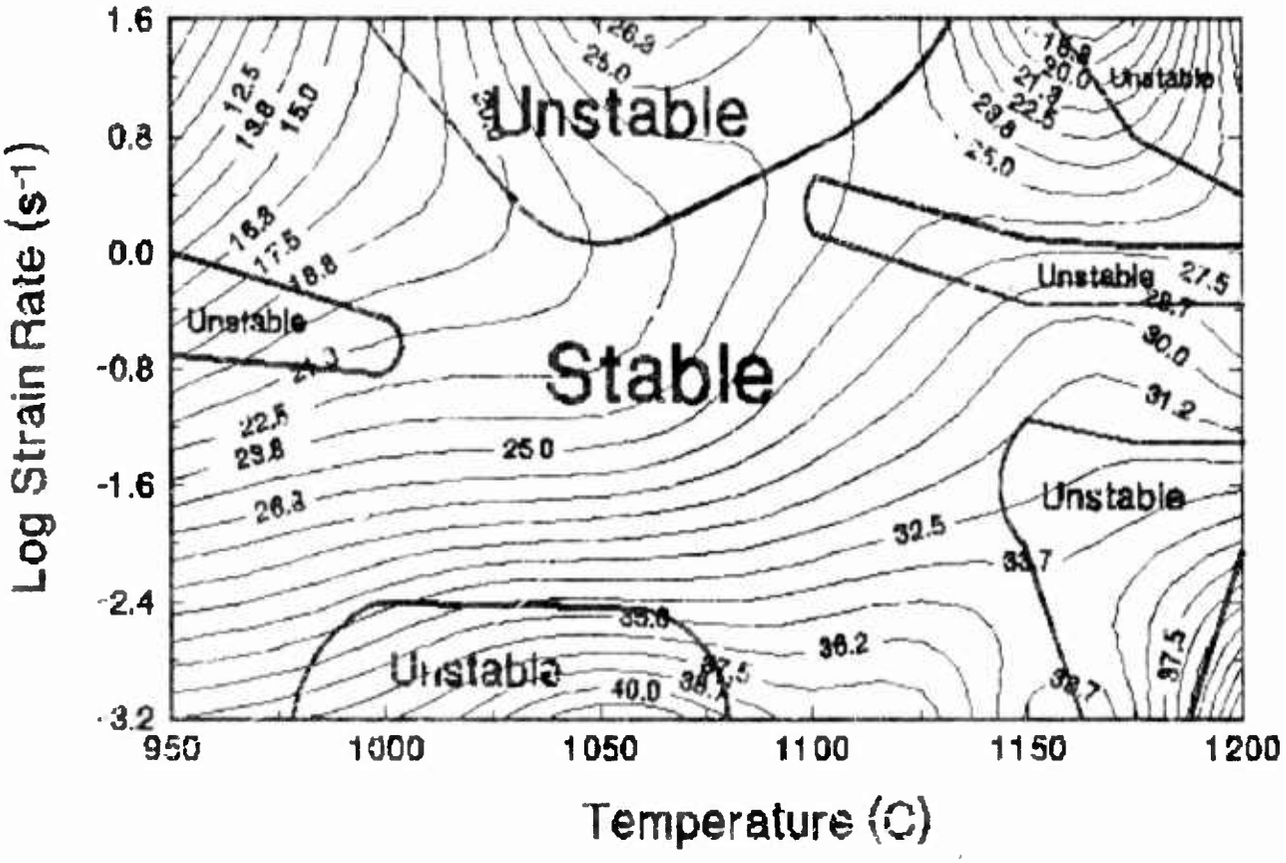

Figure 60 Processing map of Haynes 230 at a true strain of 0.30

Summary

Compression tests have been performed on Haynes alloy 230 over a wide range of temperatures and strain rates. The experimental conditions used in this work are representative of those used in metalforming practices. From the stress-strain curves, the flow behavior was characterized and a processing map indicating the optimum processing condition was generated. This condition is approximately 1100 C and 0.001 s^{-1}.

The deformed microstructures were characterized from the quenched specimens by optical microscopy and are presented with corresponding stress-strain curves.

Implementation of Data Provided by the Atlas of Formability

The Atlas of Formability program provides ample data on flow behavior of various important engineering materials in the temperature and strain rate regime commonly used in metalworking processes. The data are valuable in design and problem solving in metalworking processes of advanced materials. Microstructural changes with temperature and strain rates are also provided in the Bulletin, which helps the design engineer to select processing parameters leading to the desired microstructure.

The data can also be used to construct processing map using dynamic material modeling approach to determine stable and unstable regions in terms of temperature and strain rate. The temperature and strain rate combination at the highest efficiency in the stable region provides the optimum processing condition. This has been demonstrated in this Bulletin. In some metalworking processes such as forging, strain rate varies within the workpiece. An analysis of the process with finite element method (FEM) can ensure that the strain rates at the processing temperature in the whole workpiece fall into the stable regions in the processing map. Furthermore, FEM analysis with the data from the Atlas of Formability can be coupled with fracture criteria to predict defect formation in metalworking processes.

Using the data provided by the Atlas of Formability, design of metalworking processes, dynamic material modeling, FEM analysis of metalworking processes, and defect prediction are common practice in Concurrent Technologies Corporation. Needs in solving problems related to metalworking processes can be directed to Dr. Prabir K. Chaudhury, Manager of Forming Department, by calling (814) 269-2594.